

FINAL REPORT

**RIPRAP DESIGN FOR OVERTOPPED
EMBANKMENTS**

Prepared by

S.K. Mishra and James F. Ruff

Colorado State University
Engineering Research Center

Prepared for

U.S. Bureau of Reclamation

October, 1998

ABSTRACT

RIPRAP DESIGN FOR OVERTOPPED EMBANKMENTS

The flood potential at a dam and the resulting likelihood of dam failure must be evaluated as part of the design flood selection process. The design flood must be selected before requirements for additional spillway capacity or overtopping protection can be designed. Overtopping means using all, or a portion of, the dam crest length as an emergency spillway. Innovative overtopping protection systems for dams are being studied throughout the world. It is the hope that these studies will reduce cost and still provide a reliable level of safety to both new and existing dams. Research programs are currently underway or planned for evaluating overtopping protection concepts. If these new advancements were better known, dam owners may be more inclined to improve the level of protection of their dams at a reasonable cost.

In the construction of the new dams and rehabilitation of existing dams, riprap is usually the most economical material for erosion control. Currently, testing of large riprap sizes is lacking. Experiments have been conducted in laboratories without producing results allowing application to a full-scale dam with confidence. To address this problem, the United States Bureau of Reclamation and Colorado State University (CSU) built a near-prototype embankment overtopping facility at CSU's Engineering Research Center in 1991.

Three sizes of large riprap were tested on the overtopping facility in the summers of 1994, 1995, and 1997. Riprap gradations were obtained. Interstitial velocities of water through the rock layer as well as the flow depths were recorded for each test. These data were compared against the available riprap design equations. The need to develop a universal riprap design equation for any slope specifically steep slopes was established.

The gathered data were analyzed. A new universal riprap design equation was developed. Finally, an innovative riprap design procedure was outlined.

ACKNOWLEDGMENTS

Our appreciation to Ms. Kathleen Frizell and USBR Contract #1425-1-FC-81-17790 and Contract #1425-96-FC-81-05026, and the Colorado State University Agricultural Research Center Contract #COLO0708 for the funding support of this research and the completion of this report.

TABLE OF CONTENTS

	<u>Page</u>
ABSTRACT	i
ACKNOWLEDGMENTS	ii
LIST OF TABLES	v
LIST OF FIGURES	vi
LIST OF SYMBOLS	viii
Chapter 1: Introduction	1
1.1 The Purpose of the Current Study	3
Chapter 2: History of Embankment Protection Studies	4
2.1 Embankment Overtopping Protection Methods	4
2.2 Literature Review	6
2.3 NRC/CSU Studies for Riprap Design	12
2.4 ARS Riprap Tests	13
2.5 Need for Future Research	14
Chapter 3: Experimental Facilities, Riprap Characteristics, and Data Acquisition ..	15
3.1 Overtopping Facility	15
3.2 Characteristics of the Bedding Material	19
3.3 Characteristics of the Riprap Materials Tested	19
3.4 General Operating Procedures	21
3.5 Instrumentation and Data Acquisition	22
Chapter 4: Flow Observation	28
4.1 Riprap Flow Conditions	28
4.2 Flow Observations in 1994 and 1997	28
4.3 Flow Observations in 1995	31
Chapter 5: Data Analysis	35
5.1 Analysis of Salt Injection Method	35
5.2 Analysis of Piezometer Data	37
5.3 Velocity Calculation From Piezometer Data of 1994 and 1995	43
5.4 Velocity Calculation From Piezometer Data of 1997	43
5.5 Comparison of Interstitial Velocity Calculated From Two Methods	43

Chapter 6: Development of a Predictive Equation for Interstitial Velocity of Water Through Riprap	45
6.1 Need for Developing a New Predictive Equation for Interstitial Velocity of Water	45
6.2 Results From the Current Test Program	45
Chapter 7: Description of Riprap Failure and Toe Treatment	49
7.1 Failure of Riprap	49
7.2 Toe Treatment Test Program	53
Chapter 8: Development of the Riprap Design Equation	57
8.1 Development of Design Guidelines	57
8.2 Shield's Parameter	57
8.3 Derivation of the Universal Equation	63
8.4 Sensitivity Analysis	73
8.5 Riprap Layer Thickness and Slope Influence	73
Chapter 9: Design Procedure and Examples	79
9.1 Design Procedure	79
9.2 Example 1	81
9.3 Step by Step Solution	81
9.4 Example 2	83
9.5 Step by Step Solution	83
Chapter 10: Summary, Conclusions, and Future Research	85
10.1 Summary	85
10.2 Conclusions	86
10.3 Scope of Future Research	87
References	88
Appendix A: Interstitial Velocity Data	90
Appendix B: Manometer Data	108

LIST OF TABLES

	<u>Page</u>
Table 1.1	Mean stone diameters 2
Table 2.1	Riprap gradation for bedding layer of 1997 ($D_{50} = 48.3$ mm) 19
Table 2.2	Riprap gradation for 1994 tests ($D_{50} = 386$ mm) 20
Table 2.3	Riprap gradation for 1995 tests ($D_{50} = 655$ mm) 20
Table 2.4	Riprap gradation for 1997 tests ($D_{50} = 271$ mm) 21
Table 5.1	Comparison of interstitial velocities obtained by two methods 44
Table 6.1	Interstitial velocities 46
Table 7.1	Riprap failure characteristics 53
Table 8.1	Deviation factors σ 69

LIST OF FIGURES

		<u>Page</u>
Figure 2.1	Free body diagram of a rock in a horizontal plane	9
Figure 2.2	Free body diagram of a rock in water flow on an inclined plane	10
Figure 3.1	Overtopping facility at CSU	15
Figure 3.2	Riprap test layer configuration in 1994 and 1995	17
Figure 3.3	Riprap test layer configuration in 1997	18
Figure 3.4	Grid used for sampling rocks	20
Figure 3.5	Schematic drawing of injectors, conductivity probes, and piezometer locations	23
Figure 3.6	Plan view of the piezometers, injectors, and conductivity probes	24
Figure 3.7	1994 layout with the piezometer towers on the riprap slope before testing	25
Figure 3.8	1995 layout with the piezometer towers on the riprap slope before testing	25
Figure 3.9	1997 layout of the riprap slope with the piezometer towers before testing	26
Figure 3.10	Numbering of rocks in 1995	27
Figure 4.1	Transition of flow into the chute at $Q = 0.23 \text{ m}^3/\text{s}$, 1994	29
Figure 4.2	Flow becoming turbulent as it encountered the rock layer at $Q = 0.23 \text{ m}^3/\text{s}$, 1994	29
Figure 4.3	Visible surface water looking downstream at $Q = 0.28 \text{ m}^3/\text{s}$, 1997	30
Figure 4.4	Wet and dry areas of riprap surface at $Q = 0.42 \text{ m}^3/\text{s}$, 1997 (flow from top to bottom)	30
Figure 4.5	Wet and dry areas of riprap surface at window #2, $Q = 0.23 \text{ m}^3/\text{s}$, 1994	31
Figure 4.6	Flow (left to right) pattern due to obstruction of flow path seen through window #2 ($Q = 0.23 \text{ m}^3/\text{s}$)	32
Figure 4.7	Cascading flow (flow direction from top to bottom) (1994)	33
Figure 4.8	Water surface profile over the riprap gabion ($Q = 1.13 \text{ m}^3/\text{s}$)	33
Figure 4.9	Large plumes of water (1995) ($Q = 2.12 \text{ m}^3/\text{s}$)	34
Figure 4.10	Schematic of the velocity zones (1995)	34
Figure 5.1	Typical voltage drop indicating the interstitial flow velocity for the tests	36
Figure 5.2	Typical voltage drop seen in the bedding layer in 1997 or near the bottom layer for 1994 and 1995	37
Figure 5.3	Schematic drawing of piezometer-manometer configuration	37

Figure 5.4	Variation of depth of flow with unit discharge in 1994 and 1995	39
Figure 5.5	Variation of depth of flow with unit discharge in 1997	40
Figure 5.6	Photograph showing the profile of water flow through the riprap layer of 1994	41
Figure 5.7	Photograph showing the profile of water flow through the riprap layer of 1995	42
Figure 6.1	Comparison of current formula and formula by Abt <i>et al.</i> with existing data	48
Figure 7.1	Failure of 1994 riprap layer located 19.3 m from the crest of the flume down the slope	50
Figure 7.2	Several rocks of 1995 riprap layer caught in the trap (looking downstream)	51
Figure 7.3	Failure of 1995 layer showing removal of the top layer	51
Figure 7.4	Channelization in 1997 riprap layer with dislodgement of rocks	52
Figure 7.5	Failure of 1997 layer at 12.1 m from the crest down the slope	52
Figure 7.6	Schematic diagram of the toe shapes and sizes tested in 1997	54
Figure 7.7	Wire mesh covering the riprap	55
Figure 7.8	Catastrophic failure	56
Figure 8.1	Shield's diagram (adapted from Julien, 1995)	58
Figure 8.2a	Robinson <i>et al.</i> riprap design equation	59
Figure 8.2b	Closeup view of Robinson <i>et al.</i> (1995) riprap design equation	60
Figure 8.3a	Abt <i>et al.</i> (1991) riprap design equation	61
Figure 8.3b	Closeup view of Abt <i>et al.</i> (1991) riprap design equation	62
Figure 8.4	Fundamental equation with actual data obtained in different tests . . .	65
Figure 8.5	Universal design equation	67
Figure 8.6	Universal design equation (normal axes)	68
Figure 8.7	Error analysis at 50% slope (USBR/CSU)	71
Figure 8.8	Error analysis at 40% slope (ARS)	72
Figure 8.9	Relationship between maximum allowable surface discharge and D_{50} at various slopes	76
Figure 8.10	Relationship between maximum allowable surface discharge and the slope of the embankment at various D_{50} 's	77
Figure 8.11	Combined effect of slope and rock size on maximum allowable surface discharge	78

LIST OF SYMBOLS

a	Dimensional constant, and coefficient which varies with the cross-sectional geometry of the flow
C_f	Correction factor due to the aeration effects
C_s	Coefficient of stability of the rock layer
C_u	Coefficient of uniformity of the riprap
C_1, C_2	Constants
d	Depth of water to be determined from a stage-discharge rating curve, and representative dimension of the rock
D	Roughness height given by $3D_{84}$
D_{50}	Median stone size
D_w	Median boulder diameter
e	Absolute roughness
f	Friction factor
F_d	Drag force
F_w	Weight of the stone
g	Acceleration due to gravity
h	Water depth
i	Energy and hydraulic gradient
k_1	Function of the stone shape
k_2	Volume constant for the rock
k_s	Nikuradse roughness size
m	Hydraulic mean radius of rock voids
n	Manning's constant
n_p	Porosity
n	Exponent
q	Relationship between unit discharge
q_f	Unit discharge at failure
R	Hydraulic radius
s	Slope of energy grade line which can be approximated as the slope of the bed
S	Slope of bed (channel), and gradient expressed in decimal form
S_s	Specific gravity of rock
SF	Safety factor
t	Thickness of the riprap layer
v	Mean seepage velocity, and velocity of water
V_{ave}	Bulk velocity (average velocity)
V_i	Average interstitial velocity
W	Empirical constant for a given rockfill material
y	Average depth of water

α	Angle of the embankment with the horizontal
δs	Distance between the two probes
δt	Time elapsed between the drops of voltage at probe 1 and probe 2
γ	Specific weight (density, gravity) of water
γ_s	Specific gravity of rock
η	Roughness factor, and porosity of the rock layer
ϕ	Angle of repose of the riprap
Θ	Angle of slope
v_v	Average velocity of water through rock voids
ϕ	Angle of repose of the riprap material, and angle of internal friction
τ	Shear stress
τ_*	Non-dimensional Shield's parameter
τ_{cr}	Critical shear stress to cause the incipient motion = γRS

CHAPTER 1

INTRODUCTION

In recent years, a number of state and federal agencies have inventoried all dams within the United States to assess their overall safety. During this process, the design floods were reevaluated and often recalculated.

Previous design flood selection criteria included factors such as dam height, storage volume, downstream development, and relationships between design floods and downstream hazard classifications. Current practice is to classify dams based on the consequences of dam failure. This requires the identification of potential failure modes and quantitative evaluation of the consequences of dam failure. In addition to the traditional economic analysis of impacts such as lost project benefits and property damages, impacts from loss of life, and environmental impacts should be considered.

The revised floods were generally larger than the floods developed for the original designs because of an increased database and revised criteria for developing floods based on refined versions of the National Weather Service hydrometeorological reports (Oswalt *et al.*, 1994). In many cases, occurrence of the new or revised design floods will result in overtopping of dams due to insufficient storage and/or release capacity provided by the existing reservoirs. Traditional modification alternatives for resolving this problem, such as providing additional reservoir storage and increased spillway capacity are often very costly. As a result, some dam owners are faced with either accepting greater risks than were indicated by the original design flood calculations, or incurring significant costs to protect their facilities from failure during extreme flood events. For some time, the Federal Energy Regulatory Commission (FERC) and dam owners have maintained that finding an alternative to traditional spillway designs by protecting these embankments from failure due to overtopping would represent an important advancement in public safety and economy. Overtopping essentially means using all, or a portion of, the dam crest length as an emergency spillway.

There is an urgent need for research to develop design criteria for protective overlays as an alternative to traditional spillway design where dam safety modifications are under consideration at major embankment structures in the United States. New and innovative designs for spillways and overtopping protection systems for dams that will reduce costs and still provide a reliable level of safety are being developed throughout the world. Many of these alternatives are applicable to both new and existing dams. In addition, research programs are currently underway or planned for evaluating new spillway designs and overtopping protection concepts. If these new advancements were verified, dam owners may be more inclined to improve the level of protection of their dams at a reasonable cost. Such systems will not only save a large amount of money, but will also increase public safety.

In the construction of new dams and rehabilitation of existing dams, riprap is usually the most economical material for erosion control. The design of riprap to resist overtopping flow is dependent upon the material properties, the hydraulic gradient, and the unit discharge. Several researchers such as Stephenson (1979), Abt *et al.* (1987 and 1988), and Robinson *et al.* (1995) have provided empirical design criteria which currently offers the best approach for design. However, flow hydraulics on steep embankment slopes protected with riprap can not be analyzed by standard flow and sediment transport equations. Furthermore, testing of large riprap sizes is lacking and extrapolation to prototype sizes is difficult. All previous experiments dealing with riprap protection on slopes with overtopping flow have been performed with stone diameters of 158 mm or less and slopes of 40% or less. Experiments have been conducted in laboratory facilities and/or large-scale flumes, but have not produced results allowing application to a full-scale dam with confidence. Large-scale tests on steeper slopes where aeration effects and scale effects may not be neglected are lacking. In general, a comprehensive data set of riprap failure for D_{50} larger than 158 mm is not currently available.

Shield's parameter is a dimensionless form of the shear stress that expresses the incipient motion of stones in flowing water. Mechanics of the riprap stability is governed by the Shield's parameter. For riprap in overtopping flow, rock movement that leads to exposure of the underlying materials is the primary failure mode. Because of the many assumptions made to simplify the Shield's parameter for the present design use, it is inadequate for its applications to riprap design in overtopping flows. The simplified form of the Shield's parameter assumes the slope to be less than 10% and related forces to be neglected. This assumption is unacceptable when dealing with the steeper slopes of a typical embankment dam.

Interstitial velocities were never measured with the exception of the tests conducted jointly by the Nuclear Regulatory Commission (NRC) and Colorado State University (CSU). Even though interstitial velocity was measured during the NRC/CSU riprap testing, it was not used as a parameter for designing the riprap. Parkin *et al.* (1966), Leps (1973), and others analyzed interstitial velocities of rockfill without looking into the mechanics of failure, since it was not an immediate concern for the type of studies they were conducting. Studies carried out by Robinson *et al.* (1995) of the Agricultural Research Service at Stillwater, did not measure interstitial velocities.

Existing equations used to predict stone sizes needed on overtopped embankments produce widely varying results. Table 1.1 provides a sample of the various mean stone diameters that may be obtained by using some of the existing methods for a typical embankment dam of 2:1 downstream slope that must pass an overtopping unit discharge of 1.4 m³/s/m. These methods yield up to sevenfold difference in stone size.

Table 1.1: Mean stone diameter

Method	Predicted D_{50} stone size (mm)
Abt <i>et al.</i> (1987, 1988)	457
Robinson <i>et al.</i> (1995)	488
Stephenson (1979)	3,124

1.1 The Purpose of the Current Study

The purpose of placing riprap on an embankment is to prevent erosion of the underlying earthen materials that constitute the embankment. The need to predict the behavior of riprap protection is the very important first step in predicting the eventual breach of the dam. Design of stable riprap protection should prevent dam breaching for designed overtopping flows. Over estimation of the material needed to protect a dam can lead to excessive costs that make the project prohibitively expensive. Under estimation of the size of the material can lead to catastrophic consequences including loss of life, economic losses, and destruction of infrastructure. As a result, further tests of large size stones on steeper slopes as conducted by this project are needed to develop better design criteria for overtopped riprap.

The objective of the current investigation is to derive a universal formula for designing riprap for overtopping flows regardless of the slope of the overtopped embankment. The formula will be based on the mechanics of the riprap mixture under flowing water observed while testing in the near-prototype Embankment Overtopping Research facility located at the Engineering Research Center of CSU.

Background information for the embankment protection studies is presented in Chapter 2. A brief comparison of the different methods of riprap design is made and the need for large-scale testing and further investigation of the mechanics is established. A detailed description of the experimental facility and the procedures of the tests is given in Chapter 3. Data acquisition is also discussed in Chapter 3. Chapters 4 and 5 present flow observations and analyzes of data, respectively.

Design of riprap for embankment overtopping at a given flow condition consists of a two-step procedure. The first step involves sizing the riprap. The second step deals with predicting the minimum depth of the riprap. A fairly accurate prediction of the interstitial velocity of water through the rock layer is necessary to achieve this goal. Chapter 6 of this dissertation presents a formula to predict the interstitial velocity of water through a particular rock layer. Failure of the riprap and the toe treatment are discussed in Chapter 7.

The mechanics of riprap failure based on the complete form of the Shield's parameter is illustrated in Chapter 8. A universal equation is proposed based upon the particular flow conditions tested under this program. The universal equation is verified using test results from other researchers. The predictive equation for the velocity of water flowing through a riprap layer, obtained in Chapter 6, is used in Chapter 8 to design the thickness of the riprap layer.

This investigation provides a complete set of guidelines for designing riprap for protection of overtopped embankments. Chapter 9 shows the application of the complete riprap design guidelines through design examples. Chapter 10 summarizes the entire riprap investigation providing conclusions, recommendations, and the scope of proposed future research work in this area.

CHAPTER 2

HISTORY OF EMBANKMENT PROTECTION STUDIES

2.1 Embankment Overtopping Protection Methods

Since 1983, extensive testing has been conducted in the United States (U.S.), Great Britain, and the former Soviet Union to develop alternatives for overtopping protection for embankment dams. Protection systems tested include vegetative covers (e.g. grass-linings), roller-compacted concrete and soil cement, precast concrete block systems, geotextiles, gabions, and riprap. A review of the tests, where success and/or failure of the various systems were well documented, will help determine the most appropriate overtopping protection alternative for a particular project.

Use of vegetation is generally not accepted as sufficient erosion protection from overtopping. However, documented information is available which indicates that a vegetative cover will provide a limited amount of erosion protection. Vegetation-lined embankments may provide moderate resistance to erosion for short periods of low head and low velocity overtopping. It has been shown that embankment slopes constructed with cohesive soils and well-managed vegetation have withstood overtopping depths up to 0.6 m with velocities up to 2.74 m/sec (Powledge *et al.*, 1989). Vegetation-lined slopes require continuous maintenance by fertilizing, mowing and repairing areas of poor cover. Under local stress conditions, unvegetated areas may develop into areas of local scour that can contribute to erosive processes.

A variation on vegetation-protected embankments is the use of geotextile materials. Geotextiles can be an effective way to improve the erosion resistance of embankments (Oswalt *et al.*, 1994). Erosion, however, can be accelerated if flow develops between the material and the embankment soil. This can be prevented by appropriate anchoring of the material and a well established growth of vegetation.

Several types of individual precast concrete blocks for embankment protection have been tested and produced satisfactory results. Application of the following block systems can be found in the U.S., Russia and Great Britain (Oswalt *et al.*, 1994):

1. Wedge Concrete Blocks; and
2. Cellular Concrete Mat (CCM) system

Wedge concrete blocks will provide adequate protection on both granular embankments of medium permeability and on low permeability earthfill. Flow regime in the subsoil needs to be predicted to assess the degree of saturation and soil pore water pressures, and to design an appropriate drainage system to evacuate seepage flow. If the underlying material has low saturated shear strength, the spillway slope needs to be flatter than the general downstream slope of the dam. Wedge concrete blocks were tested in Great Britain and the U.S. to provide protection during overtopping of embankment dams (Oswalt *et al.*, 1994). In Russia, wedge-shaped block spillways have been tested to withstand

overtopping heads of 11 m and flow velocities of 22.9 m/sec (Oswalt *et al.*, 1994). The design was not very cost-effective because the resisting moment and forces were counteracted by the weight of the blocks, resulting in large blocks that may be cost prohibitive.

The United States Bureau of Reclamation (USBR) tested a modified version of the blocks, in which hydrodynamic forces help the blocks remain in place. Small-scale tests were conducted at USBR's Water Resources Laboratory and large-scale tests were conducted at CSU in 1992 and 1993. These tests confirmed that a more efficient design of concrete blocks was feasible. Blocks were placed as stepped overlay to provide a high roughness, which helps dissipate the energy of the flow and reduce flow velocity. Stepped blocks placed over a proper drainage system reduce the seepage flow within the embankment, thus reducing uplift pressure (Frizell *et al.*, 1992).

Originally designed for coastal protection in wave environments, CCM systems provide a viable option for protecting embankment slopes from potentially catastrophic erosion that can occur during overtopping flows (Oswalt *et al.*, 1994). CCM products, also called articulated concrete blocks (ACB), are prefabricated mats of precast cellular concrete blocks tied together by cables and anchored in place. These products are most commonly used in breakwater structures, streambank protection for waterways, and coastal shore protection. The Army Corps of Engineers has used heavy revetment systems of articulated concrete mats to control bank erosion along the Mississippi River.

Concrete block products can be categorized into two groups, those that simply interlock mechanically and those that are secured together with cables. Block designs vary from solid blocks to those having open cells to permit uplift pressure relief and encourage vegetation growth. Using commercially available revetments, researchers from Great Britain found that cable-tied concrete blocks provided the most effective protection against high velocity flow in the full-scale overtopping tests conducted at Jackhouse Reservoir in 1986. These systems had weights between 1,321.5 N/m² to 1,556 N/m² and were underlain by geotextiles, anchored, and covered with sod. The CCM products used in the tests withstood high velocity flows up to 7.9 m/s on a cohesive subsoil without failure (Oswalt *et al.*, 1994).

The blocks of the CCM systems are typically 0.1 m to 0.23 m thick and 0.3 m to 0.6 m square in the plan view with openings penetrating the entire block. Polyester rope or steel wire cables extend through precast holes in the blocks. All available CCM products use cables running lengthwise (longitudinally); however, some also have cables running across their width (laterally) to provide greater stability. Because of the open cells, CCM products promote infiltration into the embankment and seepage out of the embankment. The other components of typical CCM systems include an underlying woven geotextile filter fabric, mechanical anchors, and a soil/vegetative cover.

Recent documented applications of precast concrete blocks in the U.S. include Bass Lake Dam, Price Lake Dam, and Trout Lake Dam for the National Park Service. These Blue Ridge Parkway dams were the first application of CCM for overtopping protection in the U.S. The embankment dams range in height from 8.5 m to 12 m, and required over 11,706 m² of CCM products to provide protection against overtopping depths up to 1.2 m and flow velocities up to 7.9 m/s (Oswalt *et al.*, 1994).

Another common treatment used to stabilize embankments is the use of compacted soil cement. Soil cement is created when Portland cement is mixed with available soils and

then placed, spread, and compacted. The layer may be placed directly against the slope or compacted in stair step horizontal layers. Researchers have shown soil-cement layers on low dikes up to 1.2 m high to resist erosion for overtopping heads of up to 1.2 m (Chen and Anderson, 1986).

An overlay of Roller Compacted Concrete (RCC) is the most typical installation for erosion protection currently used for low to medium height dams (3 m - 48.9 m). Construction of RCC embankment protection is normally very rapid, and cost effective while affording a number of other advantages. In most cases, minimal project disruption occurs because construction is limited to the dam crest and downstream slope, with no requirement for reservoir restrictions. The performance of dams protected by RCC that have been subjected to overtopping flows has been excellent (Oswalt *et al.*, 1994).

The RCC is placed in horizontal lifts, about 4.6 m wide starting at the downstream toe and proceeding up the embankment slope. The lifts are generally about 0.3 m thick resulting in an uneven surface. This configuration provides energy dissipation with the steps acting as roughness elements to reduce flow acceleration. RCC may also be placed directly against the embankment in a thin layer parallel to the slope providing a reinforced slope. This method requires less material but construction is difficult because of compacting equipment running up and down the slope. Energy dissipation is also less on the smooth sloped surfaces than on the stepped surfaces.

Many existing embankment dams have riprap on the downstream face of the dam. Often, dam safety engineers would like to know if there will be adequate protection should the dam overtop. However, flow hydraulics on steep embankment slopes protected with riprap cannot be analyzed by standard flow and sediment transport equations. Riprap designed to resist overtopping flow is dependent upon the material properties, the hydraulic gradient, and the unit discharge.

2.2 Literature Review

Tests on riprap had generally been conducted with rocks of 153 mm diameter or less on slopes up to 5:1 (H:V). Tests were conducted to evaluate interstitial flows, resistance factors, and incipient failure of the riprap.

Parkin *et al.* (1966) studied flow through rock-filled dams and considered the use of a power function of type:

$$i = av^n \quad (2.1)$$

where i = the energy gradient, a = a dimensional constant, v = mean seepage velocity, and n = an exponent which, although varying with the rock and flow characteristics, satisfactorily approximates 1.85 for most practical flows in materials composed of convex particles coarser than 12.5 mm diameter. In free surface flows, the energy gradients in rockfill structures will generally be in the range 0.1 to 1.0.

According to Parkin *et al.* (1966), a is mainly a function of hydraulic radius and shape of the particle. A nomogram for finding a as a function of void ratio, specific surface and shape of the particles was provided by the authors. However, experimental studies are strongly recommended for determining a when designing rockfill dams.

Ruff and Gelhar (1970) investigated the velocity distributions in the porous boundary of a pipe. The velocity profiles measured in the porous boundary of a pipe indicate that shear effects penetrate to a relatively small distance (6.4 mm to 7.6 mm) into the boundary. A finite velocity exists at the surface of the porous boundary and the magnitude, when normalized with shear velocity, is about 1 to 3. The velocity decreases approximately exponentially over the penetration depth and a pressure gradient flow exists over the remainder of the porous boundary.

Wilkins (1956, 1963) performed laboratory transmissivity tests on cylindrical specimens, resulting in the relation

$$v_v = Wm^{0.5}i^{0.54} \quad (2.2)$$

where v_v = the average velocity of water through rock voids in inches per second, i = hydraulic gradient, m = the hydraulic mean radius of rock voids in inches (volume of voids divided by total surface area of the particles), and W = an empirical constant for a given rockfill material, depending primarily on the shape and roughness of the rock particles and on the viscosity of water. W , when expressed in (inch^{0.5}second) units, varies from about 33 for crushed gravel to about 46 for polished marbles. A practical determination of, m , is fairly reliable for clean, monosized rock but is very uncertain for a well-graded or nonhomogeneous rockfill. Most of the work that has been reported to date on flow through and over rockfills has consisted of tests on small models.

Stevens *et al.* (1976) developed design criteria for protecting abutments and embankments using riprap. Their method is called the safety factor method. They idealized a particle rolling around the point of contact with the adjacent downstream particle. If the driving moments produced by the lift force, drag force and the component of the weight parallel to the bed exceed the moment caused by the component of the weight normal to the bed, the particle is said to be unstable and incipient motion begins. Since the component of the weight normal to the bed is practically the only resisting force, and the weight is proportional to the volume of the particle, the resistance to motion depends on the size of the particle. The driving forces also depend upon the slope of the embankment and the angle of repose of the material.

The steps for sizing riprap using the safety factor method can be summarized as follows:

1. Choose a safety factor (SF)
2. Calculate roughness factor η :

$$\eta = \cos \alpha \left(\frac{1}{SF} - \frac{\tan \alpha}{\tan \phi} \right) \quad (2.3)$$

where: SF = safety factor, typically 1.5 for riprap;
 α = angle of the embankment with the horizontal; and
 ϕ = angle of repose of the riprap.

3. Calculate the shear stress:

$$\tau = \gamma d S \quad (2.4)$$

where: γ = specific weight of water;
 d = depth of water to be determined from a stage-discharge rating curve; and
 S = slope.

4. Calculate the median stone size from:

$$D_{50} = \frac{21\tau}{(S_s - 1)\gamma\eta} \quad (2.5)$$

where: S_s = specific gravity of rock (2.65 usually).

Carling *et al.* (1992) studied the effect of bed roughness, riprap shape, and orientation on particle entrainment. They tried to maintain flow depths greater than about five times the test particle diameter to reduce profile distortion. They concluded that for a given size and density the entrainment of a particle sitting on a rough bed depends on the shape, orientation and relative exposure to the incident flow.

Thompson and Campbell (1979) studied flow in a riprap channel in New Zealand. Using data provided by other authors and data collected in their study, a new expression for the Darcy friction factor was proposed by Thompson and Campbell:

$$f = \left(\left(1 - 0.1 \frac{k_s}{y} \right) 2 \log_{10} \left(12 \frac{y}{k_s} \right) \right)^{-2} \quad (2.6)$$

$$k_s = 2D_w \quad (2.7)$$

where: f = friction factor;
 y = depth of flow;
 k_s = Nikuradse roughness size; and
 D_w = median boulder diameter.

Hey (1979) used data from natural gravel and cobble bed streams to establish a relation between flow resistance and particle size distribution in gravel-bed rivers. Use of the Colebrook-White equation seemed to be adequate if a variation in the coefficient, a , for different shapes is allowed in the equation:

$$\frac{1}{\sqrt{f}} = 2.03 \log \left(\frac{aR}{D} \right) \quad (2.8)$$

where: f = the friction factor;
 R = hydraulic radius;

- D = roughness height given by $3D_{84}$; and
- a = coefficient which varies with the cross-sectional geometry of the flow.

The range for the value of, a , has the limits 11.1 and 13.46, and the actual value depends on the hydraulic shape (R/y) of the cross-section, in which y is the perpendicular distance from the perimeter to the point of maximum velocity. This normally is the maximum flow depth unless the channel is very narrow and deep.

Stephenson (1979) while studying the formation of rockfill embankments in flowing water, developed a general theory for the stability of individual stones on a slope in flowing water. The sliding and overturning equilibrium for a rock in a horizontal plane can be derived from Figure 2.1. Considering sliding equilibrium for a stone on a horizontal plane,

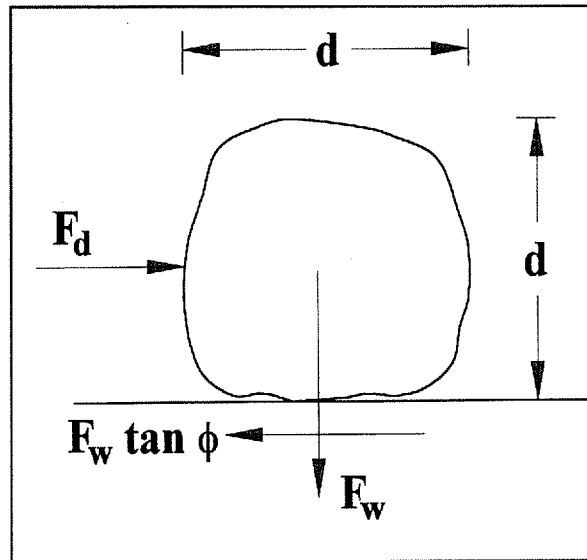


Figure 2.1: Free body diagram of a rock in a horizontal plane

he stated that the drag force had to be less than or equal to the component of the frictional force. He expressed the equation in the following form:

$$F_d \leq F_w \tan \phi = k_2 d^3 \gamma (S_s - 1) \tan \phi \quad (2.9)$$

- where:
- F_d = drag force;
 - F_w = weight of the stone;
 - k_2 = volume constant for the rock;
 - d = representative dimension of the rock;
 - γ = unit weight of water;

S_s = specific gravity of rock; and
 ϕ = angle of internal friction of the rock.

Using the same parameters, overturning equilibrium for the rock can be expressed by the following equation.

$$F_d \frac{d}{2} \leq k_2 d^3 \gamma (S_s - 1) \frac{d}{2} \quad (2.10)$$

Since $\tan\phi$ is less than unity, we can conclude that the stability against overturning is greater than that against sliding. So sliding equilibrium is taken as the limiting factor in deriving the equation for equilibrium of a stone in flowing water. Assuming the shear stress due to water flowing down the slope at an angle, θ , is τ , equilibrium of a stone can be derived from the force diagram shown in Figure 2.2.

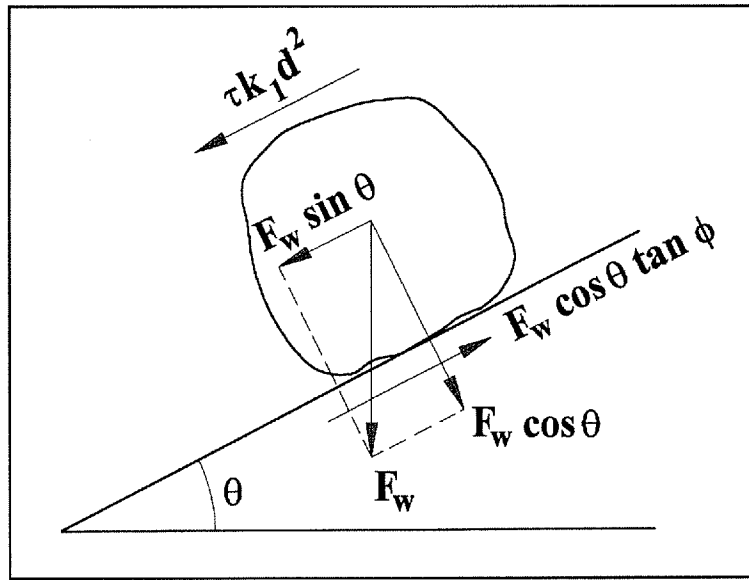


Figure 2.2: Free body diagram of a rock in water flow on an inclined plane

The summation of all the forces acting on the rock along the direction of slide yields the following equation:

$$\tau k_j d^2 + \gamma (S_s - 1) k_2 d^3 \sin\theta = \gamma (S_s - 1) k_2 d^3 \cos\theta \tan\phi \quad (2.11)$$

where: τ = shear stress due to the flowing water;
 k_j = function of the stone shape; and
 the other variables have the same meaning as described previously.

Rearranging the above equation yields

$$\tau = \gamma (S_s - 1) (k_2/k_j) d \cos\theta (\tan\phi - \tan\theta) \quad (2.12)$$

However, for shallow flow and small slopes shear stress can be given by

$$\tau = \gamma y s \quad (2.13)$$

where: y = depth of water; and
 s = slope of the bed.

Manning's equation in S.I. units is

$$v = \frac{1}{n} R^{\frac{2}{3}} s^{\frac{1}{2}} \quad (2.14)$$

where: v = velocity of water;
 n = Manning's constant;
 R = hydraulic radius; and
 s = slope of the energy grade line which can be approximated as the slope of the bed.

Strickler evaluated the Manning's coefficient, n , in terms of absolute roughness, e , given by:

$$n = \frac{0.13 e^{\frac{1}{6}}}{\sqrt{g}} \quad (2.15)$$

Combining Eqs. (2.14) and (2.15), Stephenson (1979) arrived at:

$$v = 7.7(R/e)^{1/6} \sqrt{Rsg} \quad (2.16)$$

For packed stone lining, the roughness coefficient, e , can be approximated by $n_p d$. Assuming that $R = y$ and $e = n_p d$ where, n_p , is the porosity and d is the median stone size, the unit discharge, q , is:

$$q = 7.7(y/n_p d)^{1/6} (y s g)^{1/2} y \quad (2.17)$$

Combining Eqs. (2.11), (2.12), and (2.16) and substituting $\tan\theta$ for s :

$$q = 7.7 d^{3/2} n_p^{-1/6} (\tan\theta)^{-7/6} [(k_2/k_1)(S_s - 1) \cos\theta (\tan\phi - \tan\theta)]^{5/3} \quad (2.18)$$

In Eq. (2.17) proposed by Stephenson (1979), no typical values of k_1 or k_2 have been mentioned. Moreover this equation takes into consideration only the mechanical stability of the rock and does not consider the effects of aeration and rock gradation.

2.3 NRC/CSU Studies for Riprap Design

A series of experiments were conducted from 1984 to 1987 jointly by NRC and CSU to evaluate protection for overtopped embankments. These experiments were designed to develop riprap design criteria based on unit discharge at failure. Embankment slopes of 1%, 2%, 10%, and 20% were tested. The embankments were protected by riprap layers with median stone sizes of 25, 50, 102, 127, and 158 mm. Failure of the riprap was defined as exposure of the gravel filter layer.

An equation relating the median stone size D_{50} in meters, the embankment slope S , and the unit discharge at failure, q_f ($m^3/s/m$), was developed in the Phase II report by Abt *et al.* (1988) for angular rock smaller than 6 inches and slopes of 20% or less. Based on these tests, Abt and Johnson (1991) presented the following expression relating the median riprap size to bed slope and overtopping unit discharge:

$$D_{50} = 0.503S^{0.43}q_f^{0.56} \quad (2.19)$$

It was determined that the interstitial velocity, V_i (m/s), through the riprap is a function of the material properties as well as the slope of the embankment expressed as:

$$V_i = 19.29(C_u^{-0.074}S^{0.46}n_p^{4.14})^{1.064}(gD_{50})^{0.5} \quad (2.20)$$

where C_u in the above equation represents the coefficient of uniformity of the riprap given by:

$$C_u = \frac{D_{60}}{D_{10}} \quad (2.21)$$

A sensitivity analysis was performed relating the rock size and the gradient to the interstitial velocity. Representative stone sizes were correlated to the measured interstitial velocity. The analysis showed that the D_{10} stone diameter provided the highest coefficient of correlation of the stone sizes tested. A linear regression analysis yielded the expression:

$$V_i = 0.79(gD_{10}S)^{1/2} \quad (2.22)$$

where: V_i = the average interstitial velocity in meters per second;
 g = acceleration due to gravity in m/sec^2 , D_{10} is in meters; and
 S = the gradient expressed in decimal form.

Wittler (1994) used the NRC/CSU data and introduced the idea of coefficient of stability, C_s , of the rock layer and found that the coefficient of stability is a function of the coefficient of uniformity, C_u , given by the relationship:

$$C_s = 0.75 + (\log C_u^6)^{-2} \quad (2.23)$$

The coefficient of stability is valid only for values of C_u greater than 1.1. Wittler also suggested a generalized formula to determine the median riprap size at failure for a given unit discharge as:

$$D_{50} = 2.565C_f S^{0.778} \left[\frac{q_f}{C_s} \right]^{0.667} \quad (2.24)$$

Wittler included a correction factor due to the aeration effect, C_f , given by:

$$C_f = 0.196q_f^{-0.11} S^{-0.35} \quad (2.25)$$

where: q_f = unit failure discharge in $\text{m}^3/\text{s}/\text{m}$.

This resulted in Eq. (2.26) for predicting D_{50} illustrated below:

$$D_{50} = 0.503q_f^{0.56} S^{0.43} \left[\frac{1}{C_s} \right]^{0.667} \quad (2.26)$$

2.4 ARS Riprap Tests

The Agricultural Research Service (ARS) at Stillwater, Oklahoma conducted riprap tests in three flumes (Robinson *et al.*, 1995). A 0.76-m wide and 2.44-m long flume with a fixed 40% slope was used to test riprap with D_{50} of 46 mm and 54 mm. A 1.07-m wide and 4.27-m long flume with adjustable slopes of 10%, 12.5%, 16.6%, and 22.2% was used to test riprap with D_{50} ranging from 15 mm to 98 mm. Rock chutes were also prepared with slopes of 12.5%, 22.2%, and 40% inside a 1.83-m wide and 29-m long flume with 2.44-m high walls. This large flume was used to examine rock with a D_{50} of 98 mm and 155 mm. All rock chute tests were conducted with a rock layer thickness of $2D_{50}$ measured normal to the slope. The materials used in each test were predominantly angular, crushed limestone. Based on a regression analyzes of the data, the equation for the unit failure discharge in S.I. units is:

$$D_{50} = 0.402S^{0.169} q^{0.546} \quad (2.27)$$

2.5 Need for Future Research

All previous experiments dealing with riprap protection on slopes with overtopping flow have been performed with stone diameters of 158 mm or less and on slopes of 40% or less.

Extrapolation of formulas for both steeper slopes and higher discharges might not satisfactorily predict the behavior of riprap as a protective layer. For a given rock size distribution, it is necessary to point out the limits of discharges and slopes for which equations were developed. Comparison must be made for predicted versus actual discharges at incipient failure of riprap on different slopes. Equations must be developed that include parameters for riprap that can be determined or estimated with a reasonable degree of confidence. If no equation satisfactorily predicts failure or interstitial velocities, new criteria must be developed in order to design the riprap embankment protection.

CHAPTER 3

EXPERIMENTAL FACILITIES, RIPRAP CHARACTERISTICS, AND DATA ACQUISITION

3.1 Overtopping Facility

Through the cooperative agreement signed in 1991, USBR and CSU built a near-prototype size embankment overtopping research facility. The facility is located at CSU's Engineering Research Center in Fort Collins, Colorado. It consists of a concrete head box, a chute, and a tailbox. The chute is 3.05-m wide and has a 15.24 m vertical drop on a fixed 2:1 (H:V) slope. The walls of the flume are 1.52-m high and extend the full length of the chute. Plexiglass windows, 0.9 m by 0.9 m, are located along the wall near the crest, mid-point and toe of the flume along one wall. A picture of the facility is given in Figure 3.1.

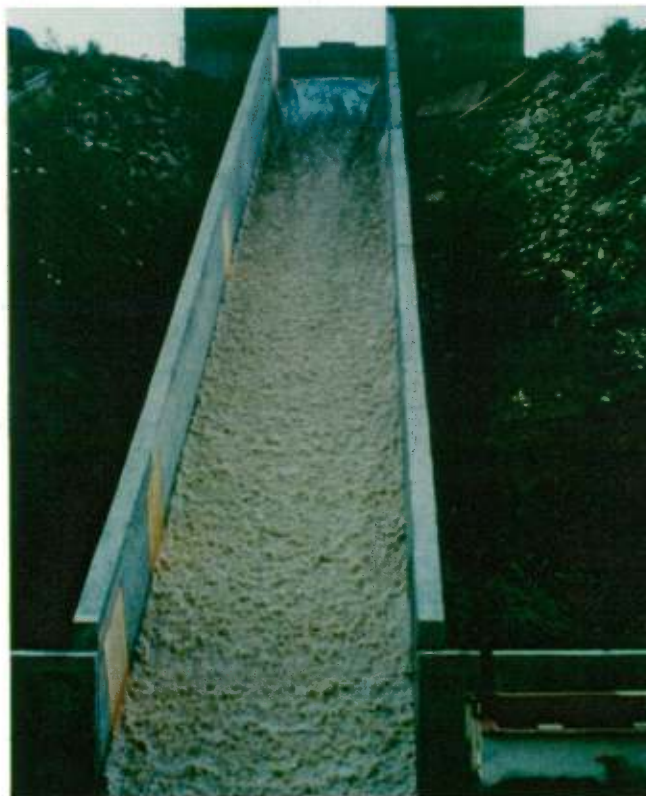


Figure 3.1: Overtopping facility at CSU

Water is supplied to the facility from adjacent Horsetooth Reservoir. Maximum reservoir level provides approximately 76.2 m of static head. A 0.9-m diameter pipe, approximately 805-m long, delivers water from the reservoir to the facility. A series of valves along the pipeline are used to control discharge. The delivery pipe diffuses into the head box to allow for prototype overtopping conditions. The pipeline can deliver a maximum discharge of approximately 3.7 m³/s with a corresponding overtopping depth of approximately 0.32 m. A diesel driven pump can provide an additional 0.85 m³/s for a total of 4.55 m³/s. The slope is fixed at 50%. Part of the flow can be bypassed through an auxiliary pipeline while changing the flow rate.

The first two riprap test sections covered the full width of the chute and extended 18.29 m down the slope from the crest. The first test (1994) consisted of an 203-mm thick gravel bedding material with a 0.61 m overlay of large riprap with a D_{50} of 386 mm. The second test (1995) utilized the first test bed with a second layer of approximately 0.61-m thick riprap with D_{50} of 655 mm. The configuration of the test layers in 1994 and 1995 is given in Figure 3.2.

The third test (1997) covered the full width of the chute and extended 30.48 m from the crest down the slope to the toe of the facility. A 203-mm thick gravel bedding material with a D_{50} of 48 mm was overlaid with a main riprap layer of thickness 533 mm with a D_{50} of 271 mm. A berm was built at the bottom of the flume to simulate toe treatment at the base of the embankment. The configuration of the test setup in 1997 is given in Figure 3.3.

For all the tests, a gabion composed of the same rocks used on the slope, was placed at the crest of the embankment. This was done to provide a smooth transition of water from the head box to the embankment and to prevent premature failure of the riprap at the transition between the concrete approach at the crest of the embankment and the concrete chute. The gabion covered the entire width of the flume and extended about 0.75 m down the flume from the crest. The top surface of the gabion was horizontal.

Placement of the riprap was accomplished by first placing the bedding material on the chute. To retain the bedding on the slope, 76 mm angle iron ribs were installed on the floor of the chute. The angle irons were bolted to the chute and had 13 mm spacers under them to provide a flow path at the chute surface. The bedding layer was 203-mm thick. The riprap was installed by using a front end loader that dumped the rock fragments into a box which was lifted by a crane to a location on the chute. Cables were removed from one end of the box and rocks were dumped by raising the box by one end.

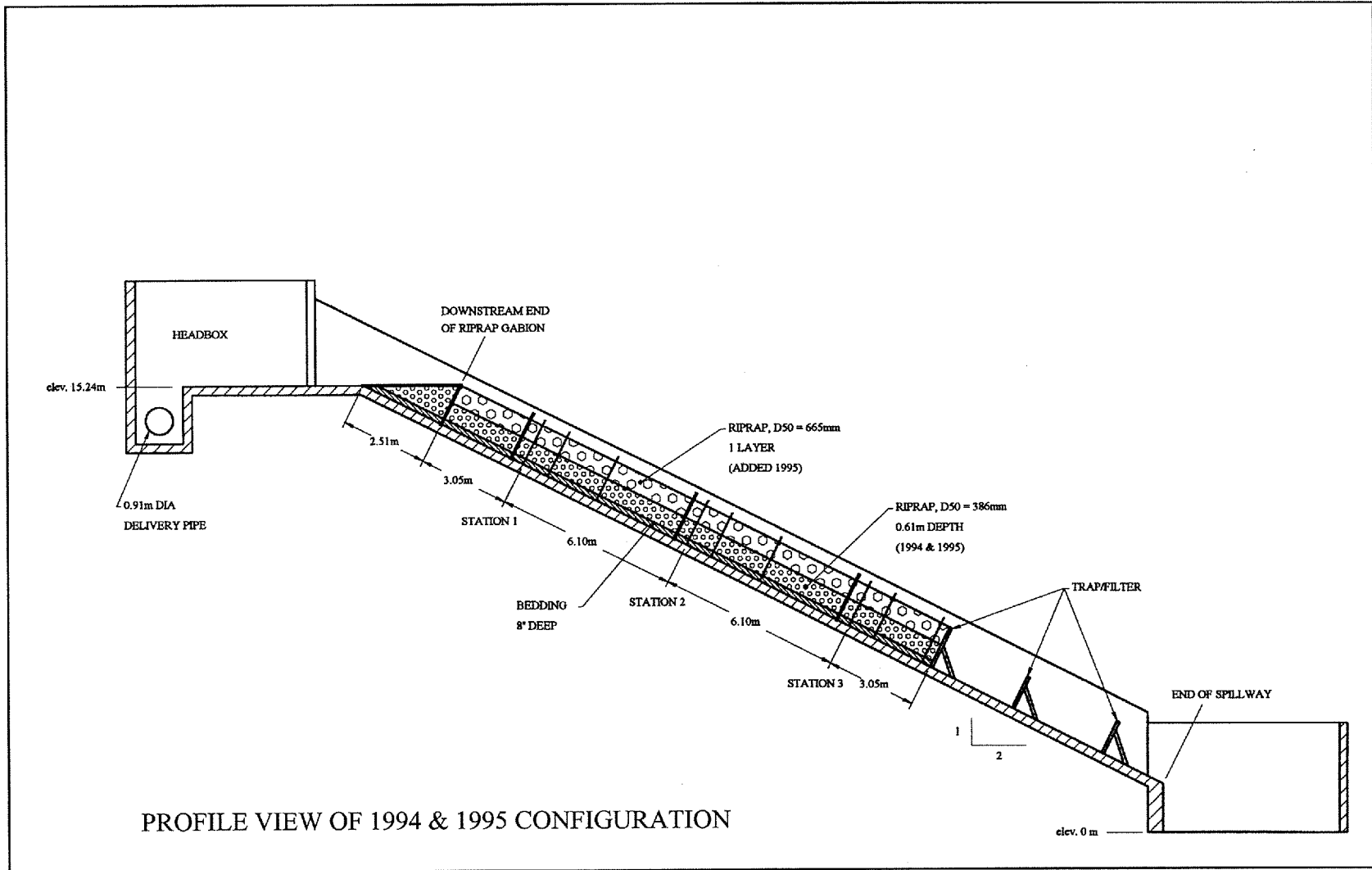


Figure 3.2: Riprap test layer configuration in 1994 and 1995

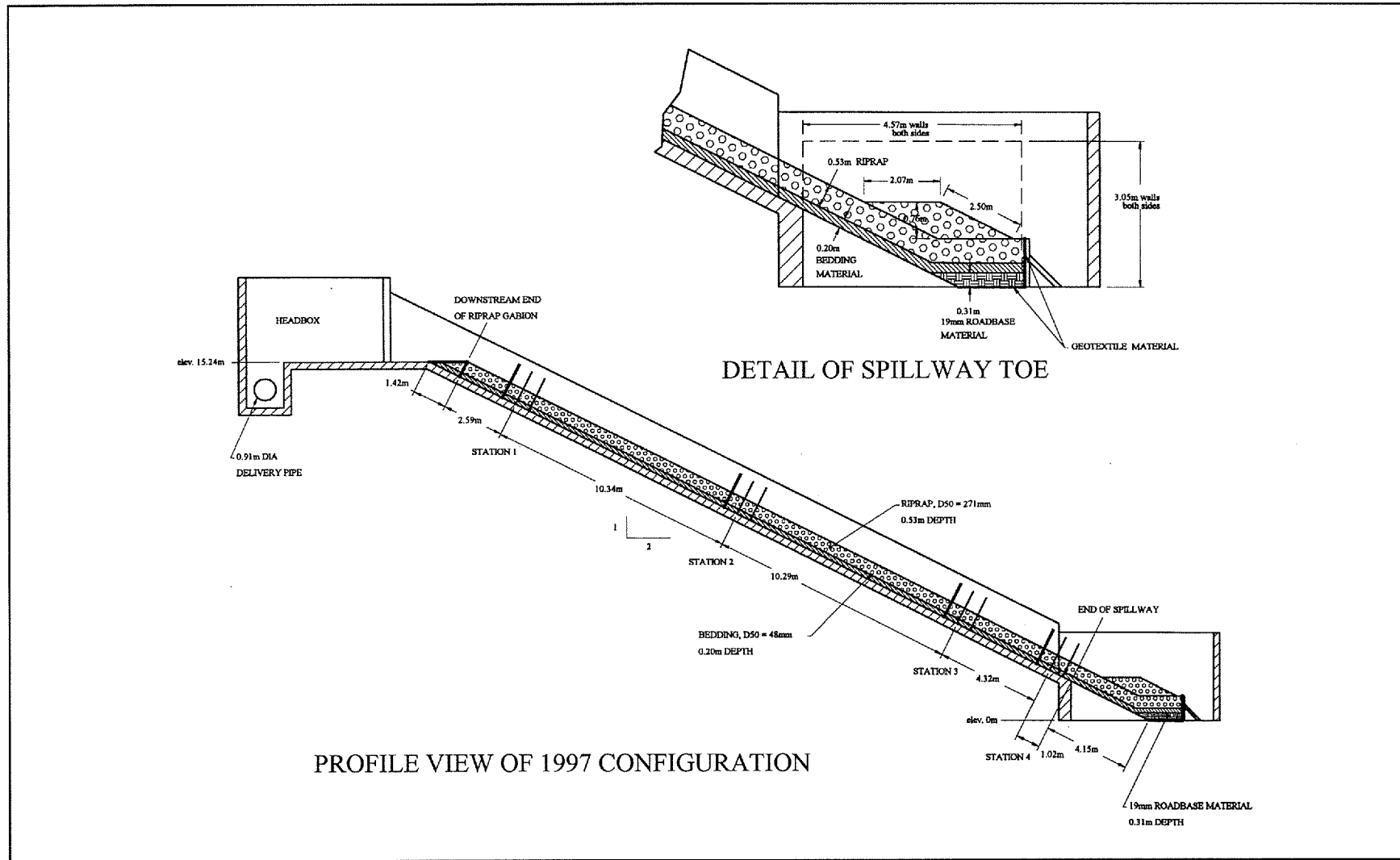


Figure 3.3: Riprap test layer configuration in 1997

3.2 Characteristics of the Bedding Material

Filters and drains are essential to safe performance of earth embankments (USBR, 1987). The earth materials for such filters and drains, where possible, should be selected from inventories of locally available material. Generally, a filter should be uniformly graded to provide adequate permeability and prevent segregation during processing, hauling, and placing. The filter design standard for embankment dams (USBR, 1987) specifies a maximum D_{90} of 60 mm for a minimum D_{10} of 10 to 50 mm.

A gravel filter was placed as bedding to simulate filters that are widely used in earth dams to prevent piping. The bedding layer was 203-mm thick. For the 1994 and 1995 tests, median diameter, D_{50} , was 38 mm, maximum diameter, D_{100} , was 76 mm, D_{10} and D_{90} were approximately 28 mm and 69 mm, respectively. Only 0.18% of the bedding material used in the 1994 and 1995 tests passed the #4 sieve. The gradation of bedding and riprap tested in 1997 was determined by sampling a large number of rocks. Gradation of the bedding layer was established by randomly selecting about 1,000 rocks and measuring them along three axes and finding the equivalent spherical diameter. Gradation of the bedding layer is given in Table 2.1.

Table 2.1: Riprap gradation for bedding layer of 1997 tests ($D_{50} = 48.3$ mm)

% of rocks less than D	D (mm)	D/D_{50}
100	88.90	1.841
90	73.03	1.512
80	63.50	1.315
70	57.20	1.184
60	52.40	1.085
50	48.30	1.000
40	47.63	0.986
30	41.91	0.868
20	38.10	0.789
10	33.35	0.690

3.3 Characteristics of the Riprap Materials Tested

The gradations of riprap tested in 1994 and 1995 were determined by measuring rocks in the surface layer within a 1.5 m x 1.5 m square grid. A photograph of the grid used for this purpose is shown in Figure 3.4. Twenty-four grid samples covered almost the entire surface area of the chute. Equivalent spherical diameters were determined from the three axes measurements of the individual rocks. Gradations for the riprap layer tested in 1994 and 1995 are summarized in Tables 2.2 and 2.3.



Figure 3.4: Grid used for sampling rocks

Table 2.2: Riprap gradation for 1994 tests ($D_{50} = 386$ mm)

% of rocks less than D	D (mm)	D/D_{50}
100	665	1.724
90	550	1.425
80	495	1.282
70	441	1.143
60	402	1.042
50	386	1.000
40	351	0.909
30	302	0.783
20	266	0.689
10	211	0.547
0	98	0.254

Table 2.3: Riprap gradation for 1995 tests ($D_{50} = 655$ mm)

% of rocks less than D	D (mm)	D/D_{50}
100	903	1.380
90	833	1.273
80	771	1.178
70	721	1.102

60	682	1.042
50	655	1.000
40	611	0.934
10	440	0.672
0	190	0.289

The gradation of the riprap layer for 1997 was determined in a similar fashion to the bedding, except that about 2,000 rock samples were measured from the surface of the riprap layer placed on the spillway. The gradation of the riprap is given in Table 2.4.

Table 2.4: Riprap gradation for 1997 tests ($D_{50} = 271$ mm)

% of rocks less than D	D (mm)	D/D_{50}
100	464	1.712
90	397	1.465
80	349	1.288
70	320	1.181
60	295	1.089
50	271	1.000
40	249	0.919
30	227	0.838
20	199	0.734
10	163	0.601

3.4 General Operating Procedures

Discharge was increased every time a new test was conducted. The flowmeter was read while the valve operator adjusted the valve to obtain the desired discharge. The discharge was initially set to a small discharge (0.06 to 0.09 m³/s) for the purpose of filling the pipeline. As the pipeline was filled, the bypass valve was opened and the discharge was gradually increased to the desired amount. As the head box filled and water started flowing down the flume, the bypass valve was slowly closed. With the bypass valve closed completely, the entire flow was going down the flume. The discharge was then set at the desired value. When data collection was completed for the particular discharge, flow was increased to the next higher discharge. The bypass valve was opened to divert water from the flume. The discharge was gradually increased to the desired value. The bypass valve was then slowly closed so that the entire discharge could flow through the flume.

While shutting down, the bypass valve was slowly opened to its fullest. Then the discharge was decreased slowly to zero flow. The bypass valve was left open for the time required to drain the pipeline.

3.5 Instrumentation and Data Acquisition

Three data acquisition stations were installed for the tests in 1994 and 1995. At each station, the instrumentation consisted of a piezometer tube, a salt injector, and a set of three conductivity probes. Figure 3.5 shows the configuration of the piezometers used to measure water depth and of the salt injector, and conductivity probes used to determine interstitial velocities. The first probe was placed 0.3 m downstream from the injector. The second probe was located 0.9 m downstream from the first probe, the third probe was located 1.8 m downstream from the second probe. To protect the probes from potential breakage by the placement of the rocks or by impact, the probes were housed inside a 64-mm diameter pipe. Holes with 51-mm diameters were drilled through the pipe at the elevations of the sensors. Wire mesh was used to cover the holes. At each station a tube and a block containing piezometers were attached perpendicular to the flume floor. Manometers were connected to the piezometers and clear acrylic tubes attached upright on a manometer board in order to read the pressure heads. The plan view of the layout of the piezometers and the conductivity probes is given in Figure 3.6. Figures 3.7 and 3.8 show photographs of the chute and the pipes containing the salt injectors and the conductivity probes in 1994 and 1995, respectively, with placement of the white manometer boards on their left.

In 1997, four data acquisition stations were installed. Each station consisted of a piezometer tube, a set of manometers, an injector, and two conductivity probes. The first probe was placed 0.6 m downstream from the salt injector and the second probe was located 0.6 m downstream of the first probe. The layout of the piezometers, the salt injector, and the conductivity probes are shown in Figure 3.6. Figure 3.9 shows the photograph of the flume with rocks painted before the 1997 tests. Pipes for injections and conductivity probes can be seen at three of the four data collection stations.

The test series provided the opportunity to gather important data regarding flow through large size riprap. The visual observations provided information on aeration, interstitial flow, stone movement, and the failure mechanism on the slope. Data were collected on discharge flowing down the chute through the riprap, the head box depth for overtopping heads, manometer readings for depth of flow down the chute and the pressure heads, and electronic recording of electrical conductivity versus time to determine interstitial velocities. In addition, portions of all runs were video taped and photographed with color print or slide film. Visual observations were made at the end of each test run (each incremented discharge) to identify scour and track a few individual rocks. For the 1994 tests, different colored lines were painted on the rocks and walls every five feet perpendicular to the direction of flow to observe movement of the painted rocks. For the 1995 tests, different numbers were painted on all the rocks placed in the flume and the positions of the rocks were recorded (Figure 3.10). For the 1997 tests, the entire riprap surface was painted with solid 1.52-m wide bands of different colors. The adjacent bands had contrasting colors for clear demarcation (Figure 3.9).

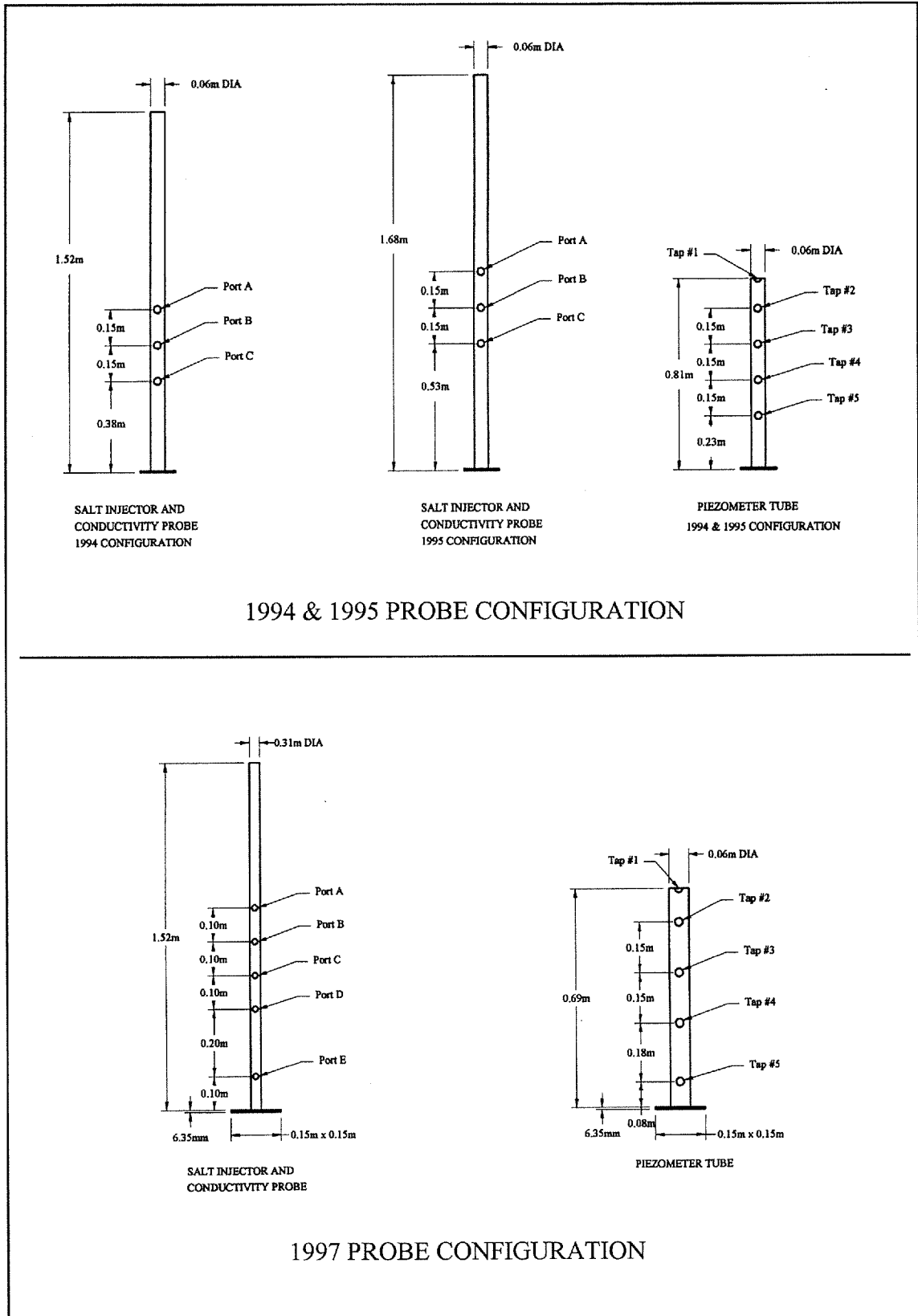


Figure 3.5: Schematic drawing of injectors, conductivity probes, and piezometer locations

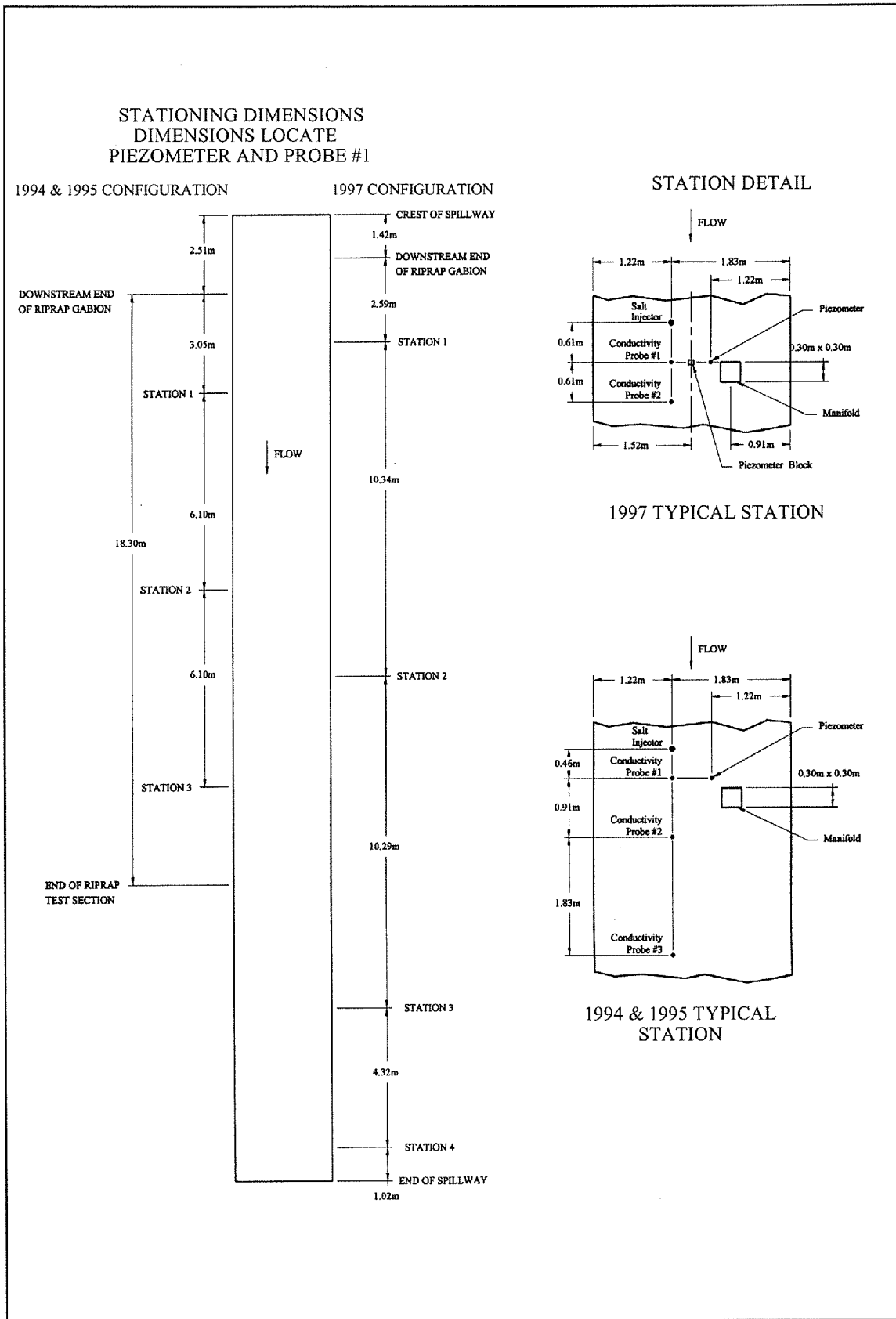


Figure 3.6: Plan view of the piezometers, injectors, and conductivity probes



Figure 3.7: 1994 layout with the piezometer towers on the riprap slope before testing



Figure 3.8: 1995 layout with the piezometer towers on the riprap slope before testing



Figure 3.9: 1997 layout of the riprap slope with the piezometer towers before testing

Discharge and head data were collected for each test. In addition, flow depths and interstitial flow velocities were recorded at all stations (3 stations in 1994/1995, and 4 stations in 1997) down the flume. Velocities were obtained by injecting salt water into the flow and measuring the time until the wave front arrived at each of the downstream probes. Each injector and probe had three different elevations to inject salt water for the tests carried out in 1994 and 1995. An electrically operated injector was used in 1994 and 1995 to inject salt at each of the three levels. The voltage decreased at each conductivity probe as the salt arrived. The voltage at the probes was monitored on a computer screen using commercially available software. Each injector and probe in 1997 had five levels of injection. However, the voltage signals were very weak when the electrical injector was used for injecting salt

solution. Therefore, a large slug of salt solution was manually supplied upstream of the injector.

Water depths were obtained by reading manometers that were connected to a piezometer at each of the data collection stations. Before taking the manometer readings, the manometer tubes were individually back flushed with water by inserting a thin metal tube at the top of the manometer board connected to a pressurized tank of water. This procedure eliminated the air bubbles inside the manometer tubes. Data recorded by the manometers were the depths of solid water flowing interstitially between the rocks, not the highly aerated flow skimming the surface.



Figure 3.10: Numbering of rocks in 1995

CHAPTER 4

FLOW OBSERVATION

4.1 Riprap Flow Conditions

Important observations and physical information were gathered during the tests of each size riprap. Observations of flow conditions provided needed insight into the physical data that were gathered.

Flow conditions through riprap covering an embankment are a function of the rock size distribution, embankment slope, and discharge. Flow conditions were well documented by making observations from the surface and through side windows located along the flume. Since the riprap characteristics of 1994 and 1997 were very similar, riprap flow conditions for these test series are described together followed by the flow conditions in 1995. Observations of flow at the failure of the riprap layers are described in Chapter 7.

4.2 Flow Observations in 1994 and 1997

The riprap surfaces tested in 1994 and 1997 are shown in the dry in Figures 3.7 and 3.9, respectively. Flow over the broad flat crest was smooth as it transitioned into the chute (Figure 4.1). There was no visible air entrainment throughout the flow depth at the crest. The surface was calm with no ripples or disturbances except near the wall boundaries. There was a drop in the water surface level just before encountering the rocks. The surface was still smooth and the drop was due to the change in slope of the chute. Almost immediately after entering the rocks, the surface flow became very turbulent and highly aerated. This occurred at approximately one to two D_{50} downstream from the start of the rock layer (Figures 4.1 and 4.2). At low discharges the flow entered the rock layer and remained below the rock surface down the entire slope. Looking through the window at the crest, aeration occurred only on the surface. The first window allowed visibility for about 1m down from the crest.

As the flow increased, the water became visible over the surface at various locations down the slope (Figure 4.3). Water would intermittently flow over or through the surface of the rocks, while other areas remained dry (Figures 4.4 and 4.5). Even at higher flow rates, some areas seemed to show the presence of a higher water surface than others. At times the flow was not visibly aerated prior to entering the rock layer about 3 m from the crest down the slope, but came out as highly aerated. As the flow came in contact with the rocks, in some cases flow impact on rocks and turbulence entrained air bubbles with the flowing water.



Figure 4.1: Transition of flow into the chute at $Q = 0.23 \text{ m}^3/\text{s}$, 1994



Figure 4.2: Flow becoming turbulent as it encountered the rock layer at $Q = 0.23 \text{ m}^3/\text{s}$, 1994



Figure 4.3: Visible surface water looking downstream at $Q = 0.28 \text{ m}^3/\text{s}$, 1997



Figure 4.4: Wet and dry areas of riprap surface at $Q = 0.42 \text{ m}^3/\text{s}$, 1997 (flow from top to bottom)



**Figure 4.5: Wet and dry areas of riprap surface at window #2,
 $Q = 0.23 \text{ m}^3/\text{s}$, 1994**

At about 7 m down the slope, entrained air became much more visible. Air bubbles were visible throughout the entire rock layer. The flow surface was highly aerated with the amount of aeration decreasing through the layer to the bedding. Air bubbles were present all the way through the bedding layer.

A lateral flow path induced by obstruction of the flow was apparent in Figure 4.6. This phenomenon is believed to be one of the factors for sometimes causing voltage signals indicating arrival of the salt solution to be observed at the downstream conductivity probes before the upstream probes. In addition, it became apparent by observing the flow that the flow path between the probes could be tremendously affected by the random placement of the riprap and the voids. Vortices were visible at essentially every location of a void. While some voids contained a single air bubble for some length of time, others were exchanging air bubbles rapidly.

As the discharge was increased, surface flows appeared to bounce down the slope as cascading flow stepping from one level to another (Figure 4.7). In some areas (possibly after rocks moved), the water appeared to pool before continuing down the slope. It appeared that flow in the bedding layer and deep in the riprap layer had lower velocity than flow near the surface based on the velocity of the air bubbles observed through the windows. Looking through different observation windows down the slope, the interstitial flow velocities appeared similar.

4.3 Flow Observations in 1995

Figure 3.8 shows the configuration of the riprap tested in 1995. The flow rates in the 1995 tests were considerably higher than the 1994 tests due to the use of larger riprap placed over the existing 0.61-m thick layer of riprap from 1994. The entrance of the flow into the flume had comparable characteristics to that of the flow in 1994. The water still

entered the rock chute in a smooth transition from the head box. The water surface was smooth but not flat. Looking through the window at the top of the flume, it appeared that the surface of water lowered and then raised (Figure 4.8). The larger riprap of 1995 was placed at the downstream end of the riprap gabion. This caused the water surface to rise as it entered the larger riprap of 1995. Because of the increase in flow rates and increases in flow depths, the point at which the surface flow became aerated was further down the slope in 1995. This break in water surface occurred in a much less uniform manner. This irregularity was due to the size of the rocks used.

As the water surface broke about 2 m downstream from the window at the top of the flume, the flow became completely aerated and turbulent over the entire surface of the slope. At very high flow, large plumes of water were formed instead of the small pools and distinctly cascading flows of 1994 (Figure 4.9).



Figure 4.6: Flow (left to right) pattern due to obstruction of flow path seen through window #2 ($Q = 0.23 \text{ m}^3/\text{s}$)

At high rates of flow, the rocks generally were completely invisible from the surface. The turbulent aerated flows and splashing water completely covered the rocks. At a unit discharge of $0.418 \text{ m}^2/\text{s}$, 0.61-m high flash boards were installed on the flume walls, to prevent water splashing over both sides of the flume (Figure 4.9). As seen in Figure 4.9, the water on the surface of the riprap was highly aerated. Even though it seemed like a large amount of water was flowing over the rock surface, in actuality there was a very little solid mass of water flowing on the surface of the riprap. This is confirmed from the recorded piezometric depths of water for various discharges presented and discussed in Chapter 5. Three separate velocity zones were very clear from observations during these tests. The flow zones are shown in the schematic depicting the velocity distribution throughout the riprap layer (Figure 4.10). Rotational flow was again prevalent in the flow through the 1995 layer.



Figure 4.7: Cascading flow (flow direction from top to bottom) (1994)



Figure 4.8: Water surface profile over the riprap gabion ($Q = 1.13 \text{ m}^3/\text{s}$)



Figure 4.9: Large plumes of water (1995) ($Q = 2.12 \text{ m}^3/\text{s}$)

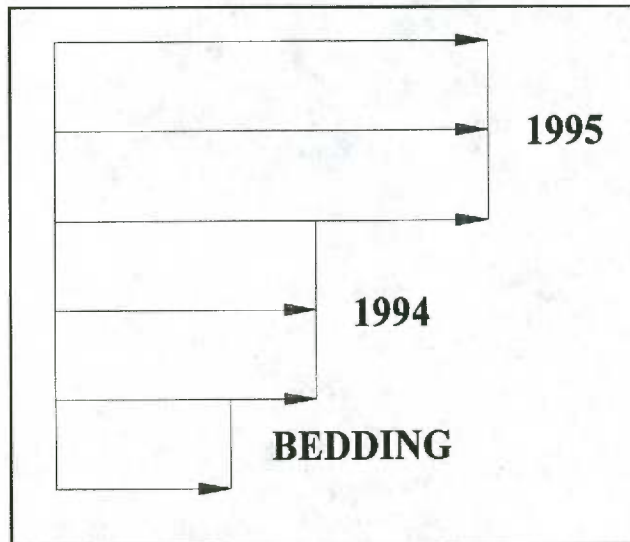


Figure 4.10: Schematic of the velocity zones (1995)

CHAPTER 5 DATA ANALYSIS

5.1 Analysis of Salt Injection Method

Interstitial velocities were obtained by injecting salt water into the flow and recording the time when the wave front arrived at each of the downstream probes. Three levels above the floor of the flume were used for injection and sensing in 1994 and 1995. An electrically operated injector was used in 1994 and 1995 to inject salt solution. The voltage decreased at each conductivity probe as the salt plume arrived at the probes. Typical voltage drops at the conductivity probes at a station are shown in Figure 5.1. Figure 5.1 shows the change of voltage with time at a particular port (level) between probes 1 and 2. The time elapsed (δt) between the drops of voltage at probe 1 and probe 2 can be calculated from Figure 5.1. Knowing the distance between the two probes (δs), the velocity of water through the riprap can be found from the simple equation:

$$v = \frac{\delta s}{\delta t} \quad (5.1)$$

In the test series in 1994 and 1995, three conductivity probes were used at each of the three stations. The velocity obtained by using Eq. (5.1) between probe 1 and probe 2 was termed as v_{12} and the velocity obtained using the probe 2 and probe 3 was termed as v_{23} . Similarly, v_{13} was obtained from the voltage readings at probes 1 and 3. The third probe was installed mainly to obtain supplemental data in case malfunctioning occurred at probe 2. In almost 80% of the cases the voltage reading at the probe 3 could not be obtained because of the dilution effect on the salt solution as well as the turbulence in the flow. The velocity obtained by using probe 1 and probe 2 data (v_{12}) was considered reliable.

Five levels were used for injection and sensing in 1997. Because of the experience gathered during the 1994 and 1995 test series, only two probes were used at each station. However, the voltage signals were very weak when the electrical injector was used for injecting the salt solution. Therefore, a salt solution was simply poured onto the rocks at each injector location. In order to obtain readings at respective ports (levels), the water depth in the riprap layer had to be above that port.

Figure 5.1 shows the change of voltage with time at a port C located 0.4 m from the flume in the riprap layer between probes 1 and 2 in 1997. The red line represents the voltage at probe 1 and the blue line represents the voltage at probe 2. It can be seen that voltage at probe 1 drops at 0.8 sec and voltage at probe 2 drops at 1.6 sec. The salt solution took 0.8 sec to travel from probe 1 to probe 2 which are 0.61 m apart. Therefore the velocity of water can be calculated by dividing 0.61 m by 0.8 sec. The interstitial velocity of water at the level of port C can be found as 0.76 m/s. Figure 5.2 shows the change of voltage with time at port E, which was located at 0.082 m from the invert of the flume. The velocity of water in the bedding layer can be calculated from Figure 5.2 by the same

method. The velocity of water at the level of port E, from Figure 5.2 was computed to be 0.5 m/s.

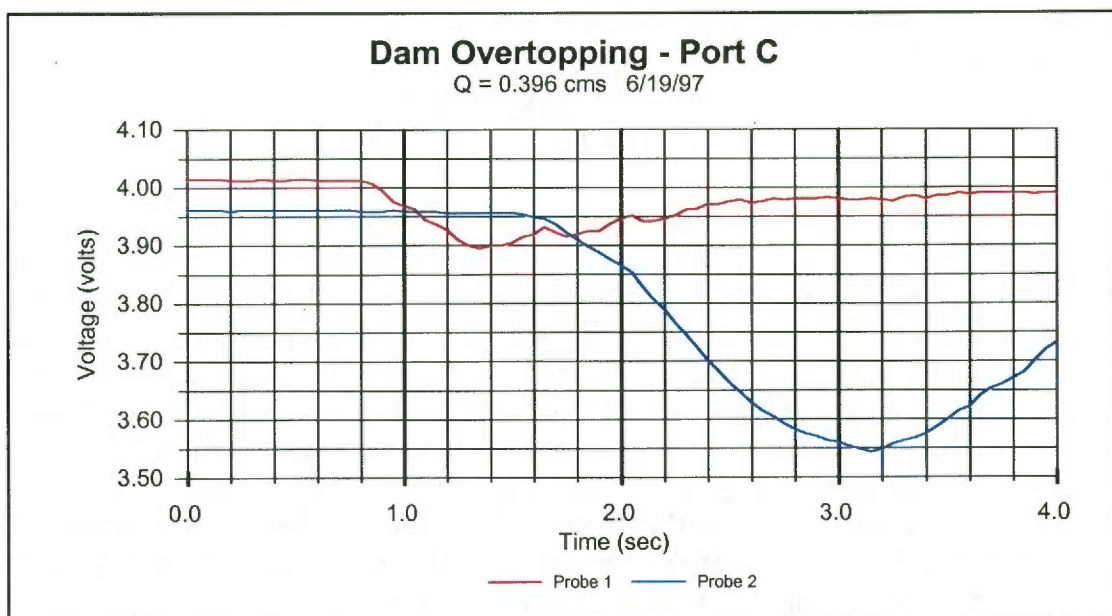


Figure 5.1: Typical voltage drop indicating the interstitial flow velocity for the tests

Voltage signals in the bedding layer (port 5) for all the probes were very strong for low discharges (up to about 6 m³/s). As the discharge increased the voltage signals at port 5 became weaker. This was because the salt solution was poured at the water surface where the high turbulence allowed little or no salt to reach the bedding layer. Velocity measurements were obtained at all the four stations for all the discharges. All the velocity measurements obtained in the tests of 1994, 1995, and 1997 are tabulated in the Appendix A.

For the 1994 riprap, the average of the interstitial velocity was computed by averaging all the velocity measurements at all three stations at the bottom two levels, since the top level was located outside of the riprap layer. This average interstitial velocity was computed to be 0.56 m/s. Similarly, the average interstitial velocity obtained in 1995 at the top probes only (top probes are the only probes which were within the rock layer of $D_{50} = 655$ mm) is 1.71 m/s. In the tests conducted in 1997 the interstitial velocities by the salt injection method, were measured in the bedding layer with a D_{50} of 48 mm as well as in the main riprap layer with a D_{50} of 271 mm. From the series of data the average interstitial velocity for the bedding layer and the main riprap layer by the salt injection method were found to be 0.46 m/sec and 0.75 m/sec, respectively.

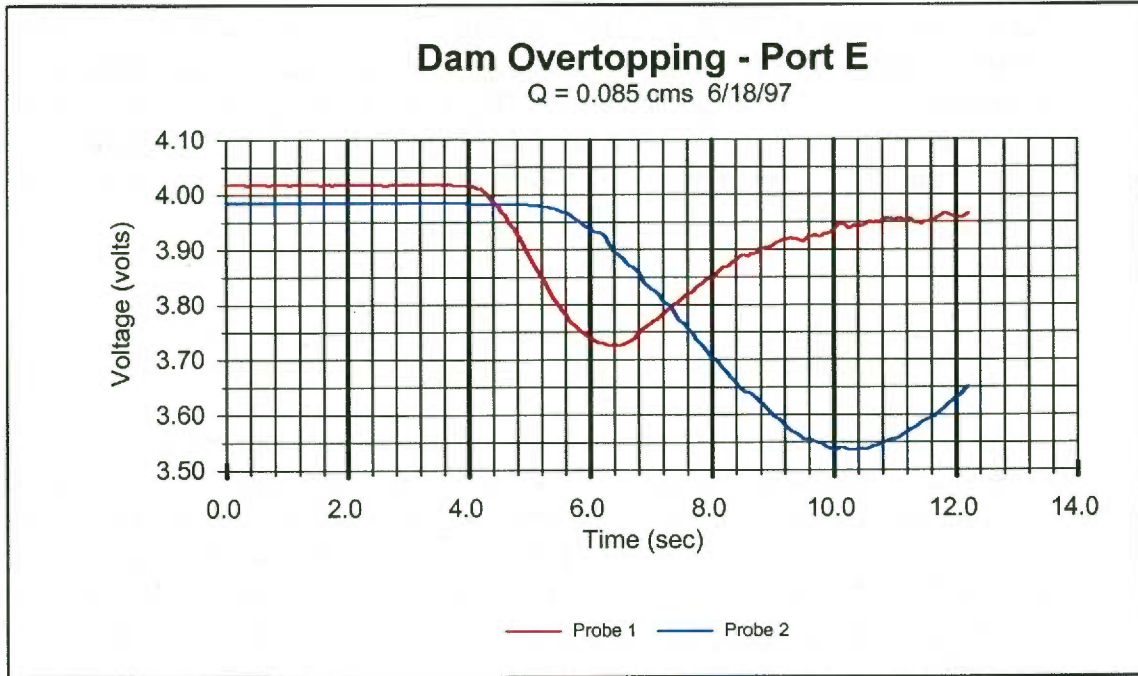


Figure 5.2: Typical voltage drop seen in the bedding layer in 1997 or near the bottom layer for 1994 and 1995

5.2 Analysis of Piezometer Data

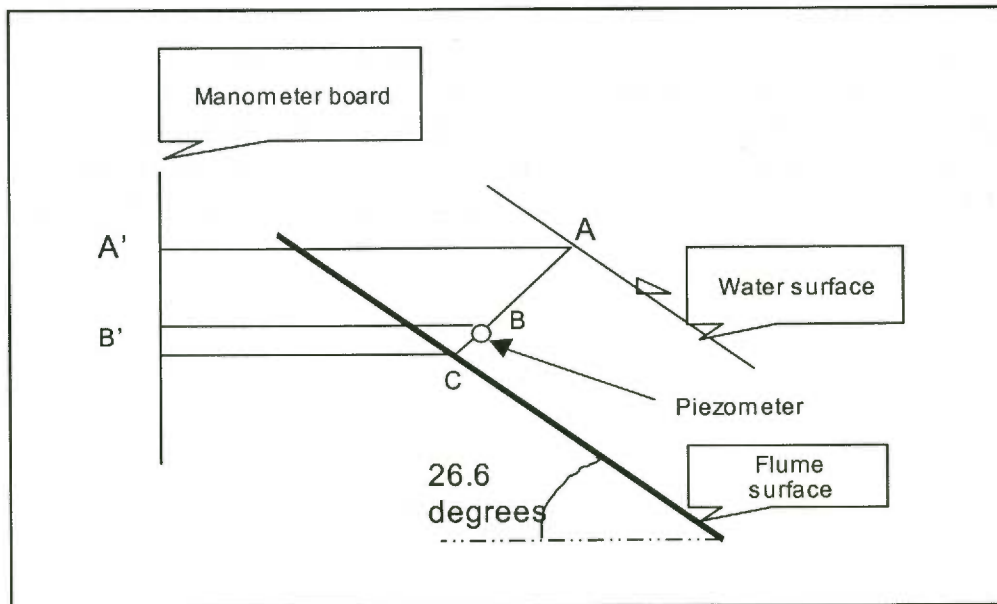


Figure 5.3: Schematic drawing of piezometer-manometer configuration

Water depths were obtained by reading manometers that were connected to a piezometer at each of the data collection stations. During data reduction, the readings for each manometer were converted to flow depths (Figure 5.3). In Figure 5.3, the depth of water, AC , is the distance normal to the slope of the flume. The manometer reading obtained at the site was $A'B'$. The desired depth of water, AC , could be computed by using the geometrical relationship as:

$$AC = \frac{A'B'}{\cos(26.6)} + BC$$

An average depth normal to the slope was determined for each discharge. The water depths at all the discharges tested in 1994, 1995, and 1997 are given in Appendix B. The average water depths, h , for 1994 and 1995 are plotted versus the unit discharge, q , in Figure 5.4. Figure 5.5 represents the relationship between unit discharge, q , and water depth, h , for 1997 tests. When the flow is purely interstitial, a linear relationship between the unit discharge, q , and depth, h , is apparent. Expressing the relationship between q and the interstitial velocity, V_i , as

$$q = V_i * \eta * h \quad (5.2)$$

where η is the porosity of the rock layer, it can be concluded that the interstitial velocity of water through the particular rock layer is constant irrespective of the magnitude of the unit discharge. The slope of the line representing the relationship between the unit discharge, q , and flow depth, h , in Figure 5.4 is $V_i * \eta$. But this is true as long as the flow is purely interstitial. As seen in the 1994 data in Figure 5.4, up to the depth of 0.8 m the flow of water is purely interstitial. As soon as the flow depth exceeds 0.8 m, severe aeration occurs resulting in flow which is no longer purely interstitial. The water flowing over the depth of 0.8 m is not a solid mass of water. The broken mass of water above the depth of 0.8 m, is caused by significant aeration of the water. Therefore, the velocity of water obtained by the salt injection method at the level higher than 0.8 m, can not give the true value of the interstitial velocity of water. Figure 5.5 shows the similar manometer data for the tests of 1997. This figure includes the data taken inside the bedding layer unlike the previous years.

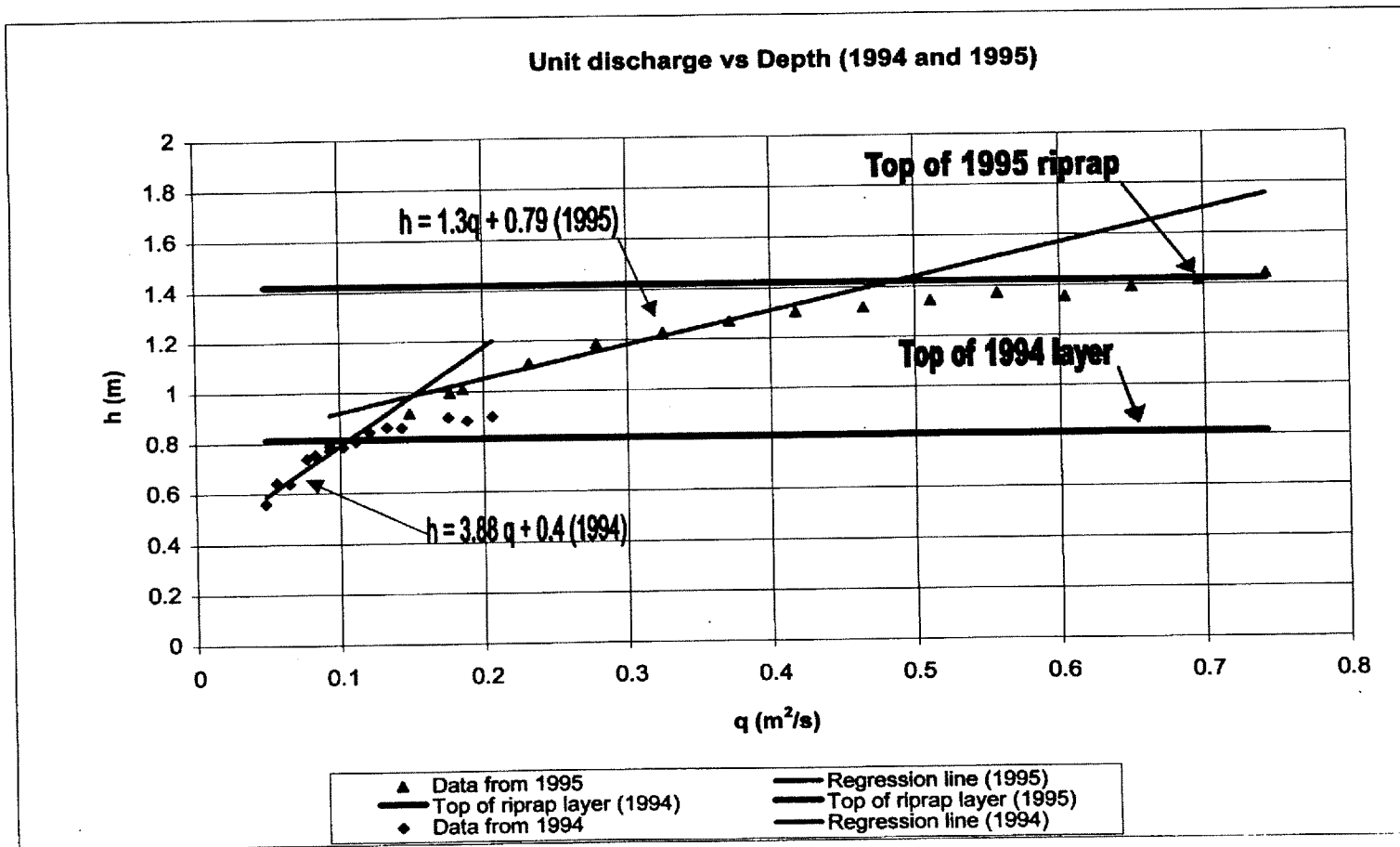


Figure 5.4 Variation of depth of flow with unit discharge in 1994 and 1995.

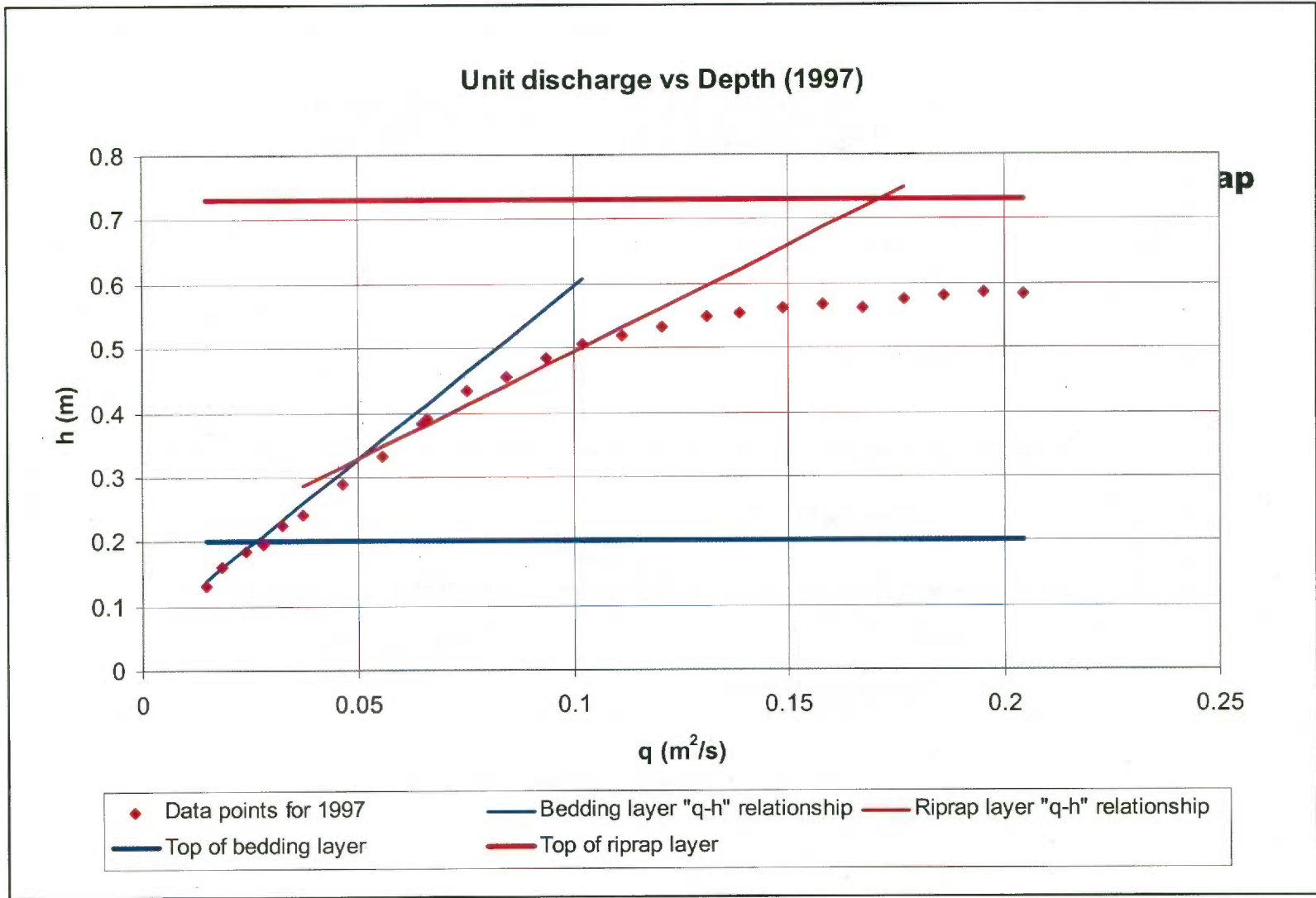


Figure 5.5: Variation of depth of flow with unit discharge in 1997

Figure 5.6 shows the photographed velocity profile through the riprap layer of 1994 ($D_{50} = 386$ mm). In the bedding layer, no bubbles can be seen in the photograph. However, bubbles could be seen by visual observations during the run throughout the bedding layer. The bubbles are stationary at some points or move at a slow velocity with minimal presence of turbulence. At higher water depths air bubbles carried by the water become prominent showing higher turbulence and increased velocity. This is the zone of interstitial flow. Above the depth of 0.8 m, the streaks show a very distinct change in their pattern indicating increased air concentration and increased turbulence. The mass of water above the depth of 0.8 m becomes highly aerated white water cascading down the slope resulting in voids and separation of the surface flow. In Figure 5.4 the line representing the variation of depth with discharge above the flow depth of 0.8 m has a flatter slope, indicating much higher velocity of water. It is important to note that the high velocity of water is caused mainly by splashing and separation of flow from the riprap surface. This is not the interstitial velocity of water.



Figure 5.6: Photograph showing the profile of water flow through the riprap layer of 1994

The piezometric data of 1995 are also shown in Figure 5.4. Since the rock layer of 1994 is covered by the rock layer of 1995, severe aeration does not occur when the water depth reaches 0.8 m and the water depth continues to rise following the linear relationship between the unit discharge and depth shown in Figure 5.4 for the 1994 data in the lower rock layer. As soon as water depth reaches the interface between 1994 and 1995 layer, water depth increases at a slower rate showing higher but constant velocity. This is because of rock properties. The voids in the 1995 rock layer were larger than those of 1994 and the velocity through the interstices was higher.

Figure 5.7 shows a photograph of the water flow through the riprap layer of 1995 ($D_{50} = 655$ mm). It is evident from the streaks of water that the velocity of water above the

depth of 0.8 m in 1995, is lower than the observed velocity at the same zone in 1994. The velocity of water remained constant until the water depth reached about 1.3 m. Afterwards, the velocity increases due to air entrainment, and the water flow is no more purely interstitial.



Figure 5.7: Photograph showing the profile of water flow through the riprap layer of 1995

The linear relationships between the unit discharge and water depth in the interstitial zone of the riprap layers of 1994 and 1995, respectively are given by (Figure 5.4):

$$h = 3.88q + 0.4 \quad (1994) \quad (5.3)$$

$$h = 1.3q + 0.79 \quad (1995) \quad (5.4)$$

The above two equations can be expressed in the general form:

$$h = C_1 q + C_2 \quad (5.5)$$

where: h = depth of flow (meters);
 q = unit discharge ($\text{m}^3/\text{s}/\text{m}$); and
 C_1, C_2 = constants.

Substituting ($V_{ave} * h$) for, q , and differentiating both sides of the above equation with respect to h , we arrive at:

$$C_1 * V_{ave} = 1 \quad (5.6)$$

where : V_{ave} = bulk velocity (average velocity).

5.3 Velocity Calculation From Piezometer Data of 1994 and 1995

Substituting the C_1 values in the Eq. (5.5) for 1994 and 1995 as 3.84 and 1.25, respectively, the bulk velocities for 1994 and 1995 were found to be 0.26 m/sec and 0.8 m/sec, respectively. Estimating the porosity η as 0.45, the interstitial velocity V_i can be found from:

$$V_i = \frac{V_{ave}}{\eta} \quad (5.7)$$

$$V_i = 0.57 \text{ m/sec} \quad (1994) \quad (5.8)$$

$$V_i = 1.71 \text{ m/sec} \quad (1995) \quad (5.9)$$

5.4 Velocity Calculation From Piezometer Data of 1997

The unit discharge is plotted against the depth of water at all four stations for the tests conducted in 1997. Figure 5.5 shows the typical variation of depth with unit discharge. As discussed in the 1994 and 1995 setup, the depth of water can be found to be linearly related to the unit discharge. The average relationships between the depth of water and the unit discharge for the bedding layer and the main riprap layer are given by:

$$h = 5.35q + 0.06 \text{ (Bedding)} \quad (5.10)$$

$$h = 3.3q + 0.162 \text{ (Riprap)} \quad (5.11)$$

Using Eqs. (5.6) and (5.7), and taking the porosity, η , to be 0.45, we can obtain the interstitial velocities to be 0.42 m/sec and 0.67 m/sec for the bedding and the main riprap, respectively.

5.5 Comparison of Interstitial Velocity Calculated From Two Methods

The interstitial velocity of water was obtained by two methods, i.e. salt injection and the unit discharge-depth ($q-h$) relationships for the tests conducted in 1994, 1995, and 1997. Table 5.1 summarizes the interstitial velocities obtained in both methods. It is clear from the data presented in Table 5.1 that the interstitial velocities obtained from the two methods discussed are in very close agreement. This evaluation confirms the accuracy of the velocity measurements obtained in the salt injection method.

Table 5.1: Comparison of interstitial velocities obtained by two methods

Test year	Interstitial velocity obtained by:	
	Salt injection	$q-h$ relationship
1994	0.56 m/s	0.57 m/s
1995	1.71 m/s	1.71 m/s
1997 (bedding)	0.46 m/s	0.42 m/s
1997 (riprap)	0.75 m/s	0.67 m/s

CHAPTER 6

DEVELOPMENT OF A PREDICTIVE EQUATION FOR INTERSTITIAL VELOCITY OF WATER THROUGH RIPRAP

As discussed in Chapter 1, several researchers (Frizell, 1990; Olivier, 1967; Abt *et al.*, 1987 & 1988; and Stephenson, 1979) have provided empirical criteria for riprap design for overtopped embankments. However, none of the previous research work focused on the importance of the velocity of water flowing through the riprap as a design parameter. Estimating flow through rockfill can be a useful procedure for designing the riprap. The velocity of water flowing through the rock voids, helps determine the depth of water flowing through the riprap, which could be the governing factor in the riprap design. In some cases it is necessary to find how much water can flow through the riprap layer in order to determine the amount of water that will flow on the surface of the riprap. Therefore, it is extremely important to be able to accurately predict the interstitial velocity of water flowing through a rockfill.

6.1 Need for Developing a New Predictive Equation for Interstitial Velocity of Water

Presently Abt *et al.* (1991) (Eq. (2.22)) is the only predictive equation available that can be used to estimate the interstitial velocity of water through a riprap layer subjected to overtopping. For steep slopes and relatively high discharges similar to 1995 test conditions, this equation does not satisfactorily predict the interstitial velocity of water. The predictive equation developed by Abt *et al.* (1991) only takes into consideration the size of the riprap and the slope of the embankment for predicting the interstitial velocity of water through the riprap. It does not take into consideration the effect of the rock layer gradation.

The interstitial velocity of water is strongly influenced by the void sizes inside the rock layer. The void sizes are determined by the gradation of the rock. Coefficient of uniformity C_u (D_{60}/D_{10}) provides a good representation of the rock gradation and should be a factor in the predictive equation for the interstitial velocity of water.

6.2 Results From the Current Test Program

The interstitial velocity data obtained by Abt *et al.* (1991), along with the data obtained at CSU in 1994, 1995, and 1997 are presented in Table 6.1. A multiple power regression analysis on the data shown in Table 6.1 with D_{50} , C_u , and slope, S , as the variables resulted in the following formula:

$$\frac{V_i}{\sqrt{(gD_{50})}} = 2.48C_u^{-2.22}S^{0.58} \quad (6.1)$$

where: V_i = interstitial velocity (m/sec);
 D_{50} = median rock size diameter (m);
 C_u = coefficient of uniformity given by D_{60}/D_{10} ;
 S = slope of the embankment in decimal form; and
 g = acceleration due to gravity = 9.81 m/s^2 .

Table 6.1: Interstitial velocities

Date and Experimenters (1)	V_i Observed (m/sec) (2)	D_{50} (mm) (3)	D_{60} (mm) (4)	D_{10} (mm) (5)	C_u (D_{60}/D_{10}) (6)	Slope (7)
1987-1988, CSU/NRC	0.03	26	27	15	1.75	0.01
1987-1988, CSU/NRC	0.04	26	27	15	1.75	0.02
1987-1988, CSU/NRC	0.07	26	27	15	1.75	0.10
1987-1988, CSU/NRC	0.07	56	59	28	2.09	0.01
1987-1988, CSU/NRC	0.02	56	59	28	2.09	0.01
1987-1988, CSU/NRC	0.11	56	59	28	2.09	0.10
1987-1988, CSU/NRC	0.11	56	59	28	2.09	0.10
1987-1988, CSU/NRC	0.22	104	109	51	2.15	0.20
1987-1988, CSU/NRC	0.30	104	109	51	2.15	0.20
1987-1988, CSU/NRC	0.32	130	142	88	1.62	0.20
1987-1988, CSU/NRC	0.27	130	142	88	1.62	0.20
1987-1988, CSU/NRC	0.46	158	163	97	1.69	0.20
1994, CSU/USBR	0.56	386	401	211	1.90	0.50
1995, CSU/USBR	1.71	655	673	440	1.55	0.50
1997, CSU/USBR	0.75	271	295	163	1.81	0.50
1997, CSU/USBR	0.46	52.4	48.3	33.4	1.57	0.5

Figure 6.1 shows a plot comparing the performance of the two separately developed interstitial velocity equation with the actually measured velocities. The left hand side Y-axis represents the new formula and the right hand side Y-axis represents the Abt *et al.* formula. The solid line on the graph describes the theoretical line for all the points on the graph, i.e., if some formula can predict, with 100% accuracy, the interstitial velocity of

water through a layer of rock, then the formula will represent the line. It may be seen, the new equation developed from this research as well as the Abt *et al.* (1991) formula accurately predict interstitial velocities for most of the existing data. However, Abt *et al.* formula does not adequately predict the actual interstitial velocity from the 1995 test, because of the large discharges combined with steep slopes. The predictive equation developed in this study computes the value of interstitial velocity which is very close to the actual velocity measured (Figure 6.1).

It is concluded in this chapter that, the new predictive equation gives a more accurate prediction of the interstitial velocity of water flowing through a rock layer of given properties than other formulas currently available. Therefore, it should be used for designing the thickness of the riprap for a given overtopping condition.

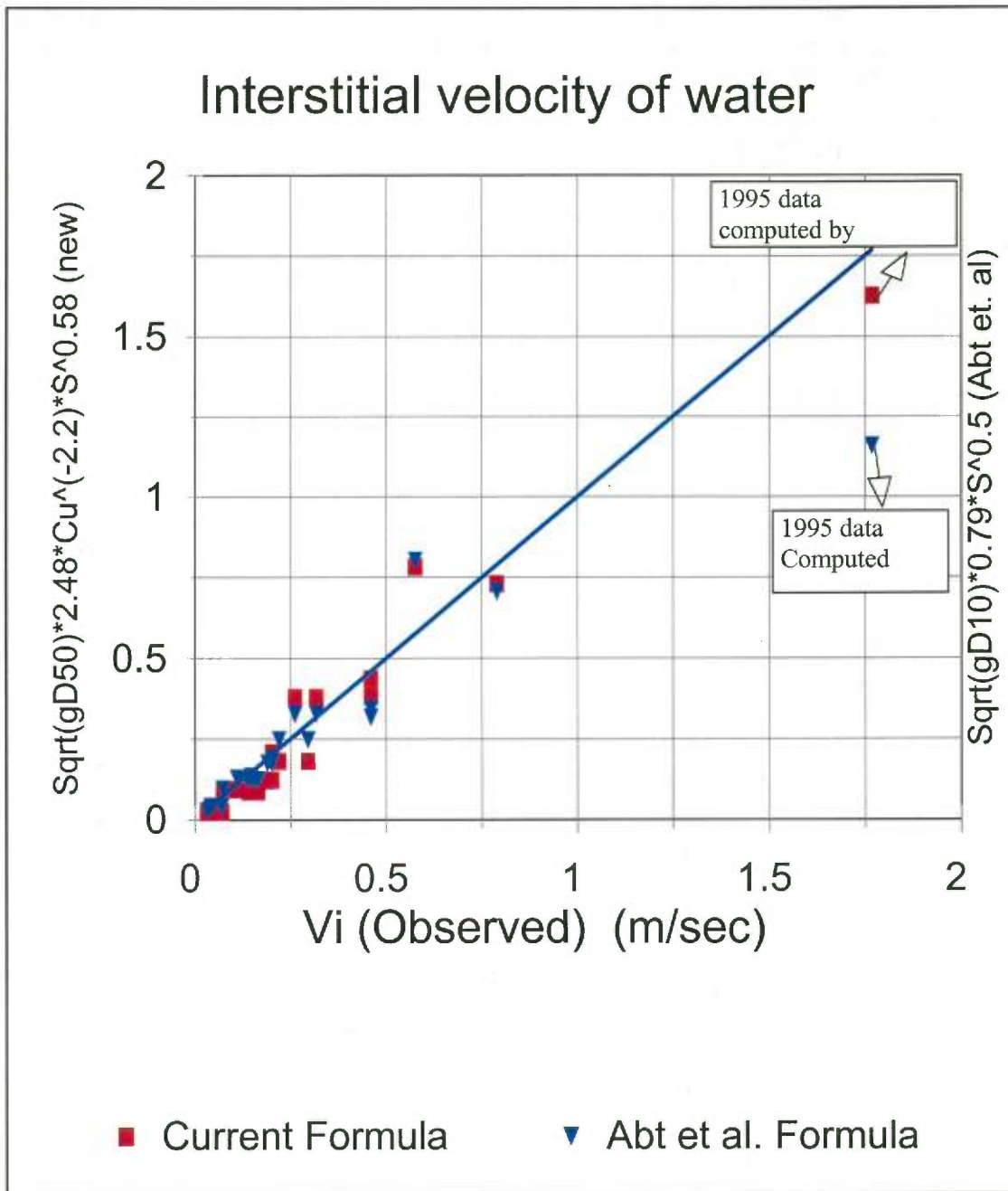


Figure 6.1: Comparison of current formula with formula by Abt *et al.* with existing data

CHAPTER 7

DESCRIPTION OF RIPRAP FAILURE AND TOE TREATMENT

7.1 Failure of the Riprap

The riprap flow conditions have been discussed in Chapter 4. Riprap failure will be discussed in this chapter. Prior to failure of the riprap slope, many individual stones moved or readjusted locations throughout the test period. Movement of these stones is referred to as incipient motion. This occurs when the displacing and overturning moments exceed the resisting moments. The force in the resisting moment is given by the component of the weight perpendicular to the embankment and interlocking between stones in the matrix. The overturning forces are the drag (or the jet impact on a stone), the lift, buoyancy, and to a lesser degree, the component of the weight parallel to the embankment depending on the point(s) of contact with other stones. Even though buoyancy plays an important role in the removal of rocks, the hydrodynamic forces have the major role in producing failure of the protective layer. This observation is supported by the depth measurements which revealed that the stones on the surface were not entirely submerged.

Failure of the riprap slope was defined as removal or dislodgement of enough material to expose the bedding material. Failure of the riprap layer occurred with the measured water depth still within the thickness of the rock layer. A layer of highly aerated water was flowing over the surface of the riprap, but this surface flow was only a small portion of the total flow and was not measurable by piezometers. A large bathtub-shaped hole down to the bedding layer was formed in the 1994 riprap layer down to the bedding layer at a distance of about 19.27 m from the crest down the slope. For these tests failure occurred at $0.223 \text{ m}^3/\text{s}/\text{m}$ (Figure 7.1).

Failure in the large 1995 material placed over the top of the previous riprap layer was more difficult to define. Failure of the 1995 material ($D_{50} = 655 \text{ mm}$) was defined as the removal of riprap to the top of the 1994 ($D_{50} = 386 \text{ mm}$) layer of rock. This criterion of one layer of approximately D_{50} thickness was used for failure. This was for fear that if the full depth of riprap was considered as failure, the number of rocks dislodged, would cause considerable damage to the flume, instrumentation, control equipment, gates, and supports. Many stones were repositioned during the tests, and several stones, as shown in Figure 7.2, were dislodged from the slope and caught in the trap below. The riprap layer was considered to have failed at a unit discharge of $0.929 \text{ m}^3/\text{s}/\text{m}$ (Figure 7.3). Many stones had repositioned or had been removed, such that the layer underneath the large stones was significantly exposed in several locations

In the summer of 1997, channelization of the rocks started at about $0.17 \text{ m}^2/\text{s}$. The picture of the channels developed on the rock surface is presented in Figure 7.4. Failure occurred at an unit discharge of $0.204 \text{ m}^3/\text{s}/\text{m}$, with the development of a large hole at 12.1 m from the crest down the slope. Figure 7.5 shows the failure of the riprap layer with the exposure of the bedding layer.

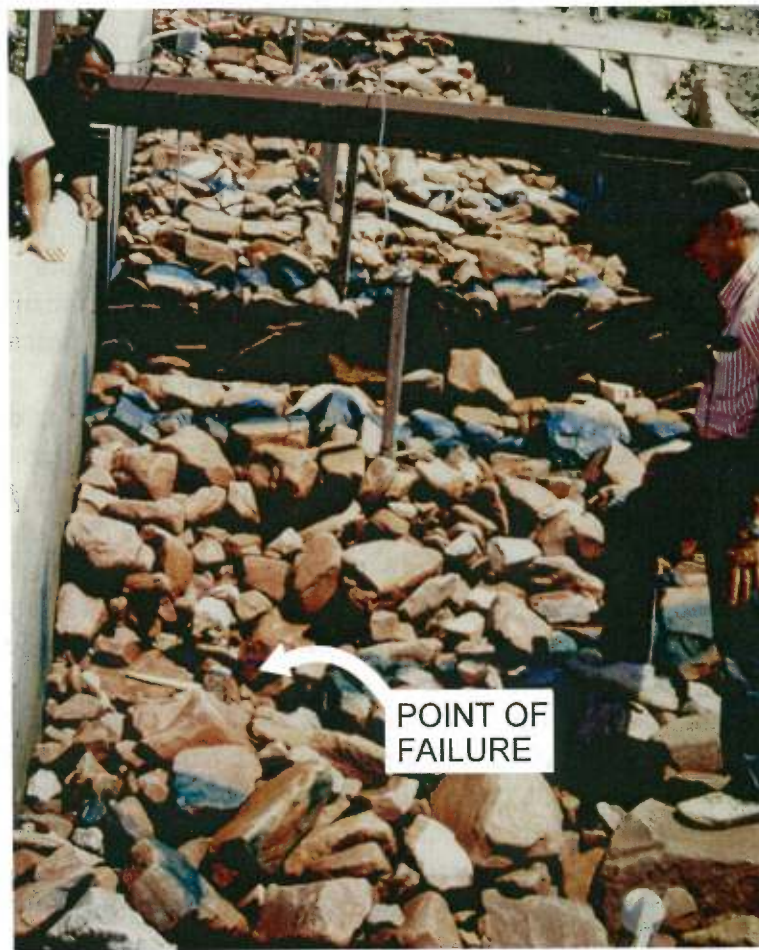


Figure 7.1: Failure of 1994 riprap layer located 19.3 m from the crest of the flume down the slope



Figure 7.2: Several rocks of 1995 riprap layer caught in the trap (looking downstream)

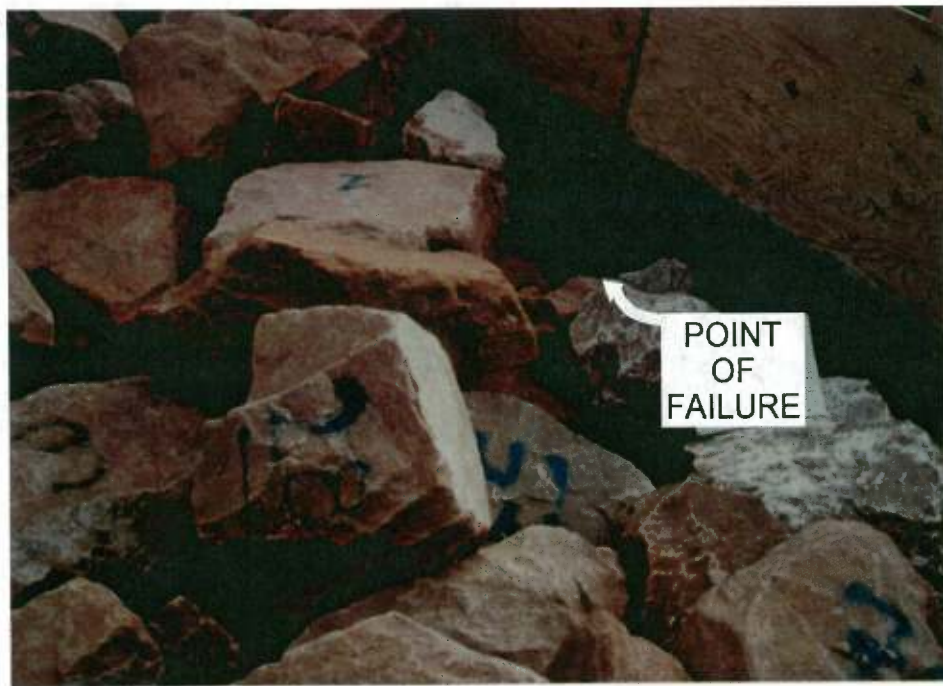


Figure 7.3: Failure of 1995 layer showing the removal of the top layer

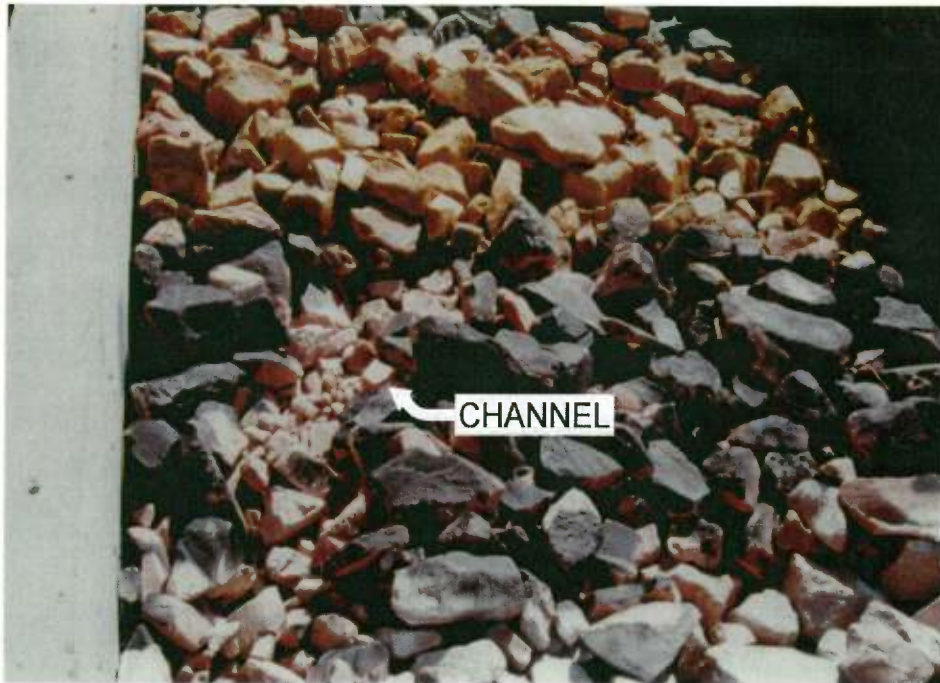


Figure 7.4: Channelization in 1997 riprap layer with dislodgement of rocks

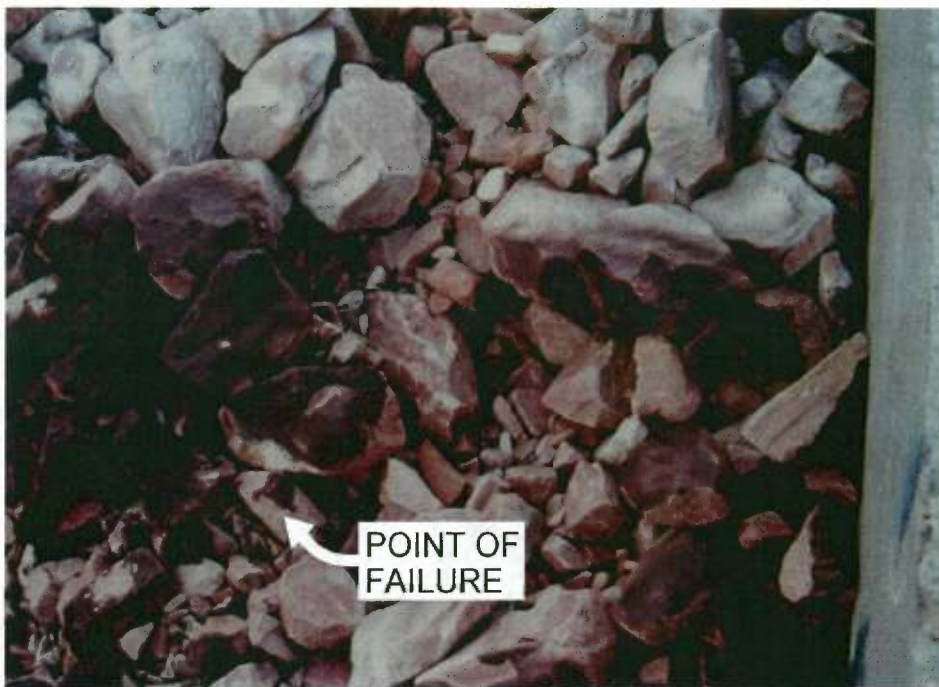


Figure 7.5: Failure of 1997 layer at 12.1 m from the crest down the slope

Table 7.1 summarizes rock characteristics and unit discharges at failure for three years of testing.

Table 7.1: Riprap failure characteristics

Year	D_{50} (mm)	Coefficient of Uniformity, C_u (D_{60}/D_{10})	Failure Discharge ($m^3/s/m$)
1994	386	1.90	0.223
1995	655	1.52	0.929
1997	271	1.81	0.204

7.2 Toe Treatment Test Program

Embankment toe treatment has always been a concern with overtopping protection. Many designers feel that, in case of overtopping, failure of the embankment will commence at the toe of the embankment because of formation of a hydraulic jump and head cutting. To address this problem, toe protection measures were tested in the summer of 1997. A berm, schematically shown in Figure 7.6(a), was constructed at the toe of the embankment.

Testing of the toe extended beyond the tests conducted to determine failure of the slope. Failure of the riprap ($D_{50} = 271$ mm) on the slope occurred at a unit discharge of $0.204 m^2/s$. The toe remained stable and there was no movement of riprap from the toe for any discharge to the point of riprap failure on the slope. Some rocks dislodged from the slope were trapped by the berm or were swept over the berm as the discharge was increased to the failure discharge of the slope, i.e., $0.204 m^2/s$. Therefore, in order to test the berm and the toe, discharges greater than the slope failure discharge were required.

In order to pass larger discharges on the riprap slope, the entire riprap surface of the flume was restrained by a wire mesh anchored to the walls of the flume. The photograph in Figure 7.7, shows the wire mesh restraint. During testing of the toe, the discharge was increased in a step-wise manner to $0.279 m^2/s$. The berm at the toe of the slope was completely stable. At this point the tailwater depth was increased by partially closing the gates located downstream of the tailbox. This resulted in formation of a hydraulic jump between the toe and the tailbox. The berm was partially submerged. The rock movement in the toe was very minimal and failure of the toe did not occur.

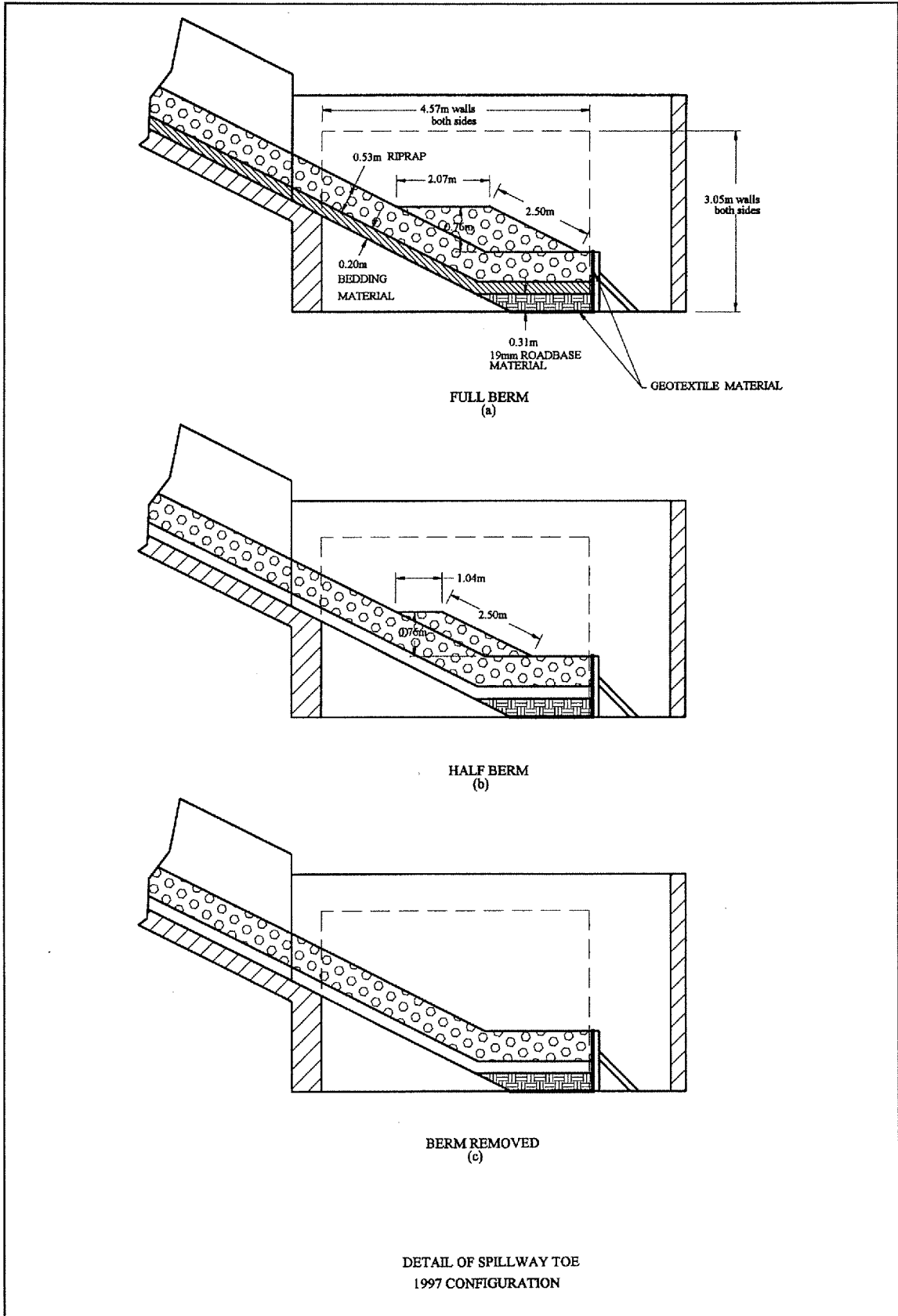


Figure 7.6: Schematic diagram of the toe shapes and sizes tested in 1997

In the next phase of the testing of the toe the original berm shown in Figure 7.6(a) was sliced into half its original size, still maintaining its original shape. The schematic of the new toe size is shown in Figure 7.6(b). The discharge was increased until the failure discharge for the slope, i.e., $0.204 \text{ m}^2/\text{s}$. The toe remained stable. The effect of increased tailwater depth, like the previous time, helped create a hydraulic jump partially submerging the modified berm without causing any failure. The berm was then completely removed (Figure 7.6(c)). Discharge was increased in a step-wise manner until $0.325 \text{ m}^2/\text{s}$. At this discharge the riprap at the top of the slope was dislodged and removed down to the flume floor. Before the $0.325 \text{ m}^2/\text{s}$ flow could be diverted, a section of the bedding and riprap approximately 3-m long was completely swept downstream exposing the concrete floor of the flume. This resulted in the catastrophic failure of the entire embankment as seen in Figure 7.8. The riprap on the entire slope appeared to move and the riprap trapped by the wire mesh caused large bulges into the mesh at several locations. Small to medium sized rocks that were able to move under the bulged wire mesh traveled down to the toe and deposited. Some rocks were swept into the tailbox and through the outlet. The toe was

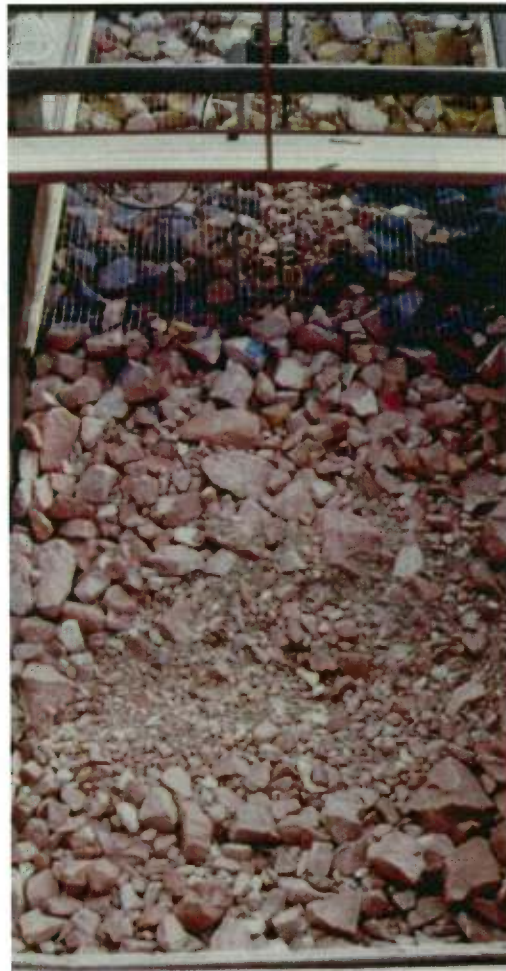


Figure 7.7: Wire mesh covering the riprap

covered with rocks in some areas and had channels in other areas. There were channels that formed and some rocks were removed. But in general the toe was still stable.

The extended riprap layer at the toe of the embankment did not fail at any discharges tested. The bedding was never exposed although some channelization did appear on the toe surface indicating some rock movement. It is, therefore, concluded from the toe treatment program that on steep embankments, riprap failure on the slope is more critical than the failure at the toe.



Figure 7.8: Catastrophic failure

CHAPTER 8

DEVELOPMENT OF THE RIPRAP DESIGN EQUATION

8.1 Development of Design Guidelines

The objective of this test program was to verify existing riprap design equations for overtopped embankments or to develop new design guidelines. Three riprap sizes were tested which were larger than any previous riprap sizes subjected to overtopping flows. The slope of the chute, fixed at 50%, is the steepest chute used so far for riprap testing.

8.2 Shield's Parameter

Fluid flow around sediment particles exerts forces that tend to initiate particle motion. The resisting force of noncohesive material relates to particle weight. Threshold conditions occur when the hydrodynamic moment of forces acting on a single particle balances the resisting moment of the force. The particle is then at the point of incipient motion where a slight increase in force will cause the particle to begin moving.

Many early definitions of incipient motion were based on the visual observations of the experimenters and were subject to the judgement of the experimenters. Shields (1936) expressed the shear on the particle by a dimensionless parameter called Shield's parameter defined as the ratio of the inertial forces and gravitational forces (F_i / F_g). Gessler (1965) concluded that the constant value of the Shield's parameter for turbulent flow is 0.047. Figure 8.1 illustrates the functional relationship between the dimensionless shear stress known as Shield's parameter and boundary Reynold's number. This figure is widely known as Shield's diagram.

The Shield's parameter is a dimensionless form of shear stress that expresses the incipient motion of particles in flowing water. In our analysis of incipient motion of riprap, it was found that assumptions made to simplify the Shield's parameter make it a poor tool to design riprap in its simplified form. For example, the simplified form of the Shield's parameter can not be used to design riprap under typical dam overtopping flow situations because this form of the Shield's parameter assumes the slope to be small. The empirical equations by Robinson *et al.* (1995) (Eq. (2.27)) and Abt *et al.* (1991) (Eq. (2.19)) are plotted with the data points in the Figures 8.2a and 8.3a. Closeup views for Figures 8.2a and 8.3a are given in Figures 8.2b and 8.3b. It can be seen that neither of the equations adequately predict the design median rock size for the embankment slope of 50%. These equations have been developed for riprap tests done for rock sizes of 0.158 m median size diameter or less at embankment slopes of 40% or less. A better riprap design criterion is needed.

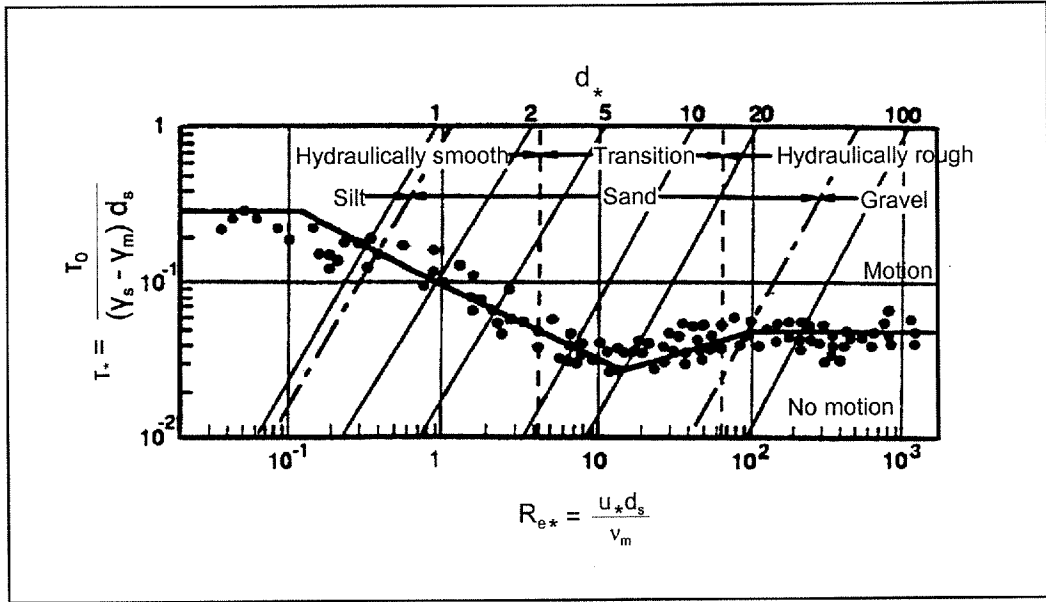


Figure 8.1 Shield's diagram (adapted from Julien, 1995)

Robinson et al. Riprap Formula for Various Slopes

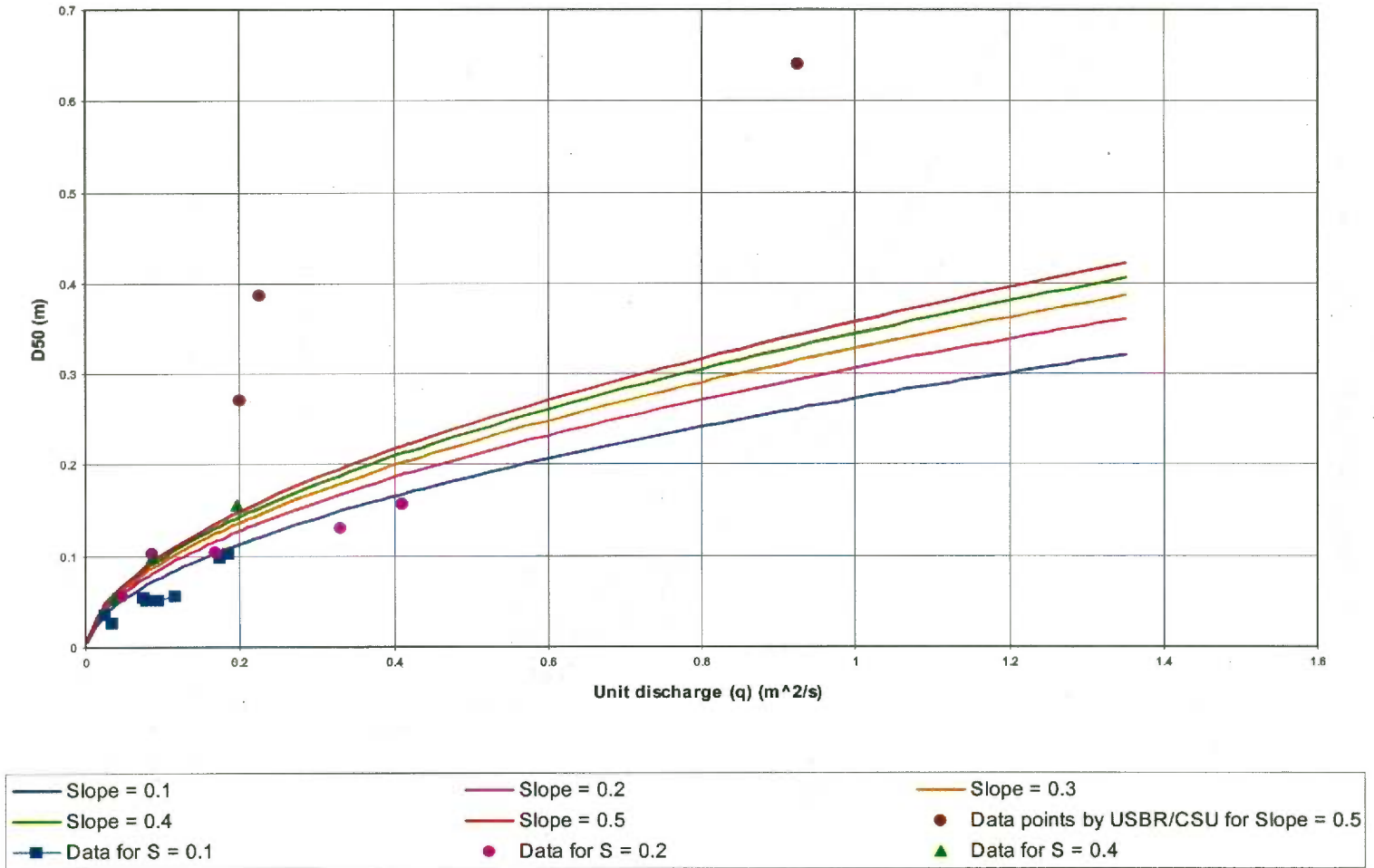


Figure 8.2a: Robinson *et al.* riprap design equation

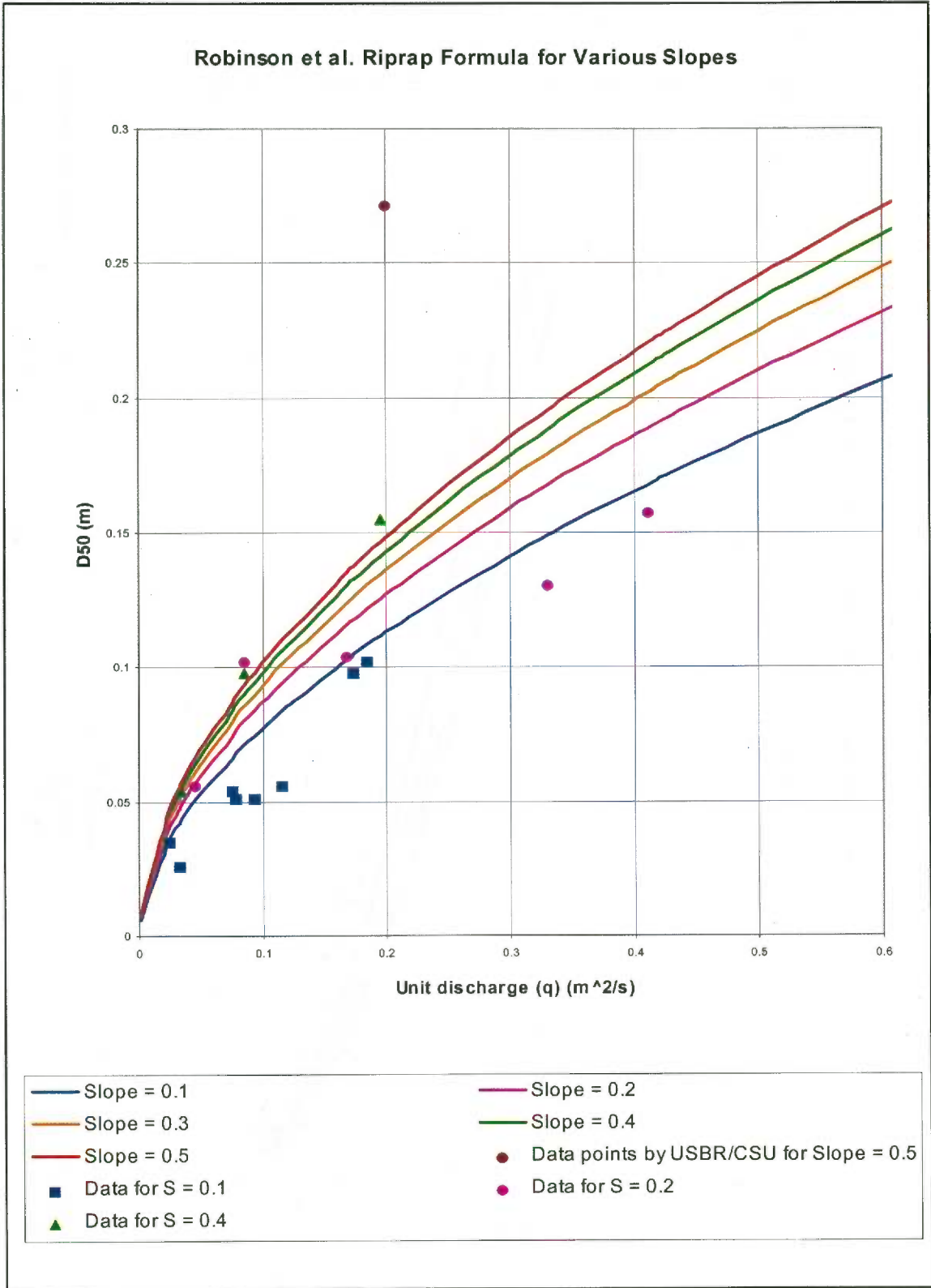


Figure 8.2b: Closeup view of Robinson *et al.* (1995) riprap design equation

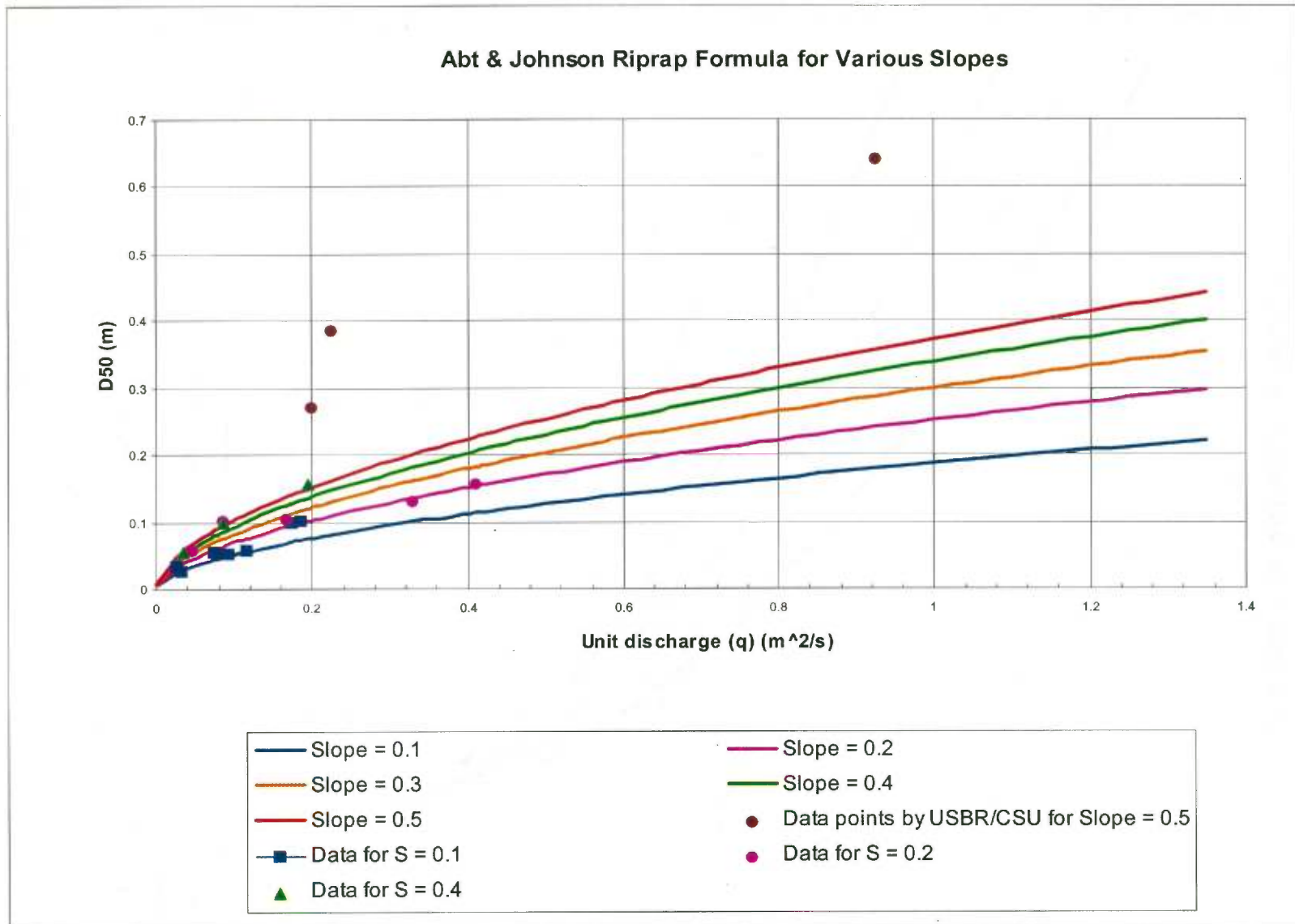


Figure 8.3a: Abt *et al.* (1991) riprap design equation

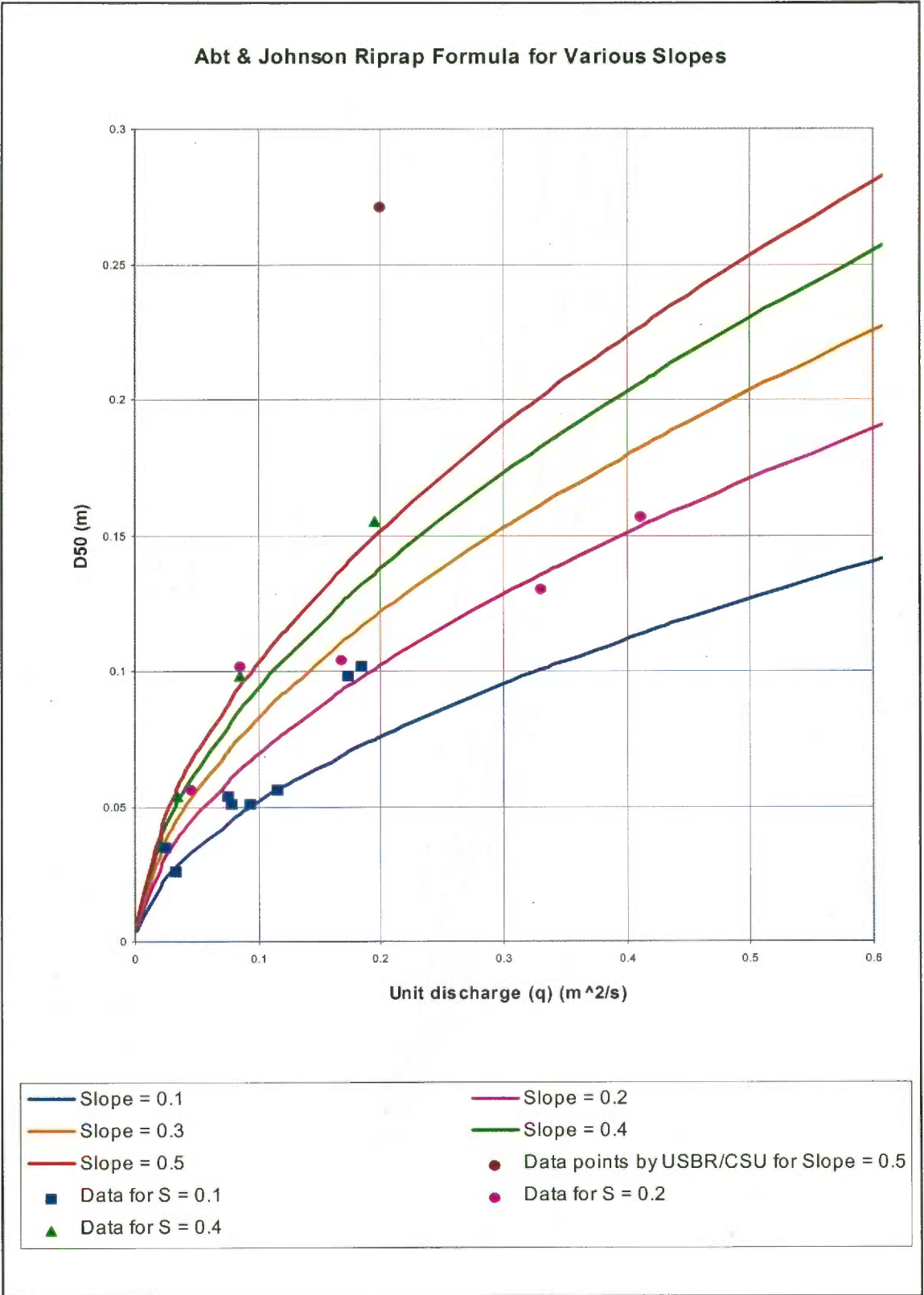


Figure 8.3b: Closeup view of Abt *et al.* (1991) riprap design equation

8.3 Derivation of the Universal Equation

Abt *et al.* (1991) and Robinson *et al.* (1995) performed regression analyzes to match their test data. Wittler's (1994) further extension of previous work by Abt *et al.* (1991) includes an extensive analysis of the application of Shield's parameter. The following derivation of a riprap equation takes the approach of fitting data to known sediment transport and flow equations. The complete equation for the Shield's parameter includes the embankment slope and the angle of repose of the material and is developed by Whittaker and Jaggi (1986) as:

$$\tau_* = \frac{\tau_{cr}}{\gamma(S_s \cos \alpha - 1)D_{50}(\cos \alpha \tan \phi - \sin \alpha)} = 0.047 \quad (8.1)$$

where:

- τ_* = non-dimensional Shield's parameter;
- τ_{cr} = critical shear stress to cause the incipient motion = γRS ;
- S_s = specific gravity of rock (2.65 for most cases);
- $\tan \alpha$ = slope of the embankment;
- γ = density of water;
- ϕ = angle of repose of the riprap material;
- D_{50} = median rock size diameter; and
- R = hydraulic radius.

From Manning's equation the hydraulic radius R in S.I. units can be written as:

$$R = \left(\frac{q n}{S^{0.5}} \right)^{3/5} \quad (8.2)$$

where:

- R = hydraulic radius (m);
- q = unit discharge (m^2/s);
- n = Manning's roughness coefficient; and
- S = slope of the channel.

Therefore for the unit failure discharge, the hydraulic radius R will be:

$$R = \left(\frac{q_f n}{S^{0.5}} \right)^{3/5} \quad (8.3)$$

where: q_f = unit discharge at failure (m^2/s).

Manning's coefficient, n , in S.I. units was described by Strickler as:

$$n = 0.0414 D_{50}^{1/6} \quad (8.4)$$

Starting with the complete form of the Shield's parameter and substituting the value of τ_{cr} with γRS :

$$\tau_* = \frac{\gamma RS}{\gamma(S_s \cos\alpha - 1)D_{50}(\cos\alpha \tan\phi - \sin\alpha)} = 0.047 \quad (8.5)$$

Substituting for R :

$$\tau_* = \frac{\gamma \left(\frac{q_f n}{S^{0.5}} \right)^{3/5} S}{\gamma(S_s \cos\alpha - 1)D_{50}(\cos\alpha \tan\phi - \sin\alpha)} = 0.047 \quad (8.6)$$

Substituting for n :

$$\tau_* = \frac{\gamma \left(\frac{q_f 0.0414 D_{50}^{1/6}}{S^{0.5}} \right)^{3/5} S}{\gamma(S_s \cos\alpha - 1)D_{50}(\cos\alpha \tan\phi - \sin\alpha)} = 0.047 \quad (8.7)$$

Solving the above equation for D_{50} and taking the specific gravity of rock (S_s) to be 2.65:

$$D_{50} = 3.56(q_f)^{0.667} S^{-0.333} \left(\frac{\sin\alpha}{(2.65 \cos\alpha - 1)(\cos\alpha \tan\phi - \sin\alpha)} \right)^{1.11} \quad (8.8)$$

This equation is hereafter referred to as the fundamental equation. This equation is plotted in Figure 8.4 with all the observed data from the riprap tests conducted in this study as well as the data available from the NRC and ARS studies. This graph was constructed using the value of D_{50} for a given value of unit discharge at failure. The value of the angle of internal friction, ϕ , is considered to be 42 degrees for all angular rocks of median stone diameter of 5 cm and over. The family of curves represents the above relation for different slope values, i.e., 0.05, 0.1, 0.2, 0.4, and 0.5. Incipient motion of rock is the governing factor in the development of Shield's parameter. The gradation of the rock layer and the factors such as the effects of air entrainment, turbulence, steep slopes, etc. are not considered in the Shield's parameter, therefore, it is not surprising, this equation does not predict the data obtained in riprap tests performed by Abt *et al.* in 1987 and 1988, Robinson *et al.* in 1995, and CSU/USBR in 1994, 1995, and 1997. In fact, the deviation of the actual data from the rock sizes predicted by the fundamental equation increases as the embankment gets steeper.

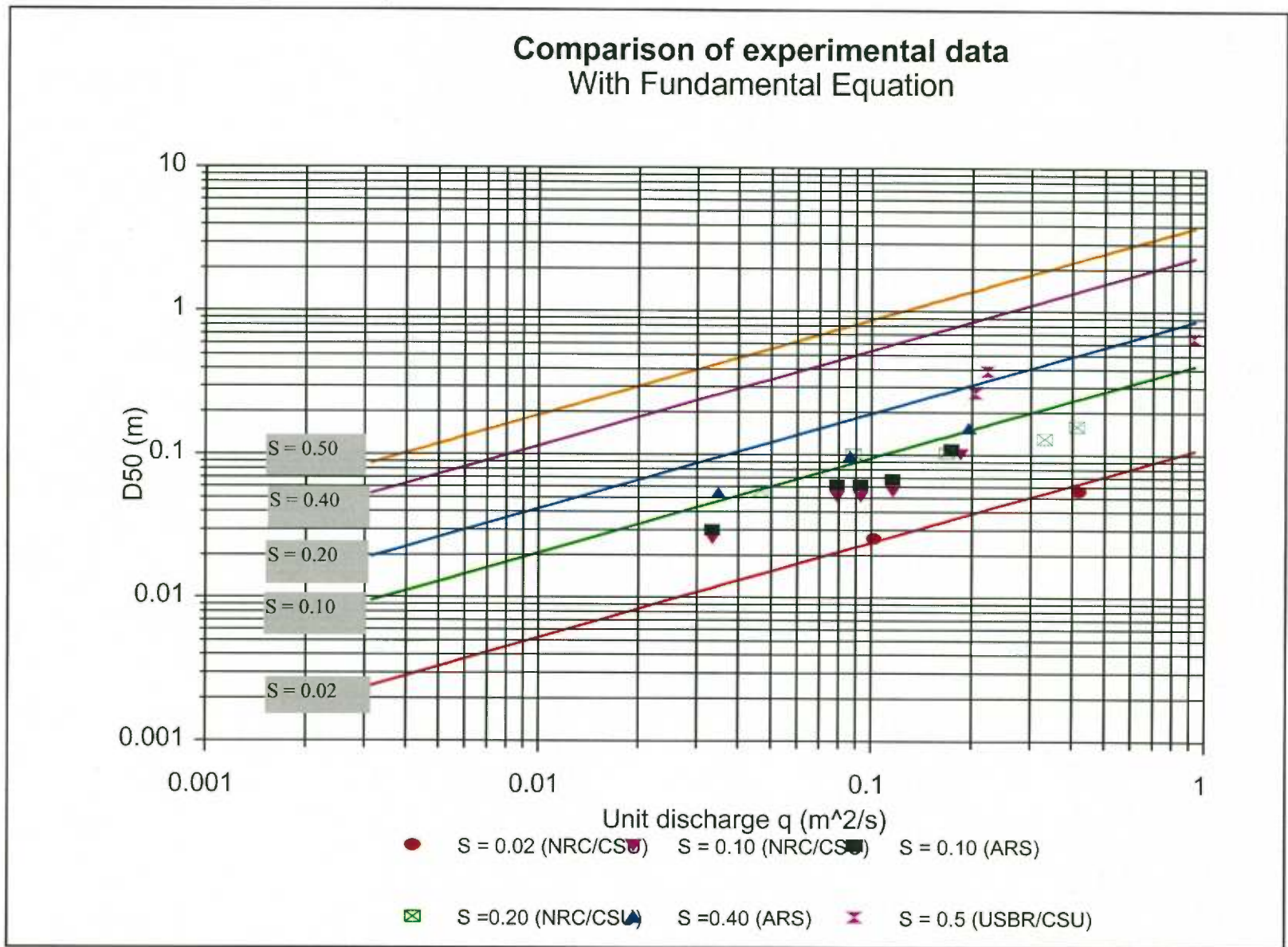


Figure 8.4: Fundamental equation with actual data obtained in different tests

This deviation can be expressed as the ratio of the actual median rock size diameter and the predicted D_{50} from the fundamental equation (Figure 8.4). This deviation factor, σ , can be expressed as a function of the rock properties, the slope of the embankment, and the unit discharge. From the data in Figure 8.4, deviation factors for each data point were calculated and are presented in Table 8.1 with the corresponding values of the coefficient of uniformity, C_u , slope of the embankment, S , and the unit discharge at failure, q_f . Performing a multiple power regression analysis on the data in Table 8.1, the deviation factor σ , can be expressed as

$$\sigma = 0.155C_u^{-0.25}q_f^{-0.15}S^{-0.415} \quad (8.9)$$

where, all the parameters have the same meaning as in Table 8.1.

The right hand side of the fundamental equation is multiplied by σ , to develop the design equation. The universal design equation can be written as:

$$D_{50} = \sigma(3.56(q_f)^{0.667}S^{-0.333}) \left(\frac{\sin\alpha}{(2.65\cos\alpha - 1)(\cos\alpha\tan\phi - \sin\alpha)} \right)^{1.11} \quad (8.10)$$

Putting the rock properties on the left hand side of the equation, the final form of the design equation can be written as:

$$D_{50}C_u^{0.25} = 0.55(q_f)^{0.52}S^{-0.75} \left(\frac{\sin\alpha}{(2.65\cos\alpha - 1)(\cos\alpha\tan\phi - \sin\alpha)} \right)^{1.11} \quad (8.11)$$

The design equation (8.11) with all the data obtained is plotted in Figure 8.5 and Figure 8.6 with log-log and normal axes, respectively. The equation produces various degrees of fit accuracy depending upon the value of the $D_{50}C_u^{0.25}$ parameter. Of particular interest is the area of most investigations, where $D_{50} * C_u^{0.25}$ is less than 0.2. The deviation distances of the data points from the design curves in log-log scale (Figure 8.5) might be misleading. Therefore, Figure 8.6 must be discussed.

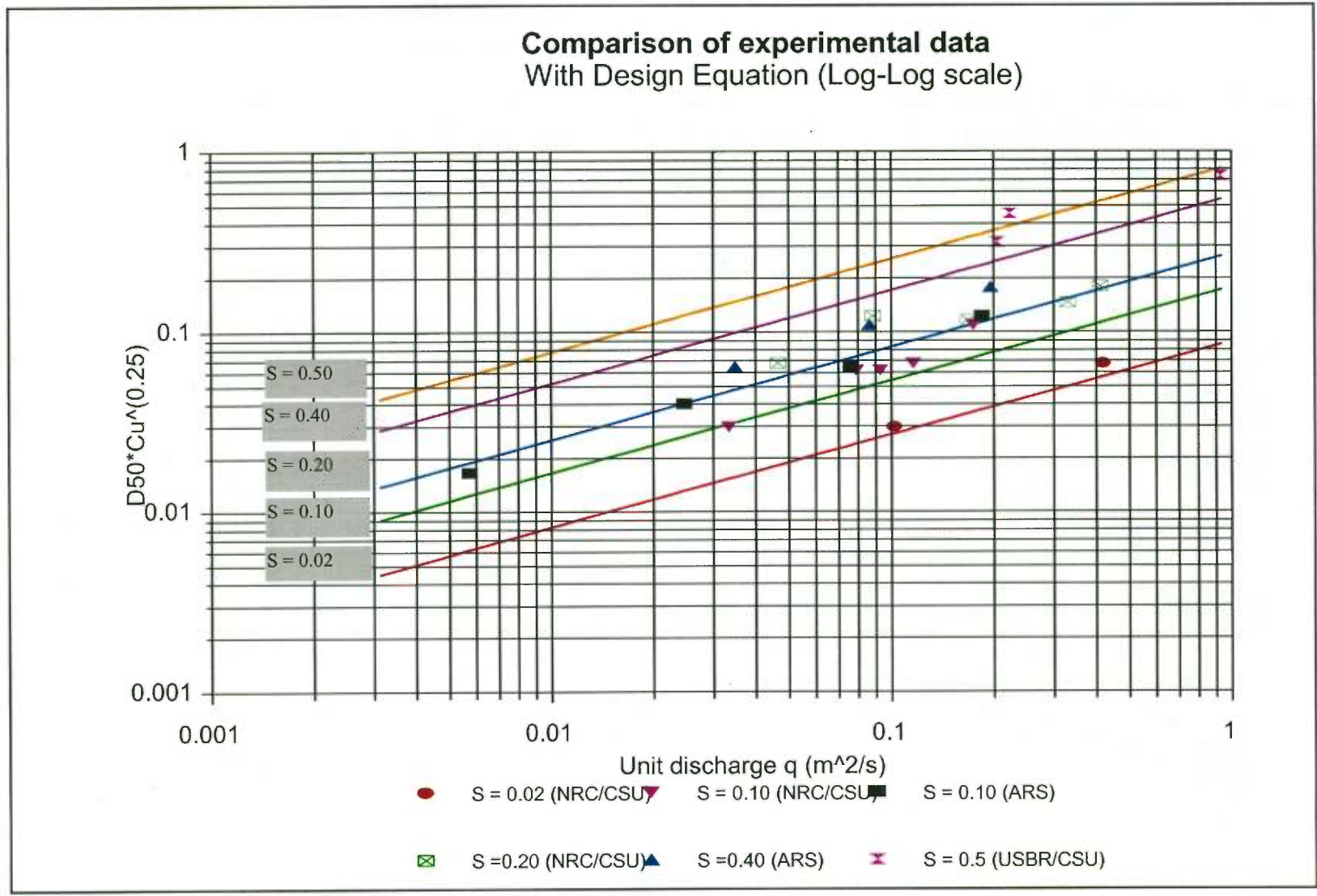


Figure 8.5: Universal design equation

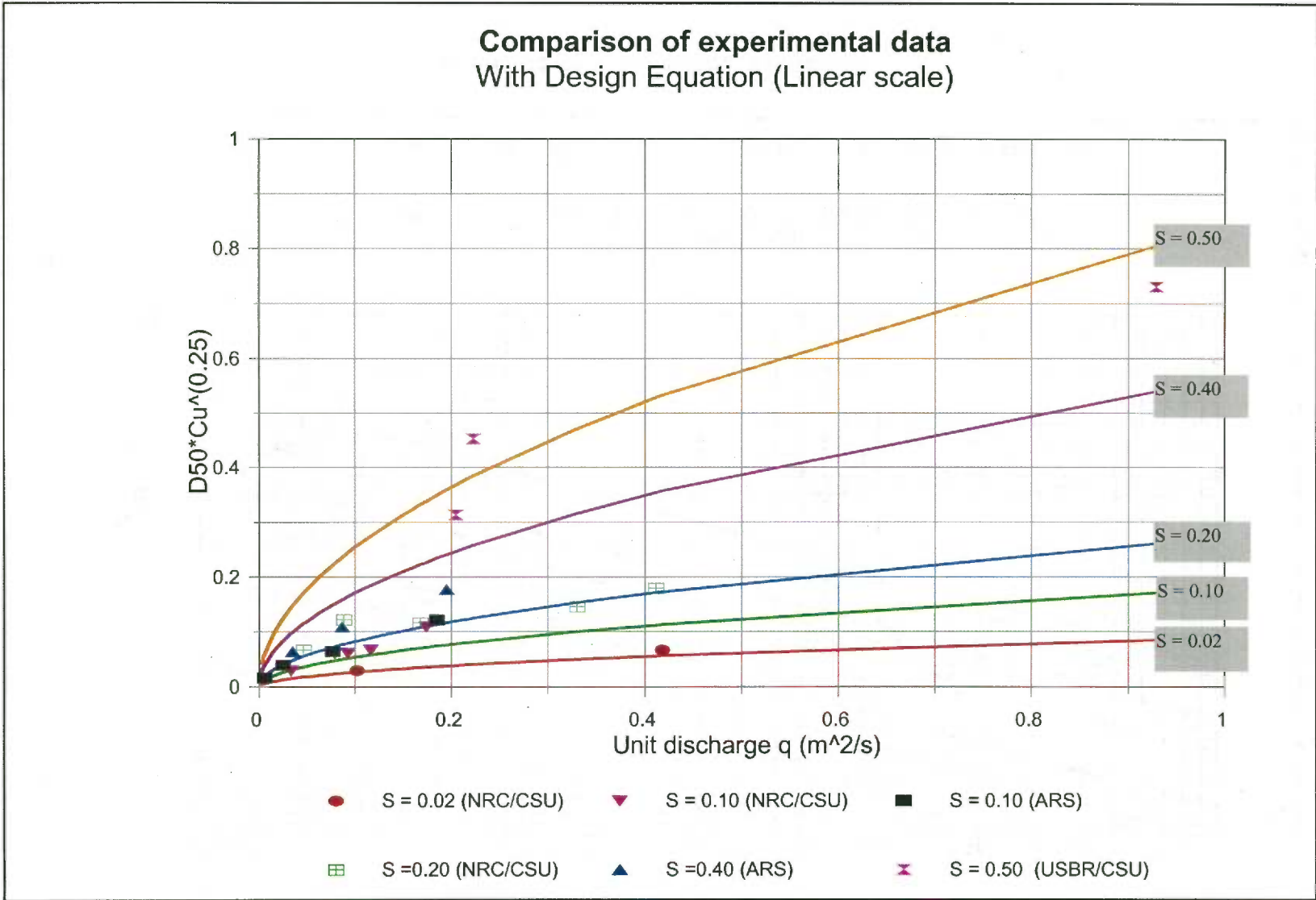


Figure 8.6: Universal design equation (normal axes)

Table 8.1: Deviation factors σ

Deviation Factor σ	C_u	S	q_f (m ² /s)
1.053	1.75	0.02	0.102
0.887	2.09	0.02	0.418
1.061	1.50	0.10	0.006
0.934	1.73	0.10	0.025
0.566	1.75	0.10	0.033
0.682	2.03	0.10	0.076
0.626	2.14	0.10	0.079
0.562	2.14	0.10	0.093
0.533	2.09	0.10	0.116
0.714	1.57	0.10	0.174
0.710	2.12	0.10	0.185
0.906	1.50	0.13	0.005
0.782	1.73	0.13	0.024
0.629	2.03	0.13	0.062
0.632	1.57	0.13	0.151
0.594	1.57	0.13	0.166
0.594	1.73	0.13	0.331
0.481	2.09	0.20	0.047
0.570	2.12	0.20	0.088
0.380	1.57	0.20	0.168
0.302	1.62	0.20	0.330
0.316	1.69	0.20	0.412
0.685	1.50	0.22	0.0003
0.574	1.73	0.22	0.015
0.400	2.03	0.22	0.048
0.446	1.57	0.22	0.100
0.418	1.57	0.22	0.111
0.412	1.73	0.22	0.224
0.205	2.03	0.40	0.035
0.203	1.57	0.40	0.086
0.186	1.73	0.40	0.195
0.260	1.90	0.50	0.386
0.171	1.52	0.50	0.929
0.193	1.81	0.5	0.204

The data obtained at ARS at 40% slope, tend to deviate from the universal design equation developed in this study. From Figure 8.6, it is very clear that, the data points obtained by ARS for the slope value of 40%, are situated at a low discharge range. Here the development of the confidence limits, was thought to be very important. In Figures 8.7 and 8.8, the confidence limits are shown for the data obtained by this study for 50% slope (Figure 8.7) and the data obtained by ARS for 40% slope (Figure 8.8). It was found that the data obtained in this study fall within a confidence level of 80%, whereas the data obtained by ARS had a confidence level of 75%. All data reported by other investigators had a confidence level of 80% or better.

A new design equation to predict median rock size for a protective riprap layer has been developed by compilation of data from the current test program and from previous investigations. A set of curves shown in Figure 8.6 for different embankment slopes combines the rock properties of the riprap material, unit discharge, and embankment slope. The curves provide an estimation of the point of initial failure of the riprap with 80% confidence that the rock size will be appropriate.

An additional simplification may be performed to the design equation. The value of coefficient of uniformity C_u can typically range from 1.5 to 2.1. Taking a general value of C_u as 1.75 the design Eq. (8.11) can be further simplified as:

$$D_{50} = 0.48(q_f)^{0.52} S^{-0.75} \left(\frac{\sin\alpha}{(2.65\cos\alpha - 1)(\cos\alpha \tan\phi - \sin\alpha)} \right)^{1.11} \quad (8.12)$$

The design curves combine empirical data with accepted sediment transport equations. To ensure stability, a safety factor should be used by the designer.

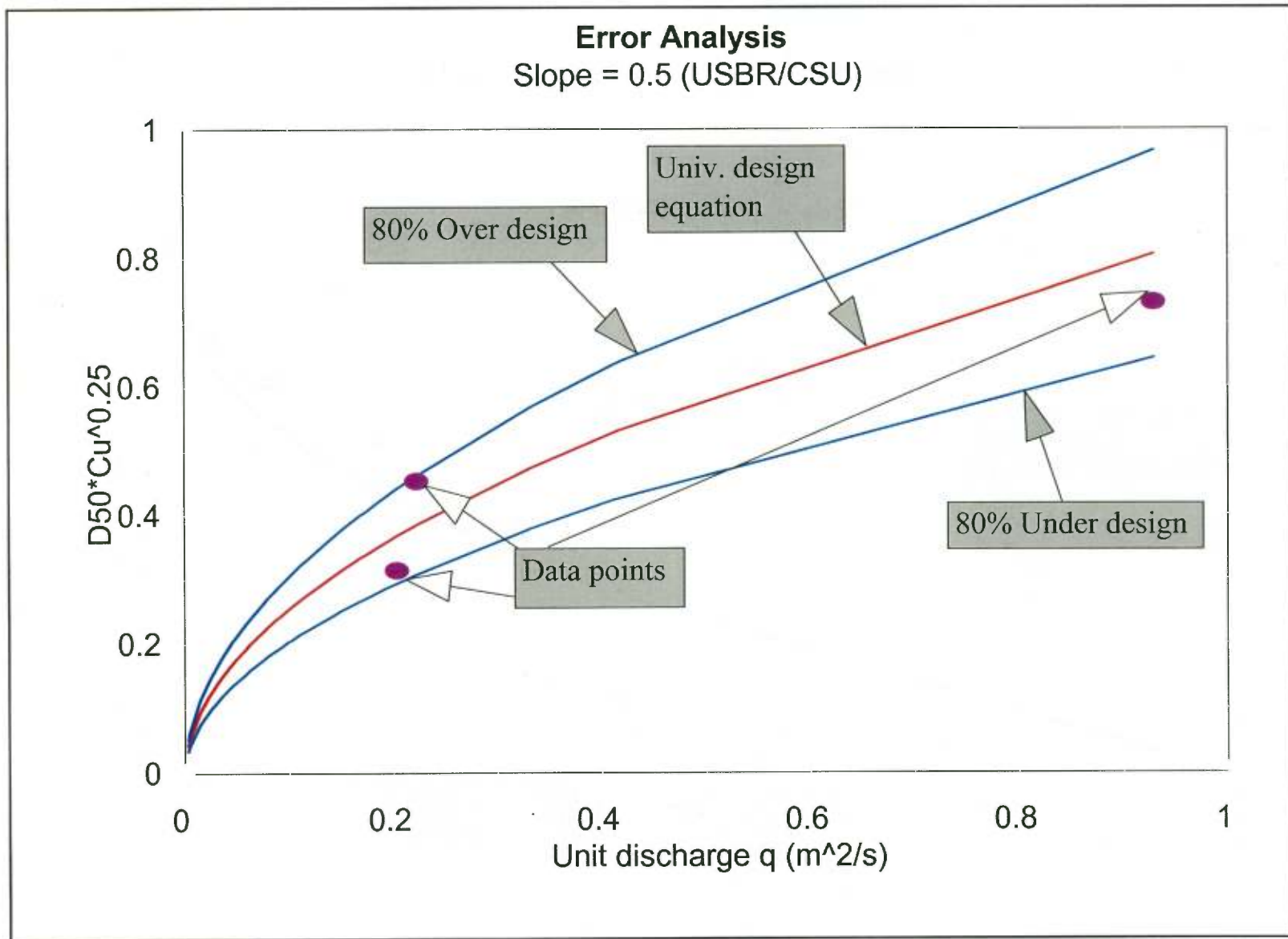


Figure 8.7: Error analysis at 50% slope (USBR/CSU)

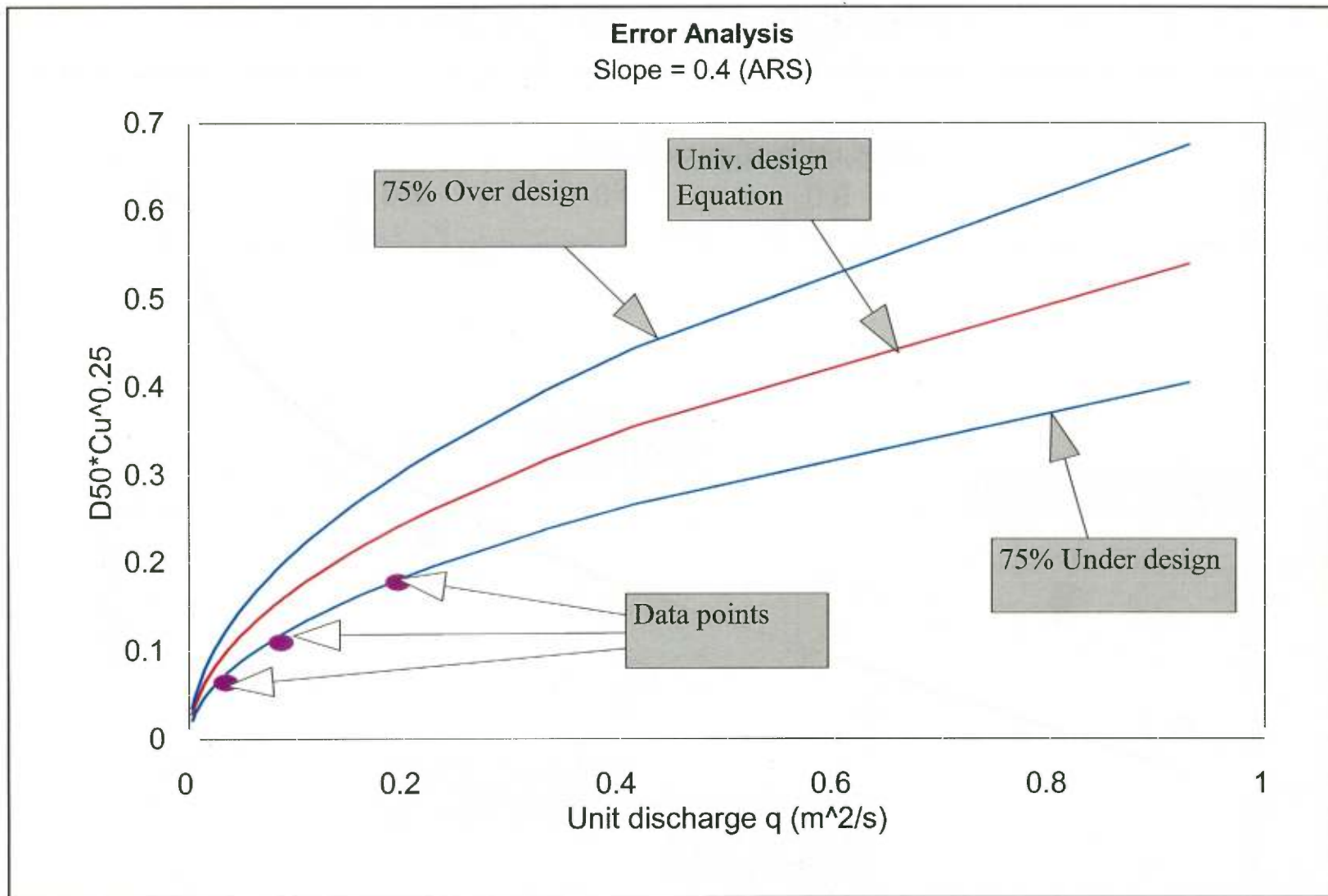


Figure 8.8: Error analysis at 40% slope (ARS)

8.4 Sensitivity Analysis

In order to test the sensitivity of the riprap design equation, Eq. (8.12) may be compared with the equations generated by using the extreme values of the coefficient of uniformity, C_u , i.e. 1.5 and 2.1. Using these two values of C_u (1.5 and 2.1) we arrive at Eqs. (8.13) and (8.14), respectively. Note the difference in the constants of 0.50 and 0.46 in the equations. It is evident from Eqs. (8.13) and (8.14) that, the results obtained from either of Eqs. (8.13) and (8.14) will be within 4.2% of the results predicted by Eq. (8.12) which uses 1.75 as a general value for C_u . It is interesting to note that, even with a C_u value of 4.0, which is quite high, the results predicted by Eq. (8.12) will be within 19% of the results predicted by Eq. (8.11) which is the universal equation.

$$D_{50} = 0.5(q_p)^{0.52} S^{-0.75} \left(\frac{\sin\alpha}{(2.65\cos\alpha - 1)(\cos\alpha\tan\phi - \sin\alpha)} \right)^{1.11} \quad (8.13)$$

$$D_{50} = 0.46(q_p)^{0.52} S^{-0.75} \left(\frac{\sin\alpha}{(2.65\cos\alpha - 1)(\cos\alpha\tan\phi - \sin\alpha)} \right)^{1.11} \quad (8.14)$$

8.5 Riprap Layer Thickness and Slope Influence

The previous section discussed the design equation to size riprap for overtopping protection. Now the thickness of the riprap layer will be addressed. The thickness of protective riprap layers is usually assumed to be twice the D_{50} or equal to the D_{100} size rock in the layer. The information obtained from this test program, combined with data from other experiments, has produced an analytical approach to determining the required riprap layer thickness. This provides the designer more confidence in the use of the riprap for overtopping applications. Also, stability may be ensured for higher discharges on steeper slopes by providing a riprap layer of designed thickness. This approach involves using the interstitial velocity, porosity, and continuity to determine the appropriate riprap layer thickness. As shown in Chapter 6 the interstitial velocity through a riprap layer is given by:

$$\frac{V_i}{\sqrt{(gD_{50})}} = 2.48C_u^{-2.22} S^{0.58} \quad (6.1)$$

The average velocity can be determined using the porosity and the interstitial flow velocity determined by the previous equation from $V_{ave} = V_i n_p$. The average depth, y , is then determined from continuity using the design unit discharge and the average velocity, $y = q/V_{ave}$. This depth is used to determine the required thickness, t , of the riprap layer. The minimum thickness of the riprap layer must always be at least $2D_{50}$.

In general, for steeper slopes, the majority of the flow will be interstitial and the " $2D_{50}$ " criteria will be met; however, this is not always the case. For smaller stone sizes on milder slopes, the riprap thickness is often greater than $2D_{50}$ and may approach a practical limit of $4D_{50}$. At less steep slopes, water has been observed to flow through and over the riprap. In cases where the flow depth exceeds the $2D_{50}$ criteria, an estimate of the

discharge above the riprap must be made using standard flow equations for the flow over rough surfaces to assure that the flow over the surface will not exceed the critical shear stress for the design D_{50} . The depth of flow that can pass over the riprap surface and the associated discharge are then determined. This flow is subtracted from the total flow to determine the interstitial discharge and depth that meets the $2D_{50}$ to $4D_{50}$ criteria.

The important task is to determine the highest slope for which the surface discharge must be accounted for. The maximum depth of flow over riprap without causing shear failure can be calculated from the formula (Julien, 1995):

$$0.97hS = 0.06(\gamma_s - \gamma)D_{50}\tan\phi \quad (8.15)$$

where:

- γ_s = specific gravity of rock;
- γ = specific gravity of water;
- h = depth of water over the riprap; and
- ϕ = angle of internal friction.

From Manning's equation the hydraulic radius R in S.I. units can be written as:

$$R = \left(\frac{q n}{S^{0.5}} \right)^{3/5} = h \quad (8.2)$$

where:

- R = hydraulic radius (m) = flow depth h (approximately);
- q = unit discharge (m^2/s);
- n = Manning's roughness coefficient; and
- S = slope of the channel.

Manning's coefficient, n , in S.I. units can be described by Strickler's equation as:

$$n = 0.0414D_{50}^{1/6} \quad (8.4)$$

where: D_{50} = median rock diameter (m).

A maximum unit surface discharge can be evaluated by finding the velocity of surface flow by using Manning's equation (Eq. (8.2)) as well as Strickler's equation (Eq. (8.4)) for predicting Manning's roughness coefficient in terms of D_{50} . Hence combining Eqs. (8.4), (8.2), and (8.15) the equation for maximum unit surface discharge can be found as:

$$D_{50}^{1.11} = 0.418(\gamma_s - \gamma)q^{1.67}S^{1.43}\tan\phi \quad (8.16)$$

Figure 8.9 shows the relationship of unit surface discharge with D_{50} for a range of slopes. It is evident from the graph that the maximum allowable unit surface discharge will increase for a particular slope as D_{50} increases. Figure 8.10 shows the relationship between maximum unit surface discharge and the slope for a range of rock sizes. It is clear from this figure that, for a given rock size the maximum allowable unit surface discharge decreases as the slope increases.

In this riprap design procedure, for a particular unit discharge, as the slope of the embankment gets steeper, the design equation predicts larger values of the rock sizes according to the equation given by:

$$D_{50} C_u^{0.25} = 0.55(q_f)^{0.52} S^{-0.75} \left(\frac{\sin \alpha}{(2.65 \cos \alpha - 1)(\cos \alpha \tan \phi - \sin \alpha)} \right)^{1.1} \quad (8.11)$$

Therefore, the maximum unit surface discharge for the riprap layer is simultaneously governed by the slope and D_{50} of the riprap layer. The combined effect of slope and the rock size must be obtained to estimate the allowable unit surface discharge. For a particular q_f , D_{50} can be obtained for a given slope from the riprap design equation (8.11), and then the maximum allowable surface discharge can be computed from Eq. (8.16). If we change the slope in this situation, the riprap design equation will predict another median stone size diameter for the same unit discharge and the maximum surface discharge must be recalculated from Eq. (8.16). This relationship of maximum allowable surface discharge, q , with slope, S , for given failure unit discharge is shown on Figure 8.11. Also shown in Figure 8.11 are the corresponding stone sizes, D_{50} , and slope, S , for the total unit discharges (q_f) of $0.5 \text{ m}^2/\text{s}$ and $1.0 \text{ m}^2/\text{s}$ used for illustration.

As the slope increases, we expect the maximum allowable unit surface discharge to decrease. Figure 8.11 shows this trend. When the slope approaches the value of 0.25, the allowable unit surface discharge starts to increase, which shows that the size of the rock becomes the dominant factor. The larger rocks result in larger voids inside the rock layer thereby making the majority of the discharge to flow interstitially. If there are no voids, the predicted discharge will be entirely surface flow. However, because of the presence of voids in the riprap, the surface discharge becomes negligible, even though the riprap has the capability to carry some surface discharge.

In the design procedure to be developed in the next chapter, it is important to keep in mind that, if the given slope is greater than or equal to 0.25 the riprap should be designed to carry the entire discharge as interstitial flow. On the other hand, if the slope is less than 25%, the unit surface discharge must be calculated to find out the true interstitial flow. This will be demonstrated in Chapter 9.

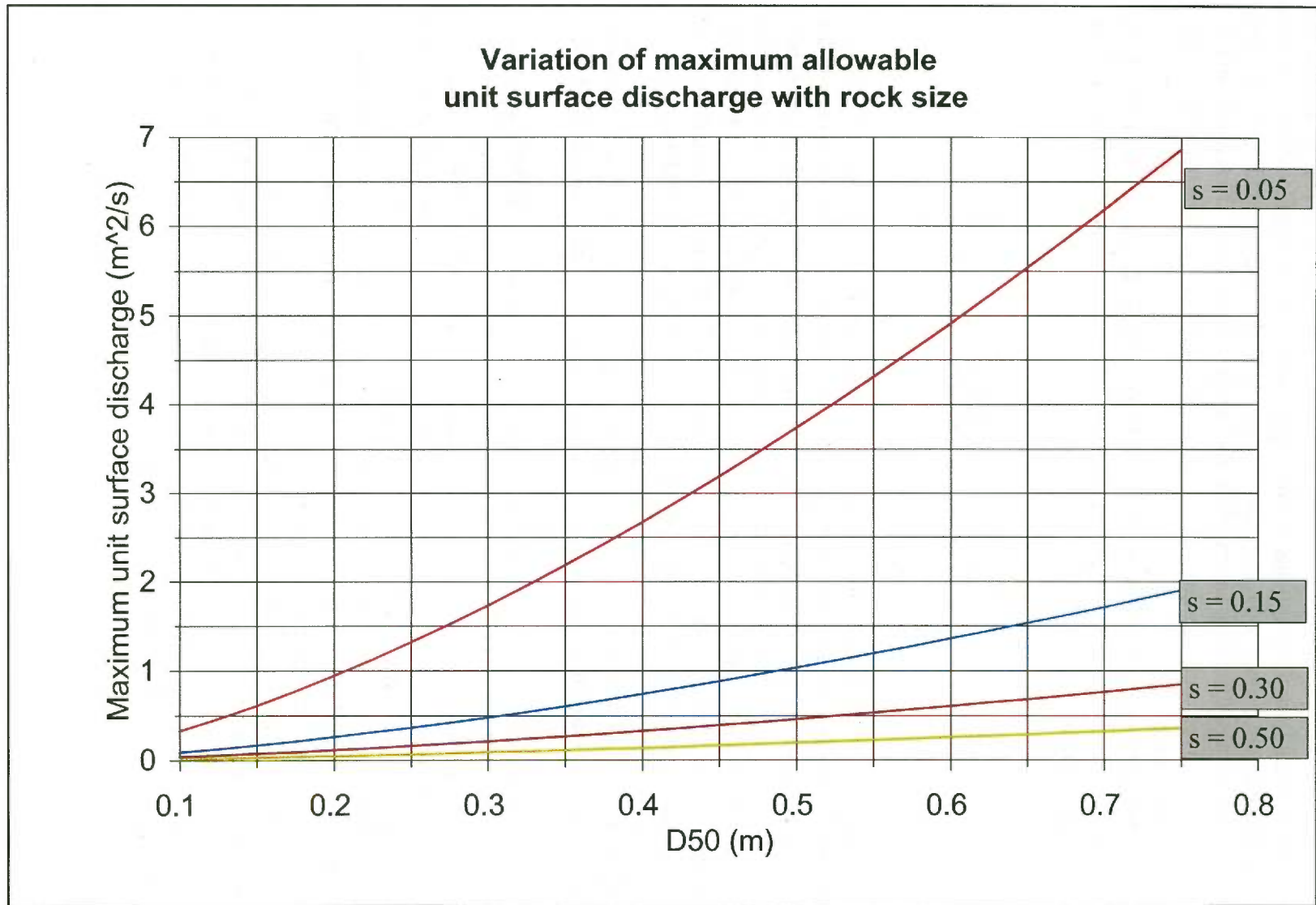


Figure 8.9: Relationship between maximum allowable surface discharge and D_{50} at various slopes

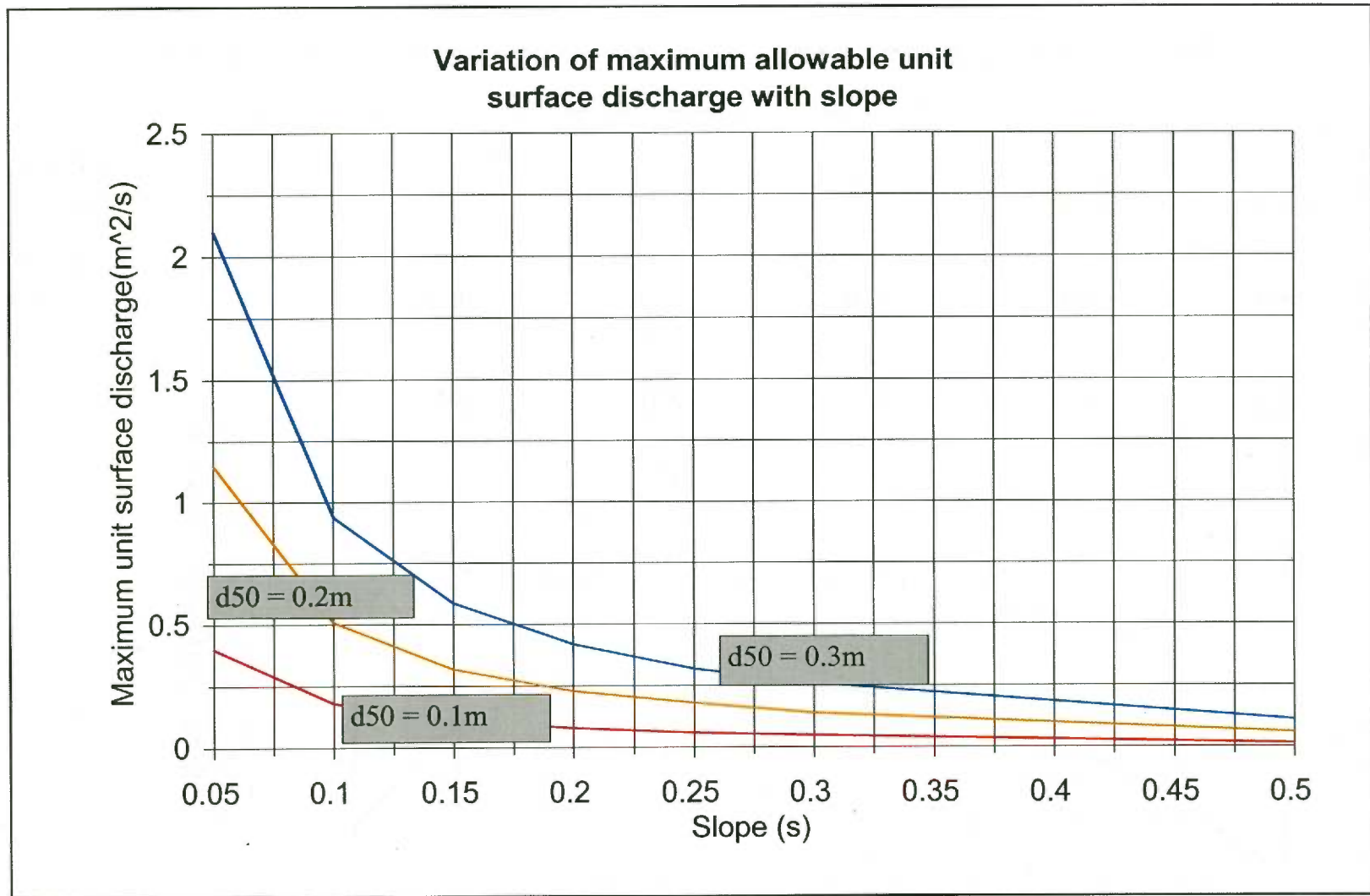


Figure 8.10: Relationship between maximum allowable surface discharge and the slope of the embankment for various D_{50} 's

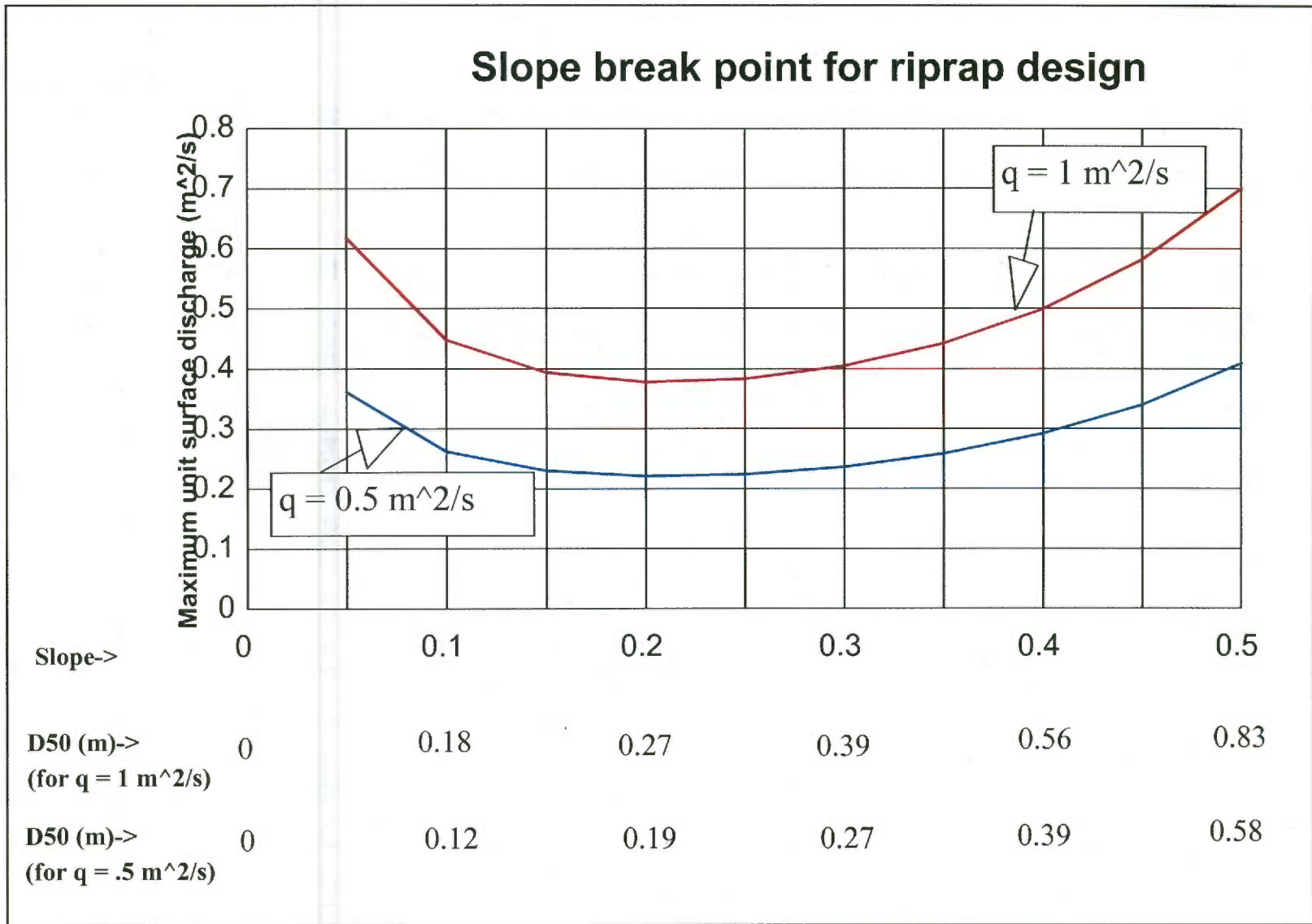


Figure 8.11: Combined effect of slope and rock size on maximum allowable surface discharge

CHAPTER 9

DESIGN PROCEDURE AND EXAMPLES

For protecting embankments from overtopping flows using riprap, the designer is usually provided with the volume of water to be overtopped, the slope of the embankment, and the length of the crest of the dam. The universal riprap design equation derived in Chapter 8 (Eq. (8.11)), can be used for sizing of the riprap required. The depth of the riprap layer can be obtained by using the interstitial velocity equation developed in Chapter 6 (Eq. (6.1)).

9.1 Design Procedure

Based on the equations developed in Chapters 6 and 8, the riprap design procedure can be summarized as follows:

STEP 1: Many designers like to know the depth of the overtopping discharge; from Q find the overtopping depth H using:

$$Q = CLH^{1.5}$$

STEP 2: Find the median rock diameter, D_{50} , from either the design equation (Eq. (8.11)) or the design curves (Figure 8.5 or 8.6) for given unit discharge and embankment slope.

$$D_{50}C_u^{0.25} = 0.55(q_f)^{0.52}S^{-0.75}\left(\frac{\sin\alpha}{(2.65\cos\alpha - 1)(\cos\alpha\tan\phi - \sin\alpha)}\right)^{1.11} \quad (8.11)$$

STEP 3: Find the interstitial velocity, V_i , from

$$V_i = 2.48(S)^{0.58}(C_u)^{-2.22}\sqrt{gD_{50}}$$

From V_i , find the average velocity, V_{ave} using

$$V_{ave} = V_i * n_p$$

STEP 4: Determine the average depth of water, y , at the point of incipient movement of the riprap,

$$y = q/v_{ave}$$

Check to see if the average depth, y , is less than, or equal to $2D_{50}$, in which case, the design is complete and the design depth of riprap is $2D_{50}$. If the depth is greater than $2D_{50}$ check if the given slope is less than or equal to 0.25. If the slope is less than or equal to 0.25, proceed with step 5. If the slope is greater than 0.25, go to step 10.

STEP 5: Find the depth of water that can flow over the surface of the riprap without causing critical shear stress,

$$0.97hS = 0.06(\gamma - \gamma_s)D_{50} \tan\phi$$

where: γ_s = specific gravity of rock (usually 2.65);
 γ = specific gravity of water; and
 h = depth of water over riprap.

STEP 6: Calculate Manning's roughness coefficient, n

$$n = 0.0414D_{50}^{1/6}$$

STEP 7: Calculate the unit discharge, q_1 , that can flow over the riprap layer,

$$q_1 = \frac{1}{n} h^{1.67} S^{1/2}$$

STEP 8: Calculate the unit discharge, q_2 , flowing through the riprap,

$$q_2 = q - q_1$$

STEP 9: Determine the new riprap thickness based on flow through the riprap

$$h_2 = \frac{q_2}{V_{ave}}$$

Check if, h_2 , is greater or smaller than $4D_{50}$. If h_2 is smaller than $4D_{50}$, the design procedure is complete and the riprap layer thickness is $4D_{50}$. Otherwise go to step 10.

STEP 10: Increase D_{50} by 10%. Proceed through steps 4 to 10 again. Repeat the procedure until convergence is reached.

The following design examples illustrate the use of the proposed method for sizing stable riprap on a typical embankment dam slope. Computations for the median stone size and minimum thickness of the protective layer are shown. A riprap embankment protection is designed for this imaginary dam using the following procedure. Flood and embankment properties that are known or assumed are listed in the following table.

9.2 Example 1

Property	Parameter	Value
Overtopping discharge	Q	56.63 m ³ /sec
Embankment length	L	304.8 m
Overtopping unit discharge	q	0.186 m ³ /s/m
Angle of repose of material	ϕ	42 degrees
Embankment crest width	W	6.1 m
Crest Discharge coefficient	C	1.57
Embankment slope	S	20% or 0.20
Embankment angle	α	11.31 degrees
Coefficient of uniformity	C_u	2.1
Porosity	η_p	0.45

9.3 Step by Step Solution

STEP 1: Many designers like to know the depth of the overtopping discharge; from Q find the overtopping depth using:

$$Q = CLH^{1.5}$$

$$H = (Q/CL)^{2/3} = \left(\frac{56.63}{1.57 \times 304.8} \right)^{0.67} = 0.24 \text{ m}$$

STEP 2: Find the median rock diameter, D_{50} , from either Eq. (8.11), the design equation or the design curves (Figure 8.5 or 8.6) for $q = 0.186 \text{ m}^3/\text{s/m}$ and an embankment slope of 0.2,

$$D_{50}^{0.25} = 0.55(q)^{0.52} S^{-0.75} \left(\frac{\sin \alpha}{(2.65 \cos \alpha - 1)(\cos \alpha \tan \phi - \sin \alpha)} \right) \quad (8.11)$$

$$D_{50} C_u^{0.25} = 0.12$$

$$D_{50} = 0.1 \text{ m}$$

STEP 3: Find the interstitial velocity, V_i , from Eq. (6.1),

$$\frac{V_i}{\sqrt{(gD_{50})}} = 2.48C_u^{-2.22}S^{0.58} \quad (6.1)$$

$$V_i = 2.48(0.2)^{0.58}(2.1)^{-2.22}\sqrt{9.81(0.1)} = 0.186 \text{ m/sec}$$

From V_i , find the average velocity, V_{ave} using

$$V_{ave} = V_i * n_p = 0.186 * 0.45 = 0.084 \text{ m/sec}$$

STEP 4: Determine the average depth of water, y , at the point of incipient movement of the riprap,

$$y = q/v_{ave} = 2.21 \text{ m}$$

Check to see if the average depth, y , is less than, or equal to $2D_{50}$, in which case, the design is complete and the design depth of riprap is $2D_{50}$. If the slope is less than or equal to 0.25, proceed with step 5. If the slope is greater than 0.25, go to step 10.

$$y = 2.21 \text{ m} > 0.2 \text{ m} = 2D_{50}$$

Slope = 0.20, so proceed to step 5

STEP 5: Find the depth of water that can flow over the surface of the riprap without causing critical shear stress,

$$0.97hS = 0.06(\gamma - \gamma_s)D_{50}\tan(42)$$

Using the appropriate values of the parameters, and solving for h ,

$$h = 0.046 \text{ m}$$

STEP 6: Calculate Manning's roughness coefficient, n

$$n = 0.0414D_{50}^{1/6} \quad n = 0.0414(0.1)^{1/6} = 0.028$$

STEP 7: Calculate the unit discharge, q_1 , that can flow over the riprap layer,

$$q_1 = \frac{1}{n}h^{1.67}S^{1/2} = 0.093 \text{ m}^2/\text{s}$$

STEP 8: Calculate the unit discharge, q_2 , flowing through the riprap,

$$q_2 = q - q_1 = 0.093 \text{ m}^2/\text{s}$$

STEP 9: Determine the new riprap thickness based on flow through riprap

$$h_2 = \frac{q_2}{V_{ave}} = 1.1 \text{ m} \geq 4D_{50} = 0.4 \text{ m}$$

Since h_2 is greater than $4D_{50}$, go to step 10.

STEP 10: Increase D_{50} by 10%. The new D_{50} is now 0.11 m. Proceed through steps 4 to 10 again. The value of h_2 obtained is 0.86 m. Increase D_{50} by 10% again. Repeating the same procedure the value of h_2 can be found as 0.7 m. Going through this iterative procedure one more time with D_{50} of 0.13 m, h_2 can be found as 0.52 m, which satisfies the criterion established in step 9. Therefore, the design median rock size diameter for this given case is 0.13 m and the riprap thickness is 0.52 m.

9.4 Example 2

Property	Parameter	Value
Overtopping discharge	Q	56.63 m ³ /sec
Embankment length	L	304.8 m
Overtopping unit discharge	q	0.186 m ³ /s/m
Angle of repose of material	ϕ	42 degrees
Embankment crest width	W	6.1 m
Crest Discharge coefficient	C	1.57
Embankment slope	S	50% or 0.50
Embankment angle	α	26.6 degrees
Coefficient of uniformity	C_u	2.1
Porosity	η_p	0.45

9.5 Step by Step Solution

STEP 1: Many designers like to know the depth of the overtopping discharge; from Q find the overtopping depth using:

$$Q = CLH^{1.5}$$

$$H = (Q/CL)^{2/3} = \left(\frac{56.63}{1.57 \times 304.8} \right)^{0.67} = 0.24 \text{ m}$$

STEP 2: Find the median rock diameter, D_{50} , from either Eq. (8.11), the design equation or the design curves (Figure 8.5 or 8.6) for $q = 0.186 \text{ m}^3/\text{s/m}$ and an embankment slope of 0.5,

$$D_{50} C_u^{0.25} = 0.55(q)^{0.52} S^{-0.75} \left(\frac{\sin \alpha}{(2.65 \cos \alpha - 1)(\cos \alpha \tan \phi - \sin \alpha)} \right)^{1.11} \quad (8.11)$$

$$D_{50} C_u^{0.25} = 0.36 \quad D_{50} = 0.3 \text{ m}$$

STEP 3: Find the interstitial velocity, V_i , from Eq. (6.1),

$$\frac{V_i}{\sqrt{(gD_{50})}} = 2.48 C_u^{-2.22} S^{0.58} \quad (6.1)$$

$$V_i = 2.48(0.5)^{0.58} (2.1)^{-2.22} \sqrt{9.81(0.3)} = 0.548 \text{ m/sec}$$

From V_i , find the average velocity, V_{ave} using

$$V_{ave} = V_i * n_p = 0.548 * 0.45 = 0.247 \text{ m/sec}$$

STEP 4: Determine the average depth of water, y , at the point of incipient movement of the riprap,

$$y = q/v_{ave} = 0.75 \text{ m}$$

Check to see if the average depth, y , is less than, or equal to $2D_{50}$, in which case, the design is complete and the design depth of riprap is $2D_{50}$. Otherwise check if the given slope is less than or equal to 0.25. If the slope is less than or equal to 0.25, proceed with step 5. If the slope is greater than 0.25, go to step 10.

$$y = 0.75 \text{ m} > 0.6 \text{ m} = 2D_{50}$$

Slope = 0.5, so proceed to step 10

STEP 10: Increase D_{50} by 10%. The new D_{50} is now 0.33 m. Proceed through steps 3 to 10 again. Going through the steps the depth was obtained as 0.72 m, which is greater than $2D_{50}$. Increasing D_{50} by 10% again, the new D_{50} is 0.36 m.

CHAPTER 10

SUMMARY, CONCLUSIONS, AND FUTURE RESEARCH

10.1 Summary

This investigation began by compiling information, historical background, and available data collected on previous riprap studies. The need for large-scale tests was established because of the widely varying results predicted by different existing methods.

Riprap tests were conducted in the summers of 1994, 1995, and 1997 on the near-prototype size embankment overtopping research facility at CSU's Engineering Research Center. The chute of the facility is 3.05-m wide and has a vertical drop of 15.24 m on a 2:1(H:V) slope. The first test (1994) consisted of a 203-mm thick gravel bedding material with a 0.61 m overlay of large riprap with a D_{50} of 386 mm. The second test (1995) utilized the first test bed with a second layer approximately 0.61-m thick with riprap having a D_{50} of 655 mm. The third test (1997), a 203-mm thick gravel bedding material with a D_{50} of 48 mm was overlaid with a riprap layer of thickness 533 mm with a D_{50} of 271 mm. A berm was built at the bottom of the flume to simulate toe treatment.

Each test series started with a very small discharge and continued by increasing the discharge until the riprap failed. Failure was defined as removal of the riprap by erosion and movement of the rock until the bedding material was exposed. Data were collected on numerous discharges flowing down the chute through the riprap. The head box depth for overtopping heads, manometer readings for depth of flow down the chute, and electronic recording of electrical conductivity versus time to determine interstitial velocities are some examples of the data collected. Each test series was concluded with the failure of the riprap. For each test series, the failure discharge was noted.

In this dissertation, a new criteria was established between the design of the riprap layer and the interstitial velocity of water flowing through the riprap layer. An equation was developed to predict the interstitial velocity of water through the rock layer, based on the median rock size diameter as well as the coefficient of uniformity of the rock layer. For 1994, 1995, and 1997 tests the failure discharges were found to be 0.223 m³/s/m, 0.929 m³/s/m, and 0.204 m³/s/m, respectively. Based on the original Shield's parameter and deviation factor containing the effects of the gradation of the rock layer, slope of the embankment, and the unit discharge a universal formula for designing the riprap was derived. This equation was tested for the data obtained in this study and previous research studies. The universal riprap design equation was found to satisfactorily predict the size of the riprap to be used for a specified unit discharge and a given embankment slope.

Design curves were derived for sizing riprap for a given condition. The thickness of the riprap layer can be determined with the help of the equation derived to predict the interstitial velocity through the riprap layer. A step by step design procedure was presented.

This iterative design procedure establishes the median size riprap diameter and the thickness of the riprap layer.

10.2 Conclusions

This investigation poses two hypotheses. The first hypothesis deals with the Shield's parameter. The Shield's parameter is a dimensionless form of shear stress that expresses the incipient motion of riprap in flowing water. In this analysis of incipient motion of riprap, it was found that the many assumptions made to simplify the Shield's parameter, render it a poor tool to design riprap in its simplified form. For example, the simplified form of the Shield's parameter cannot be used to design riprap in overtopping flows because this form of Shield's parameter assumes the slope to be small, generally less than 10%. The complete equation for the Shield's parameter includes the embankment slope and the angle of repose of the riprap material. It is given by:

$$\tau_* = \frac{\tau_{cr}}{\gamma(S_s \cos \alpha - 1)D_{50}(\cos \alpha \tan \phi - \sin \alpha)} = 0.047 \quad (8.1)$$

The factor $(\cos \alpha \tan \phi - \sin \alpha)$ indicates the behavior of the Shield's parameter on various slopes, α , and various angles of repose, ϕ . Based on the complete form of the Shield's parameter and taking into consideration the effects caused by the gradation of the rock size, and possible effect of air entrainment, the universal riprap design equation can be expressed as:

$$D_{50}C_u^{0.25} = 0.55q_f^{0.52}S^{-0.75} \left(\frac{\sin \alpha}{(2.65 \cos \alpha - 1)(\cos \alpha \tan \phi - \sin \alpha)} \right)^{1.11} \quad (8.11)$$

The predicted rock sizes based on this formula were found to be extremely close to the experimental results obtained during the current study as well as the past investigations. However, the existing riprap design equations fail to predict the results obtained experimentally for large rocks and steep slopes.

The second hypothesis concerns the prediction of the interstitial velocity of water through the riprap layer and using this interstitial velocity to design the thickness of the riprap layer in an iterative manner. The interstitial velocity equation derived in this investigation, takes into consideration the gradation of the riprap along with the median rock size diameter of the riprap and the slope of the embankment. This equation is:

$$\frac{V_i}{\sqrt{(gD_{50})}} = 2.48C_u^{-2.22}S^{0.58} \quad (6.1)$$

This research resulted in a method, by which not only the size of the riprap, but also the thickness of the riprap layer, can be predicted in a rational method.

It was demonstrated that the breakpoint at which the riprap does not need to be designed to carry surface discharge is 25%. The riprap should be designed to carry surface discharge if the slope of the embankment is less than 25%.

10.3 Scope of Future Research

This dissertation depends upon the first hypothesis, that Shield's parameter is constant and has a value of 0.047. Olivier (1967) used a similar approach, but without the assumption that the local velocity is proportional to the shear velocity. He used approximations for the lift, drag, and other hydrodynamic forces. Measuring these forces directly would provide an opportunity to check the assumptions that Olivier made.

Direct measurements of air concentration should be made with advanced air concentration probes to finalize the effects of possible air entrainment by water.

Experiments at prototype scale on an intermediate slope (between thirty and forty percent) with a riprap layer of D_{50} between 400 mm and 500 mm will be a great reinforcement to the theory proposed. Also the piezometric depth of water could be measured in a very thick riprap layer (simulating a riprap layer of infinite thickness) to further validate the theory that interstitial velocity of water remains constant with the change of unit discharge.

REFERENCES

- Abt, S.R., Khattak, M.S., Nelson, J.D., Ruff, J.F., Shaikh, A., Wittler, R.J., Lee, D.W., and Hinkle, N.E. (1987). Development of riprap design criteria by riprap testing in flumes: Phase I. NUREG/CR-4651, U.S. Nuclear Regulatory Commission, Vol. 1, 48-53.
- Abt, S.R., Wittler, R.J., Ruff, J.F., LaGrone, D.L., Khattak, M.S., Nelson, J.D., Hinkle, N.E., and Lee, D.W. (1988). Development of riprap design criteria by riprap testing in flumes: Phase II. NUREG/CR-4651, U.S. Nuclear Regulatory Commission, Vol. 2, 57-65.
- Abt, S.R., Ruff, J.F., and Wittler, R.J. (1991). Estimating flow through riprap. *ASCE Journal of Hydraulics*, Vol. 5, 670-675.
- Abt, S.R., and Johnson, T. (1991). Riprap design for overtopping flow. *ASCE Journal of Hydraulics*, Vol. 117, 959-972.
- Carling, P.A., Kelsey, A., and Glaister, M.A. (1992). Dynamics of Gravel-bed rivers, Edited by P. Bill, R.D. Hey, C.R. Thorne, and P. Tacconi, John Wiley and Sons, New York, NY, pp 23-39.
- Chen, Y.H. and Anderson, B.A. (1986). Development of a methodology for estimating embankment damage due to flood overtopping. Report No. FHWA-RD-86-126, Federal Highway Administration, Washington DC.
- Escande, L. (1953). Experiments concerning the infiltration of water through a rock mass. Proc., Minnesota Int. Hydrology Convention.
- Frizell, K.H., Mefford, B., Dodge, R.A., and Vermeyen, T.B. (1992). Protecting embankment dams subject to overtopping during major flood events.
- Gessler, J. (1965). The beginning of bedload movement of mixtures investigated as natural armoring in channels. W.M. Keck Laboratory of Hydraulics and Water Resources, California Institute of Technology, Pasadena, CA.
- Hey, R.D. (1979). Flow resistance in gravel-bed rivers. *Proc. ASCE Journal of Hydraulic Division*, Vol. 105 (4), 365-379
- Julien, P.Y. (1995). Erosion and Sedimentation. Cambridge University Press, pp. 128-129.
- Leps, T.M. (1973). Flow Through Rockfill. Embankment dam engineering, John Wiley and Sons, pp. 87-107.
- Olivier, H. (1967). Through and overflow rockfill dams- New design techniques. *J. Inst. of Civ. Engrg.*, 36, 433-471.
- Oswalt, N.R., Buck, L.E., Hepler, T.E., and Jackson, H.E. (1994). Alternatives for overtopping protection of dams. American Society of Civil Engineers, Pp 136.
- Parkin, A.K., Trollope, D.H., and Lawson, J.D. (1966). Rockfill structures subject to water flow. *J. Soil Mech. Found. Div.*, ASCE, (6), 135-151.
- Powledge, G.R., Ralston, D., Miller, P.S., Chen, Y.H., Clopper, P.E., and Temple, D.M. (1989). Mechanics of overflow erosion of embankments II: Hydraulics and design considerations. *Journal of Hydraulic Engineering*, Vol. 115, 1056-1075.

- Robinson, K.M., Rice, C.E., and Kadavy, K.C. (1995). Stability of rock chutes. Proc. Water Resources Engineering, ASCE, San Antonio, TX, Vol. 2, 1476-1480.
- Ruff, J.F., and Gelhar, L.W. (1970). Porous boundary effects in turbulent shear flow. Report No. 126, Prepared under National Science Foundation, Water Resources and hydrodynamics laboratory, Department of Civil Engineering, MIT, Cambridge, MA.
- Shields, A. (1936). Anwendung der Aehnlichkeitsmechanik und der Turbulenzforschung auf die Geschiebebewegung: Mitteilung der Preussischen Versuchsanstalt fuer Wasserbau. und Schiffbau, Heft 26, Berlin.
- Stephenson, D. (1979). Rockfill in hydraulic engineering: Developments in geotechnical engineering. Elsevier Scientific Publishing Company, Amsterdam, the Netherlands, 38-60.
- Stevens, M.A., Simons, D.B., and Lewis, G.L. (1976). Safety factors for riprap protection. *Proc. ASCE Journal of Hydraulic Division*, Vol. 102(5), 637-655.
- Thompson, S.M., and Cambell, P.L. (1979). Hydraulics of a large channel paved with boulders. *Journal of Hydraulic Research*, No. 17, 341-354.
- United States Bureau of Reclamation (1987). Design Standards Embankment Dams, No. 13.
- Wilkins, J.K. (1956). Flow of water through rockfill and its application to the design of dams. Proc., Second Australian-New Zealand Soil Conf., Mechanics and Foundation Engrg., Christchurch, New Zealand.
- Wilkins, J.K. (1963). The stability of overtopped rockfill dams. Proc. Fourth Australian Conference on soil mechanics and foundation Engrg., Adelaid, Australia, 1-7.
- Whittaker, J. and Jaggi, M. (1986). Block ramps. Reports by the Research Institute for Water Engineering, Hydrology and Glaciology, No. 91, Zurich, Translated by Inge Hollingworth, USBR Division of Foreign Activities, 169 p.
- Wittler, R.J. (1994). Mechanics of riprap in overtopping flow. Dissertation, Civil Engineering, Colorado State University, Fort Collins, CO, 89 p.

APPENDIX A

INTERSTITIAL VELOCITY DATA

INTERSTITIAL VELOCITY DATA: 1994

Bottom probes at station 1

Discharge (cfs)	Unit discharge (ft ² /s)	Unit discharge (m ² /s)	delta t (sec)	delta s (ft)	delta s (m)	V ₁₂ (ft/s)	V ₁₂ (m/s)
5.00	0.50	0.05	2.18	3.00	0.91	1.38	0.42
6.00	0.60	0.06	1.80	3.00	0.91	1.67	0.51
7.00	0.70	0.07	1.91	3.00	0.91	1.57	0.48
8.00	0.80	0.07	1.99	3.00	0.91	1.51	0.46
9.00	0.90	0.08	1.85	3.00	0.91	1.62	0.49
10.00	1.00	0.09	1.80	3.00	0.91	1.67	0.51
11.00	1.10	0.10	2.30	3.00	0.91	1.31	0.40
14.00	1.40	0.13	1.99	3.00	0.91	1.51	0.46
15.00	1.50	0.14	2.09	3.00	0.91	1.43	0.44
17.00	1.70	0.16	1.02	3.00	0.91	2.95	0.90
19.00	1.90	0.18	1.40	3.00	0.91	2.14	0.65
20.00	2.00	0.19	1.78	3.00	0.91	1.69	0.51
22.00	2.20	0.20	1.80	3.00	0.91	1.67	0.51

Middle probes at station 1

Discharge (cfs)	Unit discharge (ft ² /s)	Unit discharge (m ² /s)	delta t (sec)	delta s (ft)	delta s (m)	V ₁₂ (ft/s)	V ₁₂ (m/s)
5.00	0.50	0.05	2.22	3.00	0.91	1.35	0.41
6.00	0.60	0.06	1.05	3.00	0.91	2.85	0.87
7.00	0.70	0.07	1.16	3.00	0.91	2.59	0.79
8.00	0.80	0.07	1.37	3.00	0.91	2.19	0.67
9.00	0.90	0.08	1.40	3.00	0.91	2.14	0.65
10.00	1.00	0.09	1.69	3.00	0.91	1.77	0.54
11.00	1.10	0.10	1.49	3.00	0.91	2.01	0.61
14.00	1.40	0.13	1.80	3.00	0.91	1.67	0.51
15.00	1.50	0.14	1.98	3.00	0.91	1.52	0.46
17.00	1.70	0.16	1.60	3.00	0.91	1.88	0.57
19.00	1.90	0.18	-	3.00	0.91	-	-
20.00	2.00	0.19	1.80	3.00	0.91	1.67	0.51
22.00	2.20	0.20	1.98	3.00	0.91	1.52	0.46

Bottom probes at station 2

Discharge (cfs)	Unit discharge (ft ² /s)	Unit discharge (m ² /s)	delta t (sec)	delta s (ft)	delta s (m)	V ₁₂ (ft/s)	V ₁₂ (m/s)
5.00	0.50	0.05	1.39	3.00	0.91	2.17	0.66
6.00	0.60	0.06	1.43	3.00	0.91	2.10	0.64
7.00	0.70	0.07	1.33	3.00	0.91	2.26	0.69
8.00	0.80	0.07	1.53	3.00	0.91	1.96	0.60
9.00	0.90	0.08	-	3.00	0.91	-	-
10.00	1.00	0.09	1.78	3.00	0.91	1.69	0.51
11.00	1.10	0.10	1.38	3.00	0.91	2.18	0.66
14.00	1.40	0.13	1.85	3.00	0.91	1.62	0.49
15.00	1.50	0.14	1.29	3.00	0.91	2.32	0.71
17.00	1.70	0.16	1.20	3.00	0.91	2.51	0.77
19.00	1.90	0.18	1.65	3.00	0.91	1.82	0.56
20.00	2.00	0.19	1.78	3.00	0.91	1.69	0.51
22.00	2.20	0.20	1.59	3.00	0.91	1.89	0.58

Middle probes at station 2

Discharge (cfs)	Unit discharge (ft ² /s)	Unit discharge (m ² /s)	delta t (sec)	delta s (ft)	delta s (m)	V ₁₂ (ft/s)	V ₁₂ (m/s)
5.00	0.50	0.05	-	3.00	0.91	-	-
6.00	0.60	0.06	-	3.00	0.91	-	-
7.00	0.70	0.07	-	3.00	0.91	-	-
8.00	0.80	0.07	-	3.00	0.91	-	-
9.00	0.90	0.08	1.49	3.00	0.91	2.01	0.61
10.00	1.00	0.09	1.89	3.00	0.91	1.58	0.48
11.00	1.10	0.10	1.38	3.00	0.91	2.18	0.66
14.00	1.40	0.13	2.05	3.00	0.91	1.46	0.45
15.00	1.50	0.14	1.40	3.00	0.91	2.14	0.65
17.00	1.70	0.16	-	3.00	0.91	-	-
19.00	1.90	0.18	1.17	3.00	0.91	2.57	0.78
20.00	2.00	0.19	1.60	3.00	0.91	1.88	0.57
22.00	2.20	0.20	1.44	3.00	0.91	2.08	0.64

Bottom probes at station 3

Discharge (cfs)	Unit discharge (ft ² /s)	Unit discharge (m ² /s)	delta t (sec)	delta s (ft)	delta s (m)	V ₁₂ (ft/s)	V ₁₂ (m/s)
5.00	0.50	0.05	1.20	3.00	0.91	2.50	0.76
6.00	0.60	0.06	1.49	3.00	0.91	2.01	0.61
7.00	0.70	0.07	-	3.00	0.91	-	-
8.00	0.80	0.07	1.18	3.00	0.91	2.55	0.78
9.00	0.90	0.08	1.20	3.00	0.91	2.50	0.76
10.00	1.00	0.09	1.22	3.00	0.91	2.46	0.75
11.00	1.10	0.10	-	3.00	0.91	-	-
14.00	1.40	0.13	1.20	3.00	0.91	2.50	0.76
15.00	1.50	0.14	1.57	3.00	0.91	1.91	0.58
17.00	1.70	0.16	1.50	3.00	0.91	2.00	0.61
19.00	1.90	0.18	1.88	3.00	0.91	1.60	0.49
20.00	2.00	0.19	1.29	3.00	0.91	2.32	0.71
22.00	2.20	0.20	1.50	3.00	0.91	2.00	0.61

Middle probes at station 3

Discharge (cfs)	Unit discharge (ft ² /s)	Unit discharge (m ² /s)	delta t (sec)	delta s (ft)	delta s (m)	V ₁₂ (ft/s)	V ₁₂ (m/s)
5.00	0.50	0.05	-	3.00	0.91	-	-
6.00	0.60	0.06	1.60	3.00	0.91	1.88	0.57
7.00	0.70	0.07	1.20	3.00	0.91	2.50	0.76
8.00	0.80	0.07	1.53	3.00	0.91	1.96	0.60
9.00	0.90	0.08	1.29	3.00	0.91	2.32	0.71
10.00	1.00	0.09	-	3.00	0.91	-	-
11.00	1.10	0.10	-	3.00	0.91	-	-
14.00	1.40	0.13	-	3.00	0.91	-	-
15.00	1.50	0.14	1.37	3.00	0.91	2.19	0.67
17.00	1.70	0.16	1.50	3.00	0.91	2.00	0.61
19.00	1.90	0.18	1.91	3.00	0.91	1.57	0.48
20.00	2.00	0.19	1.99	3.00	0.91	1.51	0.46
22.00	2.20	0.20	-	3.00	0.91	-	-

INTERSTITIAL VELOCITY DATA: 1995

Bottom probes at station 1

Discharge (cfs)	Unit discharge (ft ² /s)	Unit discharge (m ² /s)	delta t (sec)	delta s (ft)	delta s (m)	V ₁₂ (ft/s)	V ₁₂ (m/s)
20.00	2.00	0.19	1.30	3.00	0.91	2.30	0.70
20.00	2.00	0.19	1.43	3.00	0.91	2.10	0.64
25.00	2.50	0.23	-	3.00	0.91	-	-
30.00	3.00	0.28	1.50	3.00	0.91	2.00	0.61
35.00	3.50	0.33	1.75	3.00	0.91	1.71	0.52
35.00	3.50	0.33	2.04	3.00	0.91	1.47	0.45
35.00	3.50	0.33	1.40	3.00	0.91	2.15	0.66
35.00	3.50	0.33	1.28	3.00	0.91	2.35	0.72
40.00	4.00	0.37	1.54	3.00	0.91	1.95	0.59
40.00	4.00	0.37	1.20	3.00	0.91	2.50	0.76
40.00	4.00	0.37	1.48	3.00	0.91	2.03	0.62
40.00	4.00	0.37	1.11	3.00	0.91	2.70	0.82
45.00	4.50	0.42	1.58	3.00	0.91	1.90	0.58
45.00	4.50	0.42	1.43	3.00	0.91	2.10	0.64
45.00	4.50	0.42	1.20	3.00	0.91	2.50	0.76
50.00	5.00	0.46	1.66	3.00	0.91	1.81	0.55
50.00	5.00	0.46	1.07	3.00	0.91	2.81	0.86
50.00	5.00	0.46	1.28	3.00	0.91	2.35	0.72
50.00	5.00	0.46	1.33	3.00	0.91	2.25	0.69
50.00	5.00	0.46	1.39	3.00	0.91	2.16	0.66
55.00	5.50	0.51	1.41	3.00	0.91	2.13	0.65
55.00	5.50	0.51	1.07	3.00	0.91	2.81	0.86
60.00	6.00	0.56	0.91	3.00	0.91	3.30	1.01
60.00	6.00	0.56	1.71	3.00	0.91	1.75	0.53
60.00	6.00	0.56	1.09	3.00	0.91	2.75	0.84
60.00	6.00	0.56	1.07	3.00	0.91	2.80	0.85
65.00	6.50	0.60	1.26	3.00	0.91	2.38	0.73
65.00	6.50	0.60	1.58	3.00	0.91	1.90	0.58
70.00	7.00	0.65	2.40	3.00	0.91	1.25	0.38
70.00	7.00	0.65	1.55	3.00	0.91	1.93	0.59
70.00	7.00	0.65	1.30	3.00	0.91	2.30	0.70
75.00	7.50	0.70	1.33	3.00	0.91	2.25	0.69
75.00	7.50	0.70	0.89	3.00	0.91	3.38	1.03
80.00	8.00	0.74	2.19	3.00	0.91	1.37	0.42

Middle probes at station 1

Discharge (cfs)	Unit discharge (ft ² /s)	Unit discharge (m ² /s)	delta t (sec)	delta s (ft)	delta s (m)	V ₁₂ (ft/s)	V ₁₂ (m/s)
20.00	2.00	0.19	0.88	3.00	0.91	3.41	1.04
25.00	2.50	0.23	-	3.00	0.91	-	-
30.00	3.00	0.28	1.12	3.00	0.91	2.68	0.82
30.00	3.00	0.28	0.82	3.00	0.91	3.65	1.11
30.00	3.00	0.28	0.82	3.00	0.91	3.65	1.11
35.00	3.50	0.33	0.84	3.00	0.91	3.58	1.09
35.00	3.50	0.33	0.93	3.00	0.91	3.21	0.98
35.00	3.50	0.33	0.89	3.00	0.91	3.38	1.03
35.00	3.50	0.33	1.18	3.00	0.91	2.54	0.77
40.00	4.00	0.37	1.07	3.00	0.91	2.80	0.85
40.00	4.00	0.37	0.94	3.00	0.91	3.20	0.98
40.00	4.00	0.37	1.11	3.00	0.91	2.70	0.82
45.00	4.50	0.42	1.07	3.00	0.91	2.80	0.85
45.00	4.50	0.42	1.30	3.00	0.91	2.30	0.70
45.00	4.50	0.42	1.43	3.00	0.91	2.10	0.64

50.00	5.00	0.46	0.79	3.00	0.91	3.81	1.16
55.00	5.50	0.51	0.97	3.00	0.91	3.08	0.94
55.00	5.50	0.51	1.29	3.00	0.91	2.32	0.71
55.00	5.50	0.51	1.20	3.00	0.91	2.51	0.77
55.00	5.50	0.51	1.09	3.00	0.91	2.75	0.84
60.00	6.00	0.56	1.00	3.00	0.91	3.00	0.91
60.00	6.00	0.56	0.94	3.00	0.91	3.20	0.98
60.00	6.00	0.56	1.09	3.00	0.91	2.75	0.84
60.00	6.00	0.56	1.15	3.00	0.91	2.61	0.80
60.00	6.00	0.56	1.21	3.00	0.91	2.48	0.76
65.00	6.50	0.60	0.86	3.00	0.91	3.50	1.07
70.00	7.00	0.65	1.85	3.00	0.91	1.62	0.49
70.00	7.00	0.65	0.89	3.00	0.91	3.38	1.03
75.00	7.50	0.70	-	3.00	0.91	-	-
80.00	8.00	0.74	1.20	3.00	0.91	2.51	0.77

Top probes at station 1

Discharge (cfs)	Unit discharge (ft ² /s)	Unit discharge (m ² /s)	delta t (sec)	delta s (ft)	delta s (m)	V ₁₂ (ft/s)	V ₁₂ (m/s)
20.00	2.00	0.19	-	3.00	0.91	-	-
25.00	2.50	0.23	-	3.00	0.91	-	-
30.00	3.00	0.28	0.55	3.00	0.91	5.48	1.67
35.00	3.50	0.33	0.60	3.00	0.91	5.00	1.52
35.00	3.50	0.33	0.65	3.00	0.91	4.63	1.41
35.00	3.50	0.33	0.40	3.00	0.91	7.51	2.29
40.00	4.00	0.37	0.68	3.00	0.91	4.38	1.34
40.00	4.00	0.37	0.60	3.00	0.91	5.00	1.52
45.00	4.50	0.42	0.70	3.00	0.91	4.30	1.31
50.00	5.00	0.46	0.41	3.00	0.91	7.26	2.21
50.00	5.00	0.46	0.50	3.00	0.91	6.00	1.83
50.00	5.00	0.46	0.57	3.00	0.91	5.27	1.61
55.00	5.50	0.51	0.40	3.00	0.91	7.51	2.29
55.00	5.50	0.51	0.45	3.00	0.91	6.72	2.05
55.00	5.50	0.51	0.55	3.00	0.91	5.44	1.66
60.00	6.00	0.56	0.55	3.00	0.91	5.49	1.67
65.00	6.50	0.60	0.70	3.00	0.91	4.30	1.31
65.00	6.50	0.60	0.63	3.00	0.91	4.75	1.45
65.00	6.50	0.60	0.65	3.00	0.91	4.60	1.40
70.00	7.00	0.65	0.47	3.00	0.91	6.38	1.94
70.00	7.00	0.65	0.55	3.00	0.91	5.45	1.66
75.00	7.50	0.70	0.60	3.00	0.91	5.00	1.52
75.00	7.50	0.70	0.45	3.00	0.91	6.70	2.04
75.00	7.50	0.70	0.50	3.00	0.91	6.05	1.84
80.00	8.00	0.74	0.40	3.00	0.91	7.50	2.29
80.00	8.00	0.74	0.50	3.00	0.91	6.00	1.83
80.00	8.00	0.74	0.56	3.00	0.91	5.39	1.64

Bottom probes at station 2

Discharge (cfs)	Unit discharge (ft ² /s)	Unit discharge (m ² /s)	delta t (sec)	delta s (ft)	delta s (m)	V ₁₂ (ft/s)	V ₁₂ (m/s)
20.00	2.00	0.19	1.00	3.00	0.91	3.00	0.91
20.00	2.00	0.19	1.16	3.00	0.91	2.58	0.79
25.00	2.50	0.23	1.24	3.00	0.91	2.42	0.74
25.00	2.50	0.23	1.11	3.00	0.91	2.70	0.82
30.00	3.00	0.28	1.20	3.00	0.91	2.50	0.76
30.00	3.00	0.28	1.55	3.00	0.91	1.93	0.59
35.00	3.50	0.33	1.34	3.00	0.91	2.24	0.68
35.00	3.50	0.33	1.15	3.00	0.91	2.61	0.80
40.00	4.00	0.37	1.18	3.00	0.91	2.55	0.78

40.00	4.00	0.37	1.07	3.00	0.91	2.81	0.86
40.00	4.00	0.37	0.88	3.00	0.91	3.41	1.04
45.00	4.50	0.42	1.42	3.00	0.91	2.12	0.65
45.00	4.50	0.42	1.62	3.00	0.91	1.85	0.56
45.00	4.50	0.42	1.58	3.00	0.91	1.90	0.58
45.00	4.50	0.42	1.25	3.00	0.91	2.40	0.73
45.00	4.50	0.42	1.06	3.00	0.91	2.82	0.86
50.00	5.00	0.46	2.50	3.00	0.91	1.20	0.37
50.00	5.00	0.46	1.11	3.00	0.91	2.71	0.83
55.00	5.50	0.51	1.43	3.00	0.91	2.10	0.64
55.00	5.50	0.51	1.34	3.00	0.91	2.24	0.68
55.00	5.50	0.51	1.72	3.00	0.91	2.49	0.76
60.00	6.00	0.56	1.57	3.00	0.91	1.74	0.53
60.00	6.00	0.56	1.43	3.00	0.91	1.91	0.58
60.00	6.00	0.56	1.27	3.00	0.91	2.10	0.64
60.00	6.00	0.56	1.20	3.00	0.91	2.36	0.72
60.00	6.00	0.56	1.69	3.00	0.91	2.50	0.76
65.00	6.50	0.60	1.69	3.00	0.91	1.78	0.54
70.00	7.00	0.65	1.42	3.00	0.91	2.12	0.65
70.00	7.00	0.65	1.54	3.00	0.91	1.95	0.59
70.00	7.00	0.65	0.91	3.00	0.91	3.29	1.00
75.00	7.50	0.70	1.16	3.00	0.91	2.59	0.79
80.00	8.00	0.74	1.71	3.00	0.91	1.75	0.53
80.00	8.00	0.74	1.42	3.00	0.91	2.12	0.65
80.00	8.00	0.74	1.07	3.00	0.91	2.81	0.86

Middle probes at station 2

Discharge (cfs)	Unit discharge (ft ² /s)	Unit discharge (m ² /s)	delta t (sec)	delta s (ft)	delta s (m)	V ₁₂ (ft/s)	V ₁₂ (m/s)
20.00	2.00	0.19	1.20	3.00	0.91	2.50	0.76
20.00	2.00	0.19	1.24	3.00	0.91	2.41	0.73
20.00	2.00	0.19	1.09	3.00	0.91	2.75	0.84
25.00	2.50	0.23	1.24	3.00	0.91	2.42	0.74
25.00	2.50	0.23	1.11	3.00	0.91	2.70	0.82
30.00	3.00	0.28	-	3.00	0.91	-	-
35.00	3.50	0.33	0.94	3.00	0.91	3.20	0.98
35.00	3.50	0.33	1.22	3.00	0.91	2.45	0.75
40.00	4.00	0.37	1.15	3.00	0.91	2.60	0.79
45.00	4.50	0.42	1.09	3.00	0.91	2.75	0.84
50.00	5.00	0.46	1.19	3.00	0.91	2.52	0.77
50.00	5.00	0.46	0.88	3.00	0.91	3.39	1.03
55.00	5.50	0.51	0.84	3.00	0.91	3.56	1.09
55.00	5.50	0.51	0.99	3.00	0.91	3.04	0.93
60.00	6.00	0.56	0.89	3.00	0.91	3.38	1.03
60.00	6.00	0.56	0.93	3.00	0.91	3.21	0.98
60.00	6.00	0.56	0.99	3.00	0.91	3.02	0.92
65.00	6.50	0.60	1.07	3.00	0.91	2.80	0.85
70.00	7.00	0.65	1.42	3.00	0.91	2.12	0.65
70.00	7.00	0.65	1.33	3.00	0.91	2.25	0.69
75.00	7.50	0.70	0.91	3.00	0.91	3.28	1.00
80.00	8.00	0.74	1.20	3.00	0.91	2.51	0.77

Top probes at station 2

Discharge (cfs)	Unit discharge (ft ² /s)	Unit discharge (m ² /s)	delta t (sec)	delta s (ft)	delta s (m)	V ₁₂ (ft/s)	V ₁₂ (m/s)
20.00	2.00	0.19	-	3.00	0.91	-	-
25.00	2.50	0.23	-	3.00	0.91	-	-
30.00	3.00	0.28	-	3.00	0.91	-	-
35.00	3.50	0.33	0.65	3.00	0.91	4.60	1.40
40.00	4.00	0.37	-	3.00	0.91	-	-
45.00	4.50	0.42	-	3.00	0.91	-	-
50.00	5.00	0.46	-	3.00	0.91	-	-
55.00	5.50	0.51	-	3.00	0.91	-	-
60.00	6.00	0.56	-	3.00	0.91	-	-
65.00	6.50	0.60	0.43	3.00	0.91	6.96	2.12
65.00	6.50	0.60	0.66	3.00	0.91	4.55	1.39
70.00	7.00	0.65	0.70	3.00	0.91	4.30	1.31
70.00	7.00	0.65	0.48	3.00	0.91	6.31	1.92
70.00	7.00	0.65	0.42	3.00	0.91	7.20	2.19
75.00	7.50	0.70	0.40	3.00	0.91	7.51	2.29
80.00	8.00	0.74	-	3.00	0.91	-	-

Bottom probes at station 3

Discharge (cfs)	Unit discharge (ft ² /s)	Unit discharge (m ² /s)	delta t (sec)	delta s (ft)	delta s (m)	V ₁₂ (ft/s)	V ₁₂ (m/s)
20.00	2.00	0.19	1.30	3.00	0.91	2.30	0.70
20.00	2.00	0.19	1.43	3.00	0.91	2.10	0.64
25.00	2.50	0.23	1.20	3.00	0.91	2.50	0.76
25.00	2.50	0.23	1.41	3.00	0.91	2.13	0.65
25.00	2.50	0.23	1.09	3.00	0.91	2.75	0.84
30.00	3.00	0.28	2.01	3.00	0.91	1.49	0.45
35.00	3.50	0.33	1.76	3.00	0.91	1.70	0.52
35.00	3.50	0.33	1.40	3.00	0.91	2.14	0.65
35.00	3.50	0.33	1.32	3.00	0.91	2.28	0.69
40.00	4.00	0.37	2.00	3.00	0.91	1.50	0.46
40.00	4.00	0.37	1.36	3.00	0.91	2.20	0.67
40.00	4.00	0.37	1.25	3.00	0.91	2.40	0.73
40.00	4.00	0.37	1.00	3.00	0.91	3.00	0.91
45.00	4.50	0.42	1.94	3.00	0.91	1.55	0.47
45.00	4.50	0.42	1.75	3.00	0.91	1.71	0.52
45.00	4.50	0.42	1.60	3.00	0.91	1.87	0.57
50.00	5.00	0.46	1.71	3.00	0.91	1.75	0.53
50.00	5.00	0.46	1.88	3.00	0.91	1.60	0.49
50.00	5.00	0.46	1.33	3.00	0.91	2.25	0.69
55.00	5.50	0.51	1.58	3.00	0.91	1.90	0.58
55.00	5.50	0.51	1.43	3.00	0.91	2.10	0.64
60.00	6.00	0.56	1.82	3.00	0.91	1.65	0.50
60.00	6.00	0.56	1.67	3.00	0.91	1.80	0.55
60.00	6.00	0.56	1.50	3.00	0.91	2.00	0.61
65.00	6.50	0.60	1.19	3.00	0.91	2.52	0.77
70.00	7.00	0.65	1.09	3.00	0.91	2.75	0.84
70.00	7.00	0.65	1.43	3.00	0.91	2.10	0.64
70.00	7.00	0.65	1.67	3.00	0.91	1.80	0.55
75.00	7.50	0.70	-	3.00	0.91	-	-
80.00	8.00	0.74	1.67	3.00	0.91	1.80	0.55
80.00	8.00	0.74	1.50	3.00	0.91	2.00	0.61
80.00	8.00	0.74	1.99	3.00	0.91	1.51	0.46

Middle probes at station 3

Discharge (cfs)	Unit discharge (ft ² /s)	Unit discharge (m ² /s)	delta t (sec)	delta s (ft)	delta s (m)	V ₁₂ (ft/s)	V ₁₂ (m/s)
20.00	2.00	0.19	1.26	3.00	0.91	2.38	0.73
20.00	2.00	0.19	1.15	3.00	0.91	2.60	0.79
20.00	2.00	0.19	1.07	3.00	0.91	2.81	0.86
25.00	2.50	0.23	1.09	3.00	0.91	2.75	0.84
25.00	2.50	0.23	0.84	3.00	0.91	3.57	1.09
30.00	3.00	0.28	1.25	3.00	0.91	2.40	0.73
30.00	3.00	0.28	1.34	3.00	0.91	2.24	0.68
35.00	3.50	0.33	1.29	3.00	0.91	2.33	0.71
35.00	3.50	0.33	1.06	3.00	0.91	2.82	0.86
35.00	3.50	0.33	0.85	3.00	0.91	3.53	1.08
35.00	3.50	0.33	0.93	3.00	0.91	3.22	0.98
40.00	4.00	0.37	1.67	3.00	0.91	1.80	0.55
40.00	4.00	0.37	2.40	3.00	0.91	1.25	0.38
40.00	4.00	0.37	1.30	3.00	0.91	2.30	0.70
40.00	4.00	0.37	1.15	3.00	0.91	2.60	0.79
40.00	4.00	0.37	0.87	3.00	0.91	3.45	1.05
45.00	4.50	0.42	1.30	3.00	0.91	2.31	0.70
45.00	4.50	0.42	1.24	3.00	0.91	2.41	0.73
45.00	4.50	0.42	1.13	3.00	0.91	2.65	0.81
45.00	4.50	0.42	1.11	3.00	0.91	2.70	0.82
45.00	4.50	0.42	1.03	3.00	0.91	2.90	0.88
50.00	5.00	0.46	1.36	3.00	0.91	2.20	0.67
50.00	5.00	0.46	1.43	3.00	0.91	2.10	0.64
50.00	5.00	0.46	1.15	3.00	0.91	2.60	0.79
50.00	5.00	0.46	1.25	3.00	0.91	2.40	0.73
55.00	5.50	0.51	1.25	3.00	0.91	2.40	0.73
55.00	5.50	0.51	1.20	3.00	0.91	2.51	0.77
55.00	5.50	0.51	0.94	3.00	0.91	3.20	0.98
55.00	5.50	0.51	1.00	3.00	0.91	3.00	0.91
60.00	6.00	0.56	0.85	3.00	0.91	3.51	1.07
60.00	6.00	0.56	1.00	3.00	0.91	3.00	0.91
60.00	6.00	0.56	1.09	3.00	0.91	2.75	0.84
60.00	6.00	0.56	1.25	3.00	0.91	2.40	0.73
60.00	6.00	0.56	1.20	3.00	0.91	2.51	0.77
65.00	6.50	0.60	0.91	3.00	0.91	3.30	1.01
70.00	7.00	0.65	1.36	3.00	0.91	2.20	0.67
70.00	7.00	0.65	1.20	3.00	0.91	2.51	0.77
75.00	7.50	0.70	0.90	3.00	0.91	3.35	1.02
75.00	7.50	0.70	1.15	3.00	0.91	2.60	0.79
80.00	8.00	0.74	1.25	3.00	0.91	2.40	0.73
80.00	8.00	0.74	1.15	3.00	0.91	2.60	0.79
80.00	8.00	0.74	0.90	3.00	0.91	3.35	1.02

Top probes at station 3

Discharge (cfs)	Unit discharge (ft ² /s)	Unit discharge (m ² /s)	delta t (sec)	delta s (ft)	delta s (m)	V ₁₂ (ft/s)	V ₁₂ (m/s)
20.00	2.00	0.19	0.60	3.00	0.91	5.00	1.52
25.00	2.50	0.23	0.50	3.00	0.91	6.00	1.83
30.00	3.00	0.28	0.69	3.00	0.91	4.32	1.32
30.00	3.00	0.28	0.64	3.00	0.91	4.68	1.43
35.00	3.50	0.33	0.65	3.00	0.91	4.65	1.42
35.00	3.50	0.33	0.60	3.00	0.91	5.00	1.52
35.00	3.50	0.33	0.50	3.00	0.91	6.00	1.83
35.00	3.50	0.33	0.55	3.00	0.91	5.48	1.67
40.00	4.00	0.37	0.60	3.00	0.91	5.00	1.52
40.00	4.00	0.37	0.70	3.00	0.91	4.31	1.31

40.00	4.00	0.37	0.65	3.00	0.91	4.61	1.41
45.00	4.50	0.42	0.69	3.00	0.91	4.32	1.32
45.00	4.50	0.42	0.65	3.00	0.91	4.61	1.41
45.00	4.50	0.42	0.60	3.00	0.91	5.00	1.52
50.00	5.00	0.46	0.69	3.00	0.91	4.32	1.32
55.00	5.50	0.51	0.55	3.00	0.91	5.50	1.68
55.00	5.50	0.51	0.66	3.00	0.91	4.52	1.38
55.00	5.50	0.51	0.66	3.00	0.91	4.54	1.38
60.00	6.00	0.56	0.60	3.00	0.91	5.00	1.52
60.00	6.00	0.56	0.50	3.00	0.91	6.00	1.83
60.00	6.00	0.56	0.46	3.00	0.91	6.52	1.99
60.00	6.00	0.56	0.45	3.00	0.91	6.60	2.01
60.00	6.00	0.56	0.40	3.00	0.91	7.50	2.29
65.00	6.50	0.60	0.60	3.00	0.91	5.00	1.52
70.00	7.00	0.65	0.45	3.00	0.91	6.60	2.01
75.00	7.50	0.70	-	3.00	0.91	-	-
80.00	8.00	0.74	-	3.00	0.91	-	-

INTERSTITIAL VELOCITY DATA: 1997

Port E at Station 1

Discharge (cfs)	Unit discharge (ft ² /s)	Unit discharge (m ² /s)	delta t (sec)	delta s (ft)	delta s (m)	V ₁₂ (ft/s)	V ₁₂ (m/s)
2.00	0.20	0.02	2.04	2.00	0.61	0.98	0.30
3.00	0.30	0.03	1.15	2.00	0.61	1.74	0.53
3.00	0.30	0.03	1.10	2.00	0.61	1.82	0.55
4.00	0.40	0.04	1.15	2.00	0.61	1.74	0.53
5.00	0.50	0.05	1.20	2.00	0.61	1.67	0.51
6.00	0.60	0.06	1.25	2.00	0.61	1.60	0.49
6.00	0.60	0.06	1.15	2.00	0.61	1.74	0.53
7.00	0.70	0.07	-	2.00	0.61	-	-
8.00	0.80	0.07	-	2.00	0.61	-	-
9.00	0.90	0.08	-	2.00	0.61	-	-
10.00	1.00	0.09	-	2.00	0.61	-	-
11.00	1.10	0.10	-	2.00	0.61	-	-
12.00	1.20	0.11	-	2.00	0.61	-	-
13.00	1.30	0.12	-	2.00	0.61	-	-
14.00	1.40	0.13	-	2.00	0.61	-	-
15.00	1.50	0.14	-	2.00	0.61	-	-
16.00	1.60	0.15	-	2.00	0.61	-	-
17.00	1.70	0.16	-	2.00	0.61	-	-
18.00	1.80	0.17	-	2.00	0.61	-	-
19.00	1.90	0.18	-	2.00	0.61	-	-
20.00	2.00	0.19	-	2.00	0.61	-	-
21.00	2.10	0.20	-	2.00	0.61	-	-
22.00	2.20	0.20	-	2.00	-	-	-

Port E at Station 2

Discharge (cfs)	Unit discharge (ft ² /s)	Unit discharge (m ² /s)	delta t (sec)	delta s (ft)	delta s (m)	V ₁₂ (ft/s)	V ₁₂ (m/s)
2.00	0.20	0.02	1.05	2.00	0.61	1.90	0.58
3.00	0.30	0.03	1.20	2.00	0.61	1.67	0.51
4.00	0.40	0.04	1.05	2.00	0.61	1.90	0.58
5.00	0.50	0.05	1.35	2.00	0.61	1.48	0.45
6.00	0.60	0.06	1.25	2.00	0.61	1.60	0.49
6.00	0.60	0.06	1.25	2.00	0.61	1.60	0.49
7.00	0.70	0.07	-	2.00	0.61	-	-
8.00	0.80	0.07	-	2.00	0.61	-	-
9.00	0.90	0.08	1.75	2.00	0.61	1.14	0.35
10.00	1.00	0.09	-	2.00	0.61	-	-
11.00	1.10	0.10	-	2.00	0.61	-	-
12.00	1.20	0.11	-	2.00	0.61	-	-
13.00	1.30	0.12	-	2.00	0.61	-	-
14.00	1.40	0.13	-	2.00	0.61	-	-
15.00	1.50	0.14	-	2.00	0.61	-	-
16.00	1.60	0.15	-	2.00	0.61	-	-
17.00	1.70	0.16	-	2.00	0.61	-	-
18.00	1.80	0.17	-	2.00	0.61	-	-
19.00	1.90	0.18	-	2.00	0.61	-	-
20.00	2.00	0.19	-	2.00	0.61	-	-
21.00	2.10	0.20	-	2.00	0.61	-	-
22.00	2.20	0.20	-	2.00	0.61	-	-

Port E at Station 3

Discharge (cfs)	Unit discharge (ft ² /s)	Unit discharge (m ² /s)	delta t (sec)	delta s (ft)	delta s (m)	V ₁₂ (ft/s)	V ₁₂ (m/s)
2.00	0.20	0.02	-	2.00	0.61	-	-
3.00	0.30	0.03	-	2.00	0.61	-	-
4.00	0.40	0.04	-	2.00	0.61	-	-
5.00	0.50	0.05	1.15	2.00	0.61	1.74	0.53
6.00	0.60	0.06	-	2.00	0.61	-	-
7.00	0.70	0.07	-	2.00	0.61	-	-
8.00	0.80	0.07	-	2.00	0.61	-	-
9.00	0.90	0.08	-	2.00	0.61	-	-
10.00	1.00	0.09	-	2.00	0.61	-	-
11.00	1.10	0.10	-	2.00	0.61	-	-
12.00	1.20	0.11	-	2.00	0.61	-	-
13.00	1.30	0.12	-	2.00	0.61	-	-
14.00	1.40	0.13	-	2.00	0.61	-	-
15.00	1.50	0.14	-	2.00	0.61	-	-
16.00	1.60	0.15	-	2.00	0.61	-	-
17.00	1.70	0.16	-	2.00	0.61	-	-
18.00	1.80	0.17	-	2.00	0.61	-	-
19.00	1.90	0.18	-	2.00	0.61	-	-
20.00	2.00	0.19	-	2.00	0.61	-	-
21.00	2.10	0.20	-	2.00	0.61	-	-
22.00	2.20	0.20	-	2.00	0.61	-	-

Port E at Station 4

Discharge (cfs)	Unit discharge (ft ² /s)	Unit discharge (m ² /s)	delta t (sec)	delta s (ft)	delta s (m)	V ₁₂ (ft/s)	V ₁₂ (m/s)
2.00	0.20	0.02	3.17	2.00	0.61	0.63	0.19
2.00	0.20	0.02	3.17	2.00	0.61	0.63	0.19
3.00	0.30	0.03	1.05	2.00	0.61	1.90	0.58
4.00	0.40	0.04	1.45	2.00	0.61	1.38	0.42
5.00	0.50	0.05	1.65	2.00	0.61	1.21	0.37
6.00	0.60	0.06	-	2.00	0.61	-	-
7.00	0.70	0.07	-	2.00	0.61	-	-
8.00	0.80	0.07	-	2.00	0.61	-	-
9.00	0.90	0.08	-	2.00	0.61	-	-
10.00	1.00	0.09	-	2.00	0.61	-	-
11.00	1.10	0.10	-	2.00	0.61	-	-
12.00	1.20	0.11	-	2.00	0.61	-	-
13.00	1.30	0.12	-	2.00	0.61	-	-
14.00	1.40	0.13	-	2.00	0.61	-	-
15.00	1.50	0.14	-	2.00	0.61	-	-
16.00	1.60	0.15	-	2.00	0.61	-	-
17.00	1.70	0.16	-	2.00	0.61	-	-
18.00	1.80	0.17	-	2.00	0.61	-	-
19.00	1.90	0.18	-	2.00	0.61	-	-
20.00	2.00	0.19	-	2.00	0.61	-	-
21.00	2.10	0.20	-	2.00	0.61	-	-
22.00	2.20	0.20	-	2.00	0.61	-	-

Port D at Station 1

Discharge (cfs)	Unit discharge (ft ² /s)	Unit discharge (m ² /s)	delta t (sec)	delta s (ft)	delta s (m)	V ₁₂ (ft/s)	V ₁₂ (m/s)
2.00	0.20	0.02	-	3.00	0.91	-	-
3.00	0.30	0.03	-	3.00	0.91	-	-
4.00	0.40	0.04	1.05	3.00	0.91	2.86	0.87
5.00	0.50	0.05	-	3.00	0.91	-	-

6.00	0.60	0.06	0.97	3.00	0.91	3.08	0.94
6.00	0.60	0.06	1.05	3.00	0.91	2.86	0.87
7.00	0.70	0.07	1.20	3.00	0.91	2.50	0.76
8.00	0.80	0.07	-	3.00	0.91	-	-
9.00	0.90	0.08	-	3.00	0.91	-	-
10.00	1.00	0.09	-	3.00	0.91	-	-
11.00	1.10	0.10	-	3.00	0.91	-	-
12.00	1.20	0.11	-	3.00	0.91	-	-
13.00	1.30	0.12	-	3.00	0.91	-	-
14.00	1.40	0.13	-	3.00	0.91	-	-
15.00	1.50	0.14	-	3.00	0.91	-	-
16.00	1.60	0.15	-	3.00	0.91	-	-
17.00	1.70	0.16	-	3.00	0.91	-	-
18.00	1.80	0.17	-	3.00	0.91	-	-
19.00	1.90	0.18	1.12	3.00	0.91	2.67	0.81
20.00	2.00	0.19	-	3.00	0.91	-	-
21.00	2.10	0.20	-	3.00	0.91	-	-
22.00	2.20	0.20	-	3.00	0.91	-	-

Port D at Station 2

Discharge (cfs)	Unit discharge (ft ² /s)	Unit discharge (m ² /s)	delta t (sec)	delta s (ft)	delta s (m)	V ₁₂ (ft/s)	V ₁₂ (m/s)
2.00	0.20	0.02	-	2.00	0.61	-	-
3.00	0.30	0.03	-	2.00	0.61	-	-
4.00	0.40	0.04	-	2.00	0.61	-	-
5.00	0.50	0.05	0.75	2.00	0.61	2.67	0.81
6.00	0.60	0.06	0.75	2.00	0.61	2.67	0.81
6.00	0.60	0.06	0.85	2.00	0.61	2.35	0.72
7.00	0.70	0.07	0.65	2.00	0.61	3.08	0.94
8.00	0.80	0.07	0.75	2.00	0.61	2.67	0.81
9.00	0.90	0.08	0.75	2.00	0.61	2.67	0.81
10.00	1.00	0.09	1.05	2.00	0.61	1.90	0.58
10.00	1.00	0.09	0.95	2.00	0.61	2.10	0.64
11.00	1.10	0.10	0.80	2.00	0.61	2.50	0.76
11.00	1.10	0.10	1.10	2.00	0.61	1.81	0.55
12.00	1.20	0.11	0.71	2.00	0.61	2.81	0.86
12.00	1.20	0.11	0.85	2.00	0.61	2.35	0.72
13.00	1.30	0.12	0.89	2.00	0.61	2.25	0.69
13.00	1.30	0.12	0.93	2.00	0.61	2.16	0.66
14.00	1.40	0.13	0.94	2.00	0.61	2.13	0.65
15.00	1.50	0.14	0.71	2.00	0.61	2.81	0.86
15.00	1.50	0.14	-	2.00	0.61	-	-
16.00	1.60	0.15	1.14	2.00	0.61	1.75	0.53
16.00	1.60	0.15	0.73	2.00	0.61	2.75	0.84
17.00	1.70	0.16	0.71	2.00	0.61	2.80	0.85
18.00	1.80	0.17	0.84	2.00	0.61	2.38	0.73
19.00	1.90	0.18	1.05	2.00	0.61	1.90	0.58
19.00	1.90	0.18	1.60	2.00	0.61	1.25	0.38
19.00	1.90	0.18	1.04	2.00	0.61	1.93	0.59
20.00	2.00	0.19	0.87	2.00	0.61	2.30	0.70
20.00	2.00	0.19	0.89	2.00	0.61	2.25	0.69
20.00	2.00	0.19	-	2.00	0.61	-	-
20.00	2.00	0.19	1.46	2.00	0.61	1.37	0.42
21.00	2.10	0.20	1.46	2.00	0.61	1.37	0.42
22.00	2.20	0.20	-	2.00	0.61	-	-

Port D at station 3

Discharge (cfs)	Unit discharge (ft ² /s)	Unit discharge (m ² /s)	delta t (sec)	delta s (ft)	delta s (m)	V ₁₂ (ft/s)	V ₁₂ (m/s)
2.00	0.20	0.02	1.05	2.00	0.61	1.90	0.58
2.00	0.20	0.02	0.85	2.00	0.61	2.35	0.72
2.00	0.20	0.02	1.25	2.00	0.61	1.60	0.49
3.00	0.30	0.03	0.90	2.00	0.61	2.22	0.68
3.00	0.30	0.03	1.05	2.00	0.61	1.90	0.58
3.00	0.30	0.03	0.90	2.00	0.61	2.22	0.68
4.00	0.40	0.04	1.00	2.00	0.61	2.00	0.61
5.00	0.50	0.05	0.90	2.00	0.61	2.22	0.68
5.00	0.50	0.05	0.70	2.00	0.61	2.86	0.87
6.00	0.60	0.06	0.80	2.00	0.61	2.50	0.76
6.00	0.60	0.06	-	2.00	0.61	-	-
6.00	0.60	0.06	0.75	2.00	0.61	2.67	0.81
7.00	0.70	0.07	-	2.00	0.61	-	-
8.00	0.80	0.07	0.80	2.00	0.61	2.50	0.76
9.00	0.90	0.08	-	2.00	0.61	-	-
10.00	1.00	0.09	-	2.00	0.61	-	-
10.00	1.00	0.09	-	2.00	0.61	-	-
11.00	1.10	0.10	0.65	2.00	0.61	3.08	0.94
12.00	1.20	0.11	0.80	2.00	0.61	2.50	0.76
12.00	1.20	0.11	0.65	2.00	0.61	3.08	0.94
13.00	1.30	0.12	0.71	2.00	0.61	2.81	0.86
14.00	1.40	0.13	-	2.00	0.61	-	-
15.00	1.50	0.14	1.14	2.00	0.61	1.75	0.53
16.00	1.60	0.15	0.73	2.00	0.61	2.75	0.84
17.00	1.70	0.16	0.71	2.00	0.61	2.80	0.85
18.00	1.80	0.17	0.84	2.00	0.61	2.38	0.73
19.00	1.90	0.18	1.05	2.00	0.61	1.90	0.58
20.00	2.00	0.19	1.60	2.00	0.61	1.25	0.38
21.00	2.10	0.20	1.04	2.00	0.61	1.93	0.59
22.00	2.20	0.20	0.87	2.00	0.61	2.30	0.70

Port D at Station 4

Discharge (cfs)	Unit discharge (ft ² /s)	Unit discharge (m ² /s)	delta t (sec)	delta s (ft)	delta s (m)	V ₁₂ (ft/s)	V ₁₂ (m/s)
2.00	0.20	0.02	-	2.00	0.61	-	-
3.00	0.30	0.03	-	2.00	0.61	-	-
4.00	0.40	0.04	-	2.00	0.61	-	-
5.00	0.50	0.05	0.90	2.00	0.61	2.22	0.68
5.00	0.50	0.05	0.85	2.00	0.61	2.35	0.72
6.00	0.60	0.06	0.80	2.00	0.61	2.50	0.76
6.00	0.60	0.06	0.70	2.00	0.61	2.86	0.87
6.00	0.60	0.06	0.85	2.00	0.61	2.34	0.71
8.00	0.80	0.07	0.70	2.00	0.61	2.86	0.87
9.00	0.90	0.08	0.65	2.00	0.61	3.08	0.94
9.00	0.90	0.08	0.90	2.00	0.61	2.22	0.68
10.00	1.00	0.09	-	2.00	0.61	-	-
10.00	1.00	0.09	0.70	2.00	0.61	2.86	0.87
11.00	1.10	0.10	0.70	2.00	0.61	2.86	0.87
11.00	1.10	0.10	0.65	2.00	0.61	3.08	0.94
12.00	1.20	0.11	0.80	2.00	0.61	2.50	0.76
12.00	1.20	0.11	0.75	2.00	0.61	2.67	0.81
13.00	1.30	0.12	0.85	2.00	0.61	2.35	0.72
14.00	1.40	0.13	1.00	2.00	0.61	2.00	0.61
14.00	1.40	0.13	0.85	2.00	0.61	2.35	0.72
15.00	1.50	0.14	0.85	2.00	0.61	2.35	0.72
16.00	1.60	0.15	1.10	2.00	0.61	1.82	0.55

16.00	1.60	0.15	0.75	2.00	0.61	2.67	0.81
17.00	1.70	0.16	0.80	2.00	0.61	2.50	0.76
18.00	1.80	0.17	0.85	2.00	0.61	2.35	0.72
19.00	1.90	0.18	1.10	2.00	0.61	1.82	0.55
19.00	1.90	0.18	0.80	2.00	0.61	2.50	0.76
20.00	2.00	0.19	0.65	2.00	0.61	3.08	0.94
20.00	2.00	0.19	0.85	2.00	0.61	2.35	0.72
21.00	2.10	0.20	-	2.00	0.61	-	-
22.00	2.20	0.20	-	2.00	0.61	-	-

Port C at Station 1

Discharge (cfs)	Unit discharge (ft ² /s)	Unit discharge (m ² /s)	delta t (sec)	delta s (ft)	delta s (m)	V ₁₂ (ft/s)	V ₁₂ (m/s)
2.00	0.20	0.02	-	2.00	0.61	-	-
3.00	0.30	0.03	-	2.00	0.61	-	-
4.00	0.40	0.04	-	2.00	0.61	-	-
5.00	0.50	0.05	-	2.00	0.61	-	-
6.00	0.60	0.06	1.00	2.00	0.61	2.00	0.61
6.00	0.60	0.06	0.80	2.00	0.61	2.50	0.76
6.00	0.60	0.06	1.00	2.00	0.61	2.00	0.61
7.00	0.70	0.07	1.00	2.00	0.61	2.00	0.61
8.00	0.80	0.07	1.00	2.00	0.61	2.00	0.61
9.00	0.90	0.08	0.95	2.00	0.61	2.11	0.64
10.00	1.00	0.09	1.05	2.00	0.61	1.90	0.58
10.00	1.00	0.09	0.80	2.00	0.61	2.50	0.76
11.00	1.10	0.10	0.85	2.00	0.61	2.35	0.72
11.00	1.10	0.10	0.85	2.00	0.61	2.35	0.72
12.00	1.20	0.11	1.10	2.00	0.61	1.82	0.55
12.00	1.20	0.11	0.90	2.00	0.61	2.22	0.68
13.00	1.30	0.12	0.90	2.00	0.61	2.22	0.68
13.00	1.30	0.12	0.75	2.00	0.61	2.67	0.81
14.00	1.40	0.13	0.85	2.00	0.61	2.35	0.72
15.00	1.50	0.14	0.65	2.00	0.61	3.08	0.94
16.00	1.60	0.15	0.70	2.00	0.61	2.86	0.87
16.00	1.60	0.15	-	2.00	0.61	-	-
17.00	1.70	0.16	0.75	2.00	0.61	2.67	0.81
18.00	1.80	0.17	0.75	2.00	0.61	2.67	0.81
19.00	1.90	0.18	0.70	2.00	0.61	2.86	0.87
19.00	1.90	0.18	0.75	2.00	0.61	2.67	0.81
20.00	2.00	0.19	0.75	2.00	0.61	2.67	0.81
20.00	2.00	0.19	-	2.00	0.61	-	-
20.00	2.00	0.19	0.80	2.00	0.61	2.50	0.76
20.00	2.00	0.19	0.75	2.00	0.61	2.67	0.81
21.00	2.10	0.20	0.85	2.00	0.61	2.35	0.72
21.00	2.10	0.20	0.80	2.00	0.61	2.50	0.76
21.00	2.10	0.20	0.75	2.00	0.61	2.67	0.81
22.00	2.20	0.20	0.70	2.00	0.61	2.86	0.87

Port C at Station 2

Discharge (cfs)	Unit discharge (ft ² /s)	Unit discharge (m ² /s)	delta t (sec)	delta s (ft)	delta s (m)	V ₁₂ (ft/s)	V ₁₂ (m/s)
2.00	0.20	0.02	-	2.00	0.61	-	-
3.00	0.30	0.03	-	2.00	0.61	-	-
4.00	0.40	0.04	-	2.00	0.61	-	-
5.00	0.50	0.05	-	2.00	0.61	-	-
6.00	0.60	0.06	-	2.00	0.61	-	-
7.00	0.70	0.07	0.80	2.00	0.61	2.50	0.76
8.00	0.80	0.07	0.80	2.00	0.61	2.50	0.76
9.00	0.90	0.08	0.95	2.00	0.61	2.11	0.64

9.00	0.90	0.08	1.05	2.00	0.61	1.90	0.58
10.00	1.00	0.09	0.80	2.00	0.61	2.50	0.76
11.00	1.10	0.10	0.85	2.00	0.61	2.35	0.72
11.00	1.10	0.10	0.85	2.00	0.61	2.35	0.72
12.00	1.20	0.11	1.10	2.00	0.61	1.82	0.55
13.00	1.30	0.12	0.90	2.00	0.61	2.22	0.68
14.00	1.40	0.13	0.85	2.00	0.61	2.35	0.72
15.00	1.50	0.14	0.65	2.00	0.61	3.08	0.94
15.00	1.50	0.14	0.70	2.00	0.61	2.86	0.87
16.00	1.60	0.15	-	2.00	0.61	-	-
17.00	1.70	0.16	-	2.00	0.61	-	-
18.00	1.80	0.17	-	2.00	0.61	-	-
19.00	1.90	0.18	-	2.00	0.61	-	-
20.00	2.00	0.19	-	2.00	0.61	-	-
21.00	2.10	0.20	-	2.00	0.61	-	-
22.00	2.20	0.20	-	2.00	0.61	-	-

Port C at Station 3

Discharge (cfs)	Unit discharge (ft ² /s)	Unit discharge (m ² /s)	delta t (sec)	delta s (ft)	delta s (m)	V ₁₂ (ft/s)	V ₁₂ (m/s)
2.00	0.20	0.02	-	2.00	0.61	-	-
3.00	0.30	0.03	-	2.00	0.61	-	-
4.00	0.40	0.04	-	2.00	0.61	-	-
5.00	0.50	0.05	0.85	2.00	0.61	2.35	0.72
6.00	0.60	0.06	-	2.00	0.61	-	-
6.00	0.60	0.06	0.70	2.00	0.61	2.86	0.87
6.00	0.60	0.06	0.65	2.00	0.61	3.08	0.94
6.00	0.60	0.06	0.70	2.00	0.61	2.86	0.87
7.00	0.70	0.07	-	2.00	0.61	-	-
8.00	0.80	0.07	-	2.00	0.61	-	-
9.00	0.90	0.08	-	2.00	0.61	-	-
10.00	1.00	0.09	-	2.00	0.61	-	-
11.00	1.10	0.10	-	2.00	0.61	-	-
12.00	1.20	0.11	-	2.00	0.61	-	-
13.00	1.30	0.12	-	2.00	0.61	-	-
14.00	1.40	0.13	-	2.00	0.61	-	-
15.00	1.50	0.14	-	2.00	0.61	-	-
16.00	1.60	0.15	-	2.00	0.61	-	-
17.00	1.70	0.16	-	2.00	0.61	-	-
18.00	1.80	0.17	-	2.00	0.61	-	-
19.00	1.90	0.18	-	2.00	0.61	-	-
20.00	2.00	0.19	-	2.00	0.61	-	-
21.00	2.10	0.20	-	2.00	0.61	-	-
22.00	2.20	0.20	-	2.00	0.61	-	-

Port C at Station 4

Discharge (cfs)	Unit discharge (ft ² /s)	Unit discharge (m ² /s)	delta t (sec)	delta s (ft)	delta s (m)	V ₁₂ (ft/s)	V ₁₂ (m/s)
2.00	0.20	0.02	-	2.00	0.61	-	-
3.00	0.30	0.03	-	2.00	0.61	-	-
4.00	0.40	0.04	-	2.00	0.61	-	-
5.00	0.50	0.05	-	2.00	0.61	-	-
6.00	0.60	0.06	0.90	2.00	0.61	2.22	0.68
6.00	0.60	0.06	0.85	2.00	0.61	2.34	0.71
6.00	0.60	0.06	0.90	2.00	0.61	2.22	0.68
8.00	0.80	0.07	0.80	2.00	0.61	2.50	0.76
9.00	0.90	0.08	0.90	2.00	0.61	2.22	0.68
9.00	0.90	0.08	1.00	2.00	0.61	2.00	0.61
10.00	1.00	0.09	0.85	2.00	0.61	2.35	0.72

10.00	1.00	0.09	0.70	2.00	0.61	2.86	0.87
11.00	1.10	0.10	0.75	2.00	0.61	2.67	0.81
11.00	1.10	0.10	0.90	2.00	0.61	2.22	0.68
12.00	1.20	0.11	0.85	2.00	0.61	2.35	0.72
13.00	1.30	0.12	0.65	2.00	0.61	3.08	0.94
14.00	1.40	0.13	0.90	2.00	0.61	2.22	0.68
15.00	1.50	0.14	0.75	2.00	0.61	2.67	0.81
16.00	1.60	0.15	1.20	2.00	0.61	1.67	0.51
16.00	1.60	0.15	0.90	2.00	0.61	2.22	0.68
17.00	1.70	0.16	0.90	2.00	0.61	2.22	0.68
18.00	1.80	0.17	0.80	2.00	0.61	2.50	0.76
19.00	1.90	0.18	1.15	2.00	0.61	1.74	0.53
19.00	1.90	0.18	0.95	2.00	0.61	2.11	0.64
20.00	2.00	0.19	0.65	2.00	0.61	3.08	0.94
20.00	2.00	0.19	0.75	2.00	0.61	2.67	0.81
21.00	2.10	0.20	1.00	2.00	0.61	2.00	0.61
21.00	2.10	0.20	-	2.00	0.61	-	-
22.00	2.20	0.20	0.70	2.00	0.61	2.86	0.87

Port B at Station 1

Discharge (cfs)	Unit discharge (ft ² /s)	Unit discharge (m ² /s)	delta t (sec)	delta s (ft)	delta s (m)	V ₁₂ (ft/s)	V ₁₂ (m/s)
2.00	0.20	0.02	-	2.00	0.61	-	-
3.00	0.30	0.03	-	2.00	0.61	-	-
4.00	0.40	0.04	-	2.00	0.61	-	-
5.00	0.50	0.05	-	2.00	0.61	-	-
6.00	0.60	0.06	-	2.00	0.61	-	-
7.00	0.70	0.07	0.70	2.00	0.61	2.86	0.87
8.00	0.80	0.07	-	2.00	0.61	-	-
9.00	0.90	0.08	0.80	2.00	0.61	2.50	0.76
10.00	1.00	0.09	0.85	2.00	0.61	2.35	0.72
10.00	1.00	0.09	0.70	2.00	0.61	2.86	0.87
11.00	1.10	0.10	-	2.00	0.61	-	-
11.00	1.10	0.10	0.90	2.00	0.61	2.22	0.68
12.00	1.20	0.11	0.70	2.00	0.61	2.86	0.87
12.00	1.20	0.11	0.70	2.00	0.61	2.86	0.87
13.00	1.30	0.12	0.80	2.00	0.61	2.50	0.76
14.00	1.40	0.13	-	2.00	0.61	-	-
15.00	1.50	0.14	0.65	2.00	0.61	3.08	0.94
15.00	1.50	0.14	0.70	2.00	0.61	2.86	0.87
16.00	1.60	0.15	-	2.00	0.61	-	-
16.00	1.60	0.15	0.70	2.00	0.61	2.86	0.87
17.00	1.70	0.16	-	2.00	0.61	-	-
18.00	1.80	0.17	0.80	2.00	0.61	2.50	0.76
19.00	1.90	0.18	-	2.00	0.61	-	-
19.00	1.90	0.18	-	2.00	0.61	-	-
19.00	1.90	0.18	-	2.00	0.61	-	-
20.00	2.00	0.19	-	2.00	0.61	-	-
20.00	2.00	0.19	-	2.00	0.61	-	-
20.00	2.00	0.19	-	2.00	0.61	-	-
20.00	2.00	0.19	-	2.00	0.61	-	-
21.00	2.10	0.20	-	2.00	0.61	-	-
21.00	2.10	0.20	-	2.00	0.61	-	-
21.00	2.10	0.20	-	2.00	0.61	-	-
22.00	2.20	0.20	-	2.00	0.61	-	-

Port B at Station 2

Discharge (cfs)	Unit discharge (ft ² /s)	Unit discharge (m ² /s)	delta t (sec)	delta s (ft)	delta s (m)	V ₁₂ (ft/s)	V ₁₂ (m/s)
--------------------	--	---------------------------------------	------------------	-----------------	----------------	---------------------------	--------------------------

2.00	0.20	0.02	-	2.00	0.61	-	-
3.00	0.30	0.03	-	2.00	0.61	-	-
4.00	0.40	0.04	-	2.00	0.61	-	-
5.00	0.50	0.05	-	2.00	0.61	-	-
6.00	0.60	0.06	0.65	2.00	0.61	3.08	0.94
7.00	0.70	0.07	-	2.00	0.61	-	-
8.00	0.80	0.07	0.75	2.00	0.61	2.67	0.81
9.00	0.90	0.08	0.70	2.00	0.61	2.86	0.87
9.00	0.90	0.08	0.80	2.00	0.61	2.50	0.76
10.00	1.00	0.09	0.70	2.00	0.61	2.86	0.87
11.00	1.10	0.10	-	2.00	0.61	-	-
11.00	1.10	0.10	0.65	2.00	0.61	3.08	0.94
12.00	1.20	0.11	0.65	2.00	0.61	3.08	0.94
12.00	1.20	0.11	-	2.00	0.61	-	-
13.00	1.30	0.12	-	2.00	0.61	-	-
14.00	1.40	0.13	0.70	2.00	0.61	2.86	0.87
14.00	1.40	0.13	-	2.00	0.61	-	-
15.00	1.50	0.14	0.65	2.00	0.61	3.08	0.94
15.00	1.50	0.14	0.65	2.00	0.61	3.08	0.94
16.00	1.60	0.15	-	2.00	0.61	-	-
17.00	1.70	0.16	0.75	2.00	0.61	2.67	0.81
18.00	1.80	0.17	-	2.00	0.61	-	-
19.00	1.90	0.18	-	2.00	0.61	-	-
20.00	2.00	0.19	-	2.00	0.61	-	-
21.00	2.10	0.20	-	2.00	0.61	-	-
22.00	2.20	0.20	-	2.00	0.61	-	-

Port B at Station 3

Discharge (cfs)	Unit discharge (ft ² /s)	Unit discharge (m ² /s)	delta t (sec)	delta s (ft)	delta s (m)	V ₁₂ (ft/s)	V ₁₂ (m/s)
2.00	0.20	0.02	-	2.00	0.61	-	-
3.00	0.30	0.03	-	2.00	0.61	-	-
4.00	0.40	0.04	-	2.00	0.61	-	-
5.00	0.50	0.05	1.05	2.00	0.61	1.90	0.58
6.00	0.60	0.06	1.05	2.00	0.61	1.90	0.58
6.00	0.60	0.06	0.80	2.00	0.61	2.50	0.76
6.00	0.60	0.06	0.90	2.00	0.61	2.22	0.68
6.00	0.60	0.06	0.80	2.00	0.61	2.50	0.76
7.00	0.70	0.07	-	2.00	0.61	-	-
8.00	0.80	0.07	-	2.00	0.61	-	-
9.00	0.90	0.08	-	2.00	0.61	-	-
10.00	1.00	0.09	-	2.00	0.61	-	-
11.00	1.10	0.10	-	2.00	0.61	-	-
12.00	1.20	0.11	-	2.00	0.61	-	-
13.00	1.30	0.12	-	2.00	0.61	-	-
14.00	1.40	0.13	-	2.00	0.61	-	-
15.00	1.50	0.14	-	2.00	0.61	-	-
16.00	1.60	0.15	-	2.00	0.61	-	-
17.00	1.70	0.16	-	2.00	0.61	-	-
18.00	1.80	0.17	-	2.00	0.61	-	-
19.00	1.90	0.18	-	2.00	0.61	-	-
20.00	2.00	0.19	-	2.00	0.61	-	-
21.00	2.10	0.20	-	2.00	0.61	-	-
22.00	2.20	0.20	-	2.00	0.61	-	-

Port B at Station 4

Discharge (cfs)	Unit discharge (ft ² /s)	Unit discharge (m ² /s)	delta t (sec)	delta s (ft)	delta s (m)	V ₁₂ (ft/s)	V ₁₂ (m/s)
2.00	0.20	0.02	-	2.00	0.61	-	-

3.00	0.30	0.03	-	2.00	0.61	-	-
4.00	0.40	0.04	-	2.00	0.61	-	-
5.00	0.50	0.05	-	2.00	0.61	-	-
6.00	0.60	0.06	-	2.00	0.61	-	-
6.00	0.60	0.06	-	2.00	0.61	-	-
6.00	0.60	0.06	-	2.00	0.61	-	-
6.00	0.60	0.06	-	2.00	0.61	-	-
7.00	0.70	0.07	-	2.00	0.61	-	-
8.00	0.80	0.07	-	2.00	0.61	-	-
9.00	0.90	0.08	0.90	2.00	0.61	2.22	0.68
9.00	0.90	0.08	0.70	2.00	0.61	2.86	0.87
10.00	1.00	0.09	0.75	2.00	0.61	2.67	0.81
10.00	1.00	0.09	0.70	2.00	0.61	2.86	0.87
11.00	1.10	0.10	-	2.00	0.61	-	-
11.00	1.10	0.10	0.70	2.00	0.61	2.86	0.87
12.00	1.20	0.11	0.75	2.00	0.61	2.67	0.81
12.00	1.20	0.11	0.70	2.00	0.61	2.86	0.87
13.00	1.30	0.12	0.85	2.00	0.61	2.35	0.72
14.00	1.40	0.13	-	2.00	0.61	-	-
14.00	1.40	0.13	-	2.00	0.61	-	-
14.00	1.40	0.13	-	2.00	0.61	-	-
15.00	1.50	0.14	-	2.00	0.61	-	-
16.00	1.60	0.15	0.85	2.00	0.61	2.35	0.72
16.00	1.60	0.15	0.85	2.00	0.61	2.35	0.72
17.00	1.70	0.16	0.65	2.00	0.61	3.08	0.94
18.00	1.80	0.17	0.70	2.00	0.61	2.86	0.87
19.00	1.90	0.18	0.90	2.00	0.61	2.22	0.68
19.00	1.90	0.18	0.80	2.00	0.61	2.50	0.76
20.00	2.00	0.19	-	2.00	0.61	-	-
20.00	2.00	0.19	-	2.00	0.61	-	-
21.00	2.10	0.20	0.80	2.00	0.61	2.50	0.76
21.00	2.10	0.20	0.75	2.00	0.61	2.67	0.81
22.00	2.20	0.20	0.75	2.00	0.61	2.67	0.81

APPENDIX B
MANOMETER DATA

1994 Manometer Data

Unit discharge q (m ² /s)	WATER DEPTHS			
	Station 1 (m)	Station 2 (m)	Station 3 (m)	Average (m)
0.048	0.604	0.518	-	0.561
0.056	0.644	-	-	0.644
0.065	0.699	0.580	-	0.639
0.077	0.745	0.730	-	0.738
0.083	0.813	0.734	0.714	0.753
0.093	0.826	0.753	0.738	0.772
0.102	0.823	0.770	0.758	0.783
0.111	0.839	0.791	0.783	0.804
0.121	0.868	0.833	0.828	0.843
0.133	0.880	0.841	-	0.861
0.143	0.891	0.855	0.829	0.858
0.176	0.909	0.885	-	0.897
0.189	0.910	0.858	-	0.884
0.206	0.924	0.874	-	0.899

1995 Manometer Data

Unit discharge q (m ² /s)	WATER DEPTHS			
	Station 1 (m)	Station 2 (m)	Station 3 (m)	Average (m)
0.093	0.859	-	0.750	0.804
0.149	0.985	0.876	0.886	0.916
0.177	1.088	0.901	0.996	0.995
0.186	1.085	0.939	1.000	1.008
0.232	1.184	1.026	1.116	1.109
0.279	1.253	1.115	1.188	1.185
0.325	1.299	1.141	1.243	1.228
0.372	1.359	1.180	1.273	1.270
0.418	1.419	1.198	1.291	1.303
0.465	1.411	1.248	1.294	1.318
0.511	1.384	1.248	1.400	1.344
0.557	1.466	1.254	1.389	1.370
0.604	1.491	1.224	1.348	1.354
0.650	1.534	1.256	1.380	1.390
0.697	1.536	1.279	1.433	1.416
0.743	1.558	1.300	1.464	1.440

1997 Manometer Data

Unit discharge q (m^2/s)	WATER DEPTHS				
	Station 1 (m)	Station 2 (m)	Station 3 (m)	Station 4 (m)	Average (m)
0.015	0.118	0.146	0.140	0.126	0.133
0.019	0.164	0.164	0.146	0.174	0.162
0.024	0.175	0.196	0.196	0.179	0.187
0.028	0.175	0.193	0.190	0.229	0.197
0.033	0.214	0.229	0.225	0.245	0.228
0.037	0.244	0.236	0.231	0.265	0.244
0.046	0.290	0.290	0.279	0.308	0.292
0.056	0.350	-	0.296	0.358	0.335
0.065	0.393	0.389	0.366	0.399	0.387
0.066	0.396	-	-	-	0.396
0.075	0.419	0.450	-	0.450	0.440
0.085	0.461	0.480	0.405	0.498	0.461
0.094	0.488	0.514	0.419	0.541	0.490
0.102	0.503	0.535	0.433	0.578	0.512
0.111	0.519	0.551	0.439	0.593	0.525
0.121	0.534	0.569	0.448	0.606	0.539
0.131	0.545	0.583	0.464	0.629	0.555
0.138	0.553	0.586	0.473	0.634	0.561
0.149	0.560	0.596	0.480	0.644	0.570
0.158	0.564	0.606	0.474	0.650	0.573
0.167	0.571	0.610	0.446	0.654	0.570
0.177	0.583	0.615	0.476	0.659	0.583
0.186	0.586	0.610	0.484	0.674	0.588
0.195	0.590	0.616	0.476	0.688	0.593
0.204	0.599	0.610	0.473	0.685	0.592